DISSERTATION

DOWNWIND QUANTIFICATION OF METHANE EMISSIONS: MODELS UNCERTAINTIES AND VARIABILITY ACROSS OIL AND GAS AND NON-OIL-AND-GAS SOURCES

Submitted by

Mercy W. Mbua

Department of Systems Engineering

In partial fulfillment of the requirements

For the Degree of Doctor of Philosophy

Colorado State University

Fort Collins, Colorado

Spring 2026

Doctoral Committee:

Advisor: Anna Hodshire
Co-Advisor: Daniel Zimmerle

Thomas Bradley
Ellison Carter

ABSTRACT

DOWNWIND QUANTIFICATION OF METHANE EMISSIONS:
MODELS' UNCERTAINTIES AND VARIABILITY ACROSS OIL AND GAS AND NON-OIL-AND-GAS SOURCES

Methane (CH_4) is a potent greenhouse gas, and accurate quantification of emissions across oil and gas and non–oil and gas sectors is critical for climate mitigation and inventory reconciliation. This dissertation investigates methane emissions using two complementary objectives: (1) evaluating the feasibility of using downwind methods to quantify point source oil and gas emissions using continuously monitoring fence-line sensors, and (2) a comparison of bottom-up, measurement-based and EPA inventory methane emission estimates for non–oil and gas sources in the Denver–Julesburg basin, Colorado, while assessing seasonal variability and consistency with existing inventories.

For Objective 1, controlled-release experiments were conducted to test the performance of closed-path eddy covariance (EC), backward Lagrangian stochastic (bLs) modeling, and Gaussian plume inverse method (GPIM). The closed-path EC system was unsuitable due to instrumentation limitations, including non-synchronous data logging, low sampling frequency, and a slow analyzer response, resulting in invalid flux estimates. The GPIM and bLs models demonstrated higher quantification accuracy for single-release single-point (SRSP) emissions, with bLs achieving slopes near unity and moderate R^2 values, but both methods showed reduced accuracy for multi-release single-point (MRSP) scenarios due to plume interference and complex flow conditions. These results highlight the feasibility of GPIM and bLs for isolated point sources while

emphasizing that method performance strongly depends on source complexity, wind conditions, and data quality.

Objective 2 focused on generating measurement-based emission factors (EFs) and annualized CH_4 inventories for concentrated animal feeding operations (CAFOs), municipal solid waste (MSW) landfills, wastewater treatment plants (WWTPs), and lakes/reservoirs. Annualized emissions totaled 123 ± 21 Gg CH_4 yr^{-1}, closely aligning with the EPA's bottom-up estimate of 119 Gg CH_4 yr^{-1}. CAFOs were identified as the dominant non–oil and gas source, contributing 78% of total emissions using study-derived EFs, while MSW landfills and WWTPs contributed 11% and 1%, respectively. Seasonal variability was evident for lakes/reservoirs, and landfill emissions but inconsistent for CAFOs and WWTPs, indicating that representative measurements at any time of year can reliably inform annual inventories for the latter sectors. This study's measurement-based framework differed from the EPA's approach in that it relied on direct, field-based quantification rather than process-based activity data and static emission factors. By integrating weighted probabilities within Monte Carlo simulations, this study produced annualized EFs that reflect the distribution of both large, episodic emissions and numerous smaller, continuous sources, rather than assuming uniform emission behavior. Despite these methodological differences, the resulting annualized inventory reconciled closely with the EPA's estimate, underscoring the robustness of both approaches when temporal and spatial variability are appropriately captured. This convergence suggests that measurement-informed weighting techniques can enhance existing inventory frameworks without necessitating entirely new models, ultimately improving transparency and confidence in methane reporting across non–oil and gas sectors.

This dissertation provides several key contributions: (1) a systematic, field-tested comparison of CH_4 quantification methods under controlled-release oil and gas scenarios; (2) improved evidence-based guidance on practical methane quantification, including the strengths and limitations of each method and conditions under which accuracy and uncertainty are optimized; (3) a detailed, field-data-derived methane inventory for non–oil and gas sources in the DJ Basin, providing new emission factors, seasonal insights, and identification of primary emission drivers; and (4) a field-based methodology for scaling snapshot measurements to annual scales for inventory comparisons.

Finally, this research emphasizes a system-of-systems perspective for methane mitigation, highlighting the importance of integrating measurements, models, and teams across sectors to assess total emissions and track reduction progress. By combining methodological rigor with field-based inventories, this work informs both sector-specific mitigation strategies and broader global efforts to reduce atmospheric methane growth.

Keywords: Methane; continuous monitoring; oil and gas; point source; closed-path eddy covariance; Gaussian plume inverse method; backward Lagrangian stochastic model; livestock emissions; landfills; wastewater treatment; lakes and reservoirs; measurement-based inventory; reconciliation; systems engineering; systems thinking; methane reduction

ACKNOWLEDGEMENTS

God: Dear God, thank you so much for bringing me this far. I am where I am today because of your favor and grace.

Professor Daniel Zimmerle: Dan, I still remember the day I interviewed with you back in early 2021. I did not have much to say then because of my limited knowledge and experience in the field, but you still gave me a chance to join your research group. I could not believe it when I saw your "Congratulations" email. Since then, I have always told myself that I hope I am working hard enough to make you proud and that you never regret giving me that opportunity. You have supported me through my MSc, my PhD, and even as I plan for what comes next. Thank you so much, Dan, and God bless you. I will always carry forward your example by supporting others and giving them a chance the same way you did for me. I have deep gratitude.

Dr. Stuart Riddick: Stuart, you were my advisor for a long time, through my MSc and a large part of my PhD, and you taught me almost everything I know. I still remember our first meeting during my master's when you told me about the above ground detection for underground pipelines project, and I said, "Why don't we just install alarm sensors?" Ha! You supported me when I said I wanted to pursue a PhD, and you made sure I always had enough projects to see it through. When you left, you had set me up so well that I did not struggle to reach the end. Thank you so much, Stuart, for being such a great advisor. God bless you.

Dr. Anna Hodshire: Anna, you were my second advisor, and you truly held my hand to the finish line. We may not have worked together for long, but over the past year your support and guidance made all the difference. Thank you for your timely feedback and input on my research progress. Thank you so much, Anna. I am deeply grateful.

Dr. Thomas Bradley: Thank you so much for agreeing to be part of my PhD committee despite your busy schedule, and for providing great feedback during my preliminary exam and the PhD proposal writing class. I sincerely appreciate your time and insights.

Dr. Elisson Carter: Dr. Carter, I first interacted with you through the "Statistics for Environmental Monitoring" class, one of the few classes that directly related to what I do. Thank you for the excellent lessons and for your preliminary feedback, which have helped me tremendously.

METEC Team: I have been at METEC for the last four and a half years, since I started my master's and transitioned to my PhD. I have worked with so many amazing people, some of whom are no longer there. I have gained so much and learned even more. METEC has been a home to me. To the staff and fellow graduate students, some of whom became close friends, I could not have reached this point without your help and support. You have been my family. Thank you so much, and maybe in the future we will work together again.

My Family: To my beautiful family-my husband Francis Otinga and my son Harvey Otinga-you were the most affected by my decision to pursue graduate school. I have been away for almost five years, and it was hard being apart. But despite everything, we held on. Francis, you were the first to support me emotionally and financially, even knowing how hard it would be for you. You always said the PhD belongs to the family. You were strong when I fell apart, and you have taken great care of Harvey. Thank you so much for your patience and sacrifice. It was all worth it.

My Friends: To my amazing friends who have offered advice, love, and support, thank you so much. In a special way, I would like to mention Elijah Kiplimo, and Dr. Victor Kebande among many. Thank you for being part of my graduate school journey, and for the incredible mentorship, support and numerous advice. Elijah worked with me for long hours during both projects, thanks a lot Elijah. Victor taught me how to navigate the difficult graduate school, "PhD is not about the

product, but the process - skills, independence, and quality".

To the beautiful Colorado mountains, rivers, parks and St. John 23rd Catholic Church, thank you for keeping my sanity.

Lastly, I thank the Cogen Fellowship, Department of Systems Engineering, and the Site-Aerial-Basin Emissions Reconciliation (SABER) project for funding my studies and research projects.

DEDICATION

My family: Dr. Francis Wanjala Otinga and Leo Harvey Otinga, Mbuas, Otingas, and my wonderful friends.

To all who believed in me and offered unconditional love and support throughout this journey, I am deeply grateful!

TABLE OF CONTENTS

LIST OF FIGURES

LIST OF TABLES

CHAPTER 1: INTRODUCTION AND BACKGROUND

1.0 Introduction

1.1 Systems engineering context and application to methane emissions

This PhD dissertation focuses on methane (CH_4) emissions as a discipline situated within the Department of Systems Engineering. INCOSE (2025) defines *Systems Engineering* as a "transdisciplinary and integrative approach to enable the successful realization, use, and retirement of engineered systems, using systems principles and concepts, and scientific, technological, and management methods." Systems engineering emphasizes on:

i. establishing, balancing, and integrating stakeholders' goals, purposes, and success criteria;
ii. defining lifecycle models, process approaches, and governance structures that address complexity, uncertainty, and change;
iii. generating and evaluating alternative solution concepts and architectures; and
iv. integrating diverse subsystems to ensure successful overall system performance.

A notable example of a complex systems engineering challenge is the Boeing 787 program, launched in April 2004 with an anticipated completion in 2008. The program's objective was to design a lightweight, fuel-efficient, long-range commercial aircraft—composed of 50% composite materials compared to 12% in the Boeing 777—to reduce airline operating costs and enhance passenger comfort. Initially estimated at $5–6 billion, the program eventually experienced delays of up to 40 months and cost overruns approaching $40 billion (adaorah, 2024; Mudavadi et al., 2011; Niazi et al., 2006). The main challenge stemmed from Boeing's outsourcing strategy. The company collaborated with more than 50 suppliers, each responsible for distinct subsystems, intending to lower development costs and distribute design risks. This shifted Boeing's role from

that of a manufacturer to that of a system integrator. However, deficiencies in integration management, particularly in managing interfaces, requirements, configuration, and verification and validation, resulted in significant delays and cost growth. This example highlights that systems engineering is fundamentally a *holistic approach* to problem-solving that cuts across multiple disciplines and requires the coordinated integration of data, technologies, and teams. It is essential in addressing complex, large-scale challenges where subsystems cannot be effectively solved in isolation.

In this context, this dissertation examines *Downwind quantification of methane emissions: models' uncertainties and variability across oil and gas and non-oil-and-gas sources*. This work represents one component within the broader global effort to reduce methane emissions. While different research teams and organizations often specialize in distinct subsystems—such as oil and gas, landfills, or agriculture—and within these, employ diverse measurement technologies (e.g., aircraft-, satellite-, or vehicle-based instruments) and modeling tools, achieving collective success requires integrating data and insights across all sources (Figure 1). Only through such integration can we identify which subsystems are optimized, which offer opportunities for further mitigation, and how success can be measured at the system level, namely, total global methane reduction.

This dissertation demonstrates that by viewing methane quantification as part of a larger system, cross-domain learning becomes possible. Concepts and methodologies proven in one subsystem (e.g., oil and gas) can be adapted to others (e.g., non–oil and gas sectors), enabling faster and more effective adoption. Ultimately, methane reduction requires a *system-of-systems perspective*—understanding emissions collectively across all sources to achieve meaningful global progress.

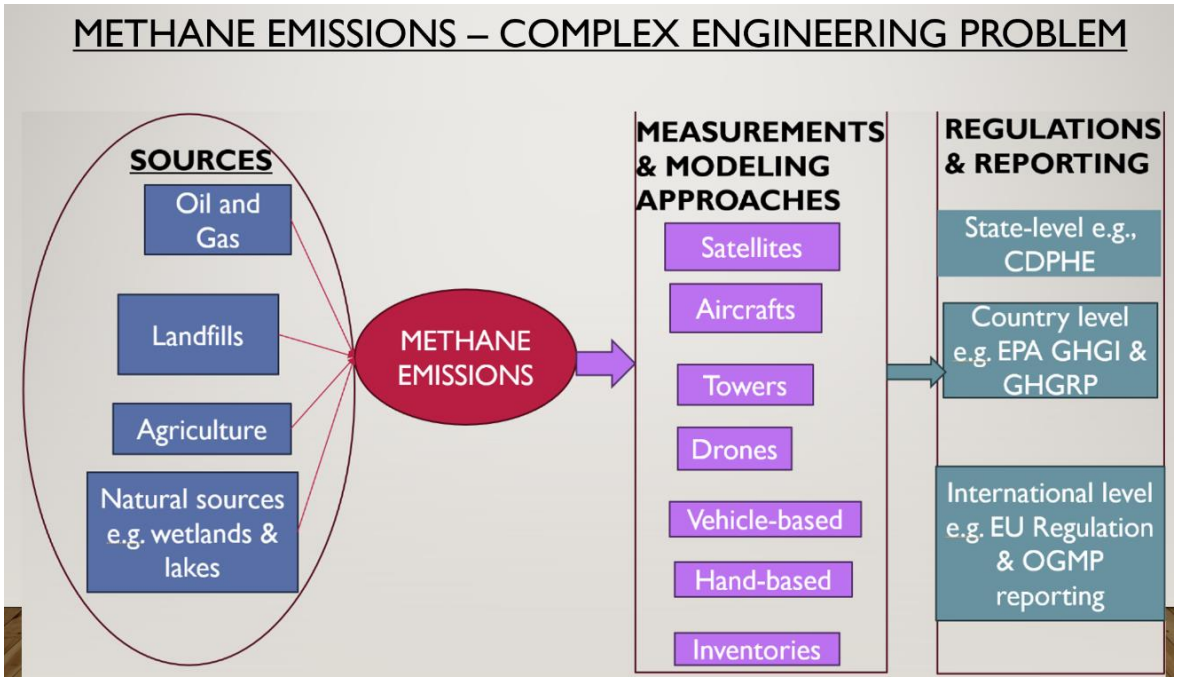

Figure 1. An illustration of methane emissions reductions as a complex systems engineering problem

1.2 Methane emissions

Methane (CH_4) is a hydrocarbon that is a primary component of natural gas. It is also a greenhouse gas that is 28 times more potent than carbon dioxide in trapping heat in the atmosphere (US EPA, 2016). Methane affects the earth's temperature and climate system. Over the last two centuries, CH_4 concentrations in the atmosphere have more than doubled mainly due to human-related activities. Methane is produced from both natural and human-influenced (anthropogenic) sources. These include oil and gas systems; agriculture; wastewater treatment; coal mining; stationary and mobile combustion; industrial processes; and wetlands, lakes, and reservoirs (US EPA, 2016). Methane is both powerful but short-lived in the atmosphere meaning targeting its reduction would have a significant effect of reducing global warming (US EPA, 2016).

The global atmospheric CH_4 budget is generally categorized into total emissions, where CH_4 is added to the atmosphere, and total sinks, through which CH_4 is removed from the atmosphere. In a perfectly balanced system, these two processes would offset each other. However,

increasing human activities have disrupted this balance, leading to higher CH_4 emissions from sources such as fossil fuel extraction and use, agriculture, the waste sector, and biofuel combustion, compared to removal processes such as chemical oxidation in the atmosphere and soil absorption (Figure 2). According to Saunois et al. (2025), global CH_4 emissions during the 2010–2019 decade were estimated at 669 Tg CH_4 yr^{-1} based on bottom-up approaches and 575 Tg CH_4 yr^{-1} using top-down approaches (Figure 2). Generally, bottom-up approaches estimate emissions from all potential sources at the source level and scale up by summing emissions from individual sources, whereas top-down approaches estimate emissions by using atmospheric methane concentration measurements to infer emission rates at larger spatial scales, such as regional or basin levels (Vaughn et al., 2018).

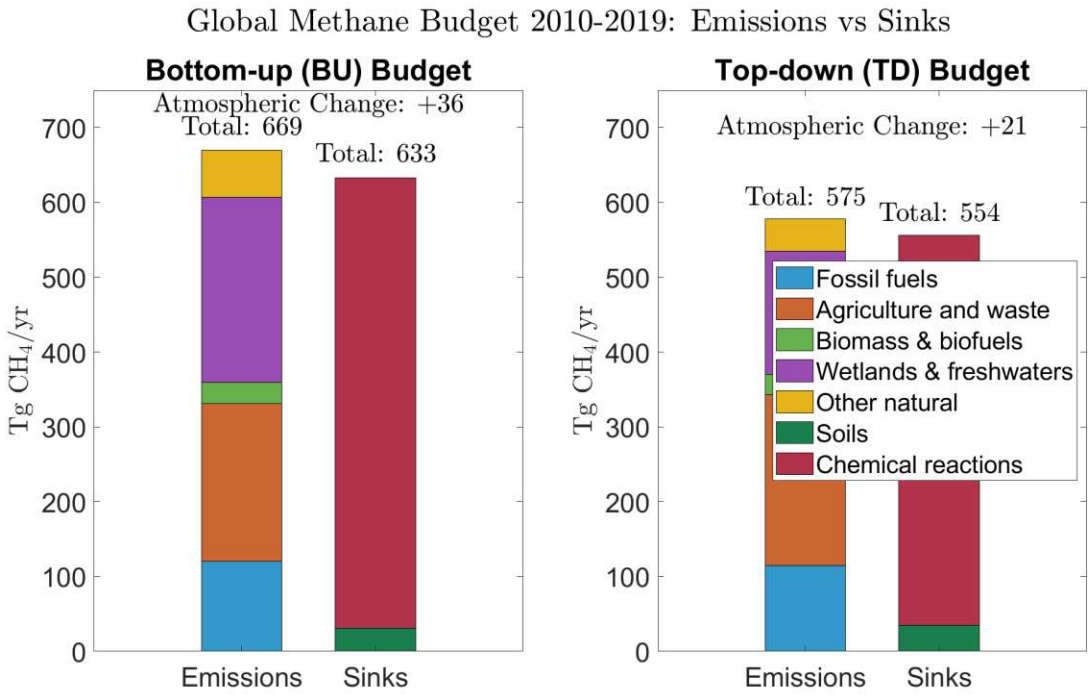

Figure 2. Adapted from Saunois et al. (2025): The Global Methane Budget 2010-2019. Stacked bars show contributions from individual sources (emissions) and removal processes (sinks) for both bottom-up (left) and top-down (right) approaches. Values represent decadal averages in Tg CH_4 yr^{-1}.

In the Saunois et al. (2025) study, top-down CH_4 emission estimates are based on in situ and Greenhouse Gases Observing Satellite (GOSAT) atmospheric observations and an ensemble of atmospheric inverse-model results while bottom-up estimates are based on process-based models for estimating land surface emissions and atmospheric chemistry, inventories of anthropogenic emissions, and data-driven extrapolations (Saunois et al., 2025). Corresponding global CH_4 sinks were estimated at 633 Tg CH_4 yr^{-1} (bottom-up) and 554 Tg CH_4 yr^{-1} (top-down). The resulting imbalance, representing the observed atmospheric CH_4 growth rate, was approximately 36 Tg CH_4 yr^{-1} for the bottom-up and 21 Tg CH_4 yr^{-1} for the top-down estimates. Based on the top-down assessment, anthropogenic activities accounted for roughly 65% of total CH_4 emissions, while natural sources contributed the remaining 35% (Saunois et al., 2025). Bottom-up estimates attribute 57% of emissions to direct anthropogenic and the 43% to natural plus indirect anthropogenic emissions (Saunois et al., 2025). This shows that human-related emissions are the biggest source of CH_4 in the atmosphere.

As a result, significant efforts are underway to reduce anthropogenic CH_4 emissions. Several international initiatives have been established to address this challenge, including the Oil and Gas Methane Partnership 2.0 (OGMP 2.0), led by the United Nations Environment Programme (UNEP, 2025), which focuses on emissions from the oil and gas sector. Additionally, programs supported by the Global Methane Hub and the Climate and Clean Air Coalition (CCAC) target methane mitigation across agriculture, waste, and energy systems (Global Methane Initiative, 2004). In the United States, the Environmental Protection Agency (EPA) estimates that CH_4 emissions originate primarily from natural gas and petroleum systems (28%), followed by enteric fermentation (25%), landfills (16%), manure management (9%), coal mining (6%), flooded land (6%), and other sources (11%) (US EPA, 2025a).

Extensive efforts have been undertaken within the oil and gas sector to reduce fossil fuel emissions. For instance, through voluntary reporting programs such as OGMP 2.0, member companies disclose their emissions using a comprehensive, measurement-based international reporting framework. This proactive approach enables companies to stay ahead of regulatory compliance requirements, respond to investor and market expectations, enhance corporate reputation, and prevent revenue losses by reducing emissions. Beyond meeting Environmental, Social, and Governance (ESG) objectives and alleviating external pressures, these actions significantly contribute to global methane mitigation efforts for climate benefit.

Companies also measure and mitigate their CH_4 emissions to comply with state, federal, and international regulations. At the state level, Colorado has implemented some of the most progressive methane regulations, including the phase-out of all CH_4-emitting pneumatics by May 2027 (CDPHE, 2025a) and through the Oil and Gas Annual Emission Inventory Reporting (ONGAEIR), which requires operators to submit annual emissions data (CDPHE, 2025b). At the federal level, methane emissions from U.S. oil and gas production are compiled by the Environmental Protection Agency (EPA) under Subpart W (EPA, 2023). Internationally, the European Union (EU) is developing regulations requiring oil and gas exporters to measure, report, and verify CH_4 emissions throughout the supply chain (EU, 2024).

Regulations in the oil and gas sector are generally more stringent than in other sectors, as leaks can often be more readily identified and mitigated compared to methane sources from livestock or waste. Collectively, all emission sources illustrated in Figure 2 contribute to the global methane budget and represent opportunities for targeted mitigation.

1.3 Research motivation

This PhD dissertation comprises two distinct studies. The first, titled *"Evaluating the Feasibility of Using Downwind Methods to Quantify Point Source Oil and Gas Emissions Using Continuously Monitoring Fence-Line Sensors,"* focuses on the quantification of CH_4 emissions at oil and gas facilities using continuous monitoring sensors. Specifically, this study aimed to address challenges associated with quantifying emissions using these technologies, as reported by Ilonze et al. (2024). Continuous monitoring solutions are increasingly employed in the oil and gas sector to detect and quantify CH_4 emissions. These systems are particularly valuable because they provide both temporal and spatial characterization of emissions, offering advantages over traditional survey methods such as aerial flyovers. Figure 3 illustrates a sample configuration of multiple continuous monitoring sensors deployed within an oil and gas facility.

Figure 3. Sample configuration of continuous monitoring sensor deployment in an oil and gas facility (AI-generated image). Source: Created with ChatGPT (2025) based on concept adapted from Herrick (2019).

However, these solutions are often associated with high uncertainties in emission quantification. In a controlled release study, Ilonze et al. (2024) reported that emissions were misestimated by continuous monitoring solutions by factors ranging from 0.2 to 42 for releases between 0.1 and 1 kg CH_4 h^{-1}, and from 0.08 to 18 for emissions greater than 1 kg CH_4 h^{-1}. A CH_4 continuous monitoring system typically consists of three main components: the sensor, the deployment configuration, and the data analytics used to estimate emissions in mass per unit time. This study focuses on uncertainties associated with the *analytics* phase; wherein atmospheric dispersion models are applied to infer emission rates (Figure 4). Specifically, this first study evaluates three atmospheric dispersion models suitable for oil and gas quantification using an Off-

Axis Integrated Cavity Output Spectroscopy (latest evolution in tunable diode laser absorption spectroscopy) instrument collocated with an ultrasonic anemometer. The models examined include the closed-path eddy covariance method, the backward Lagrangian stochastic model, and the Gaussian plume inverse model.

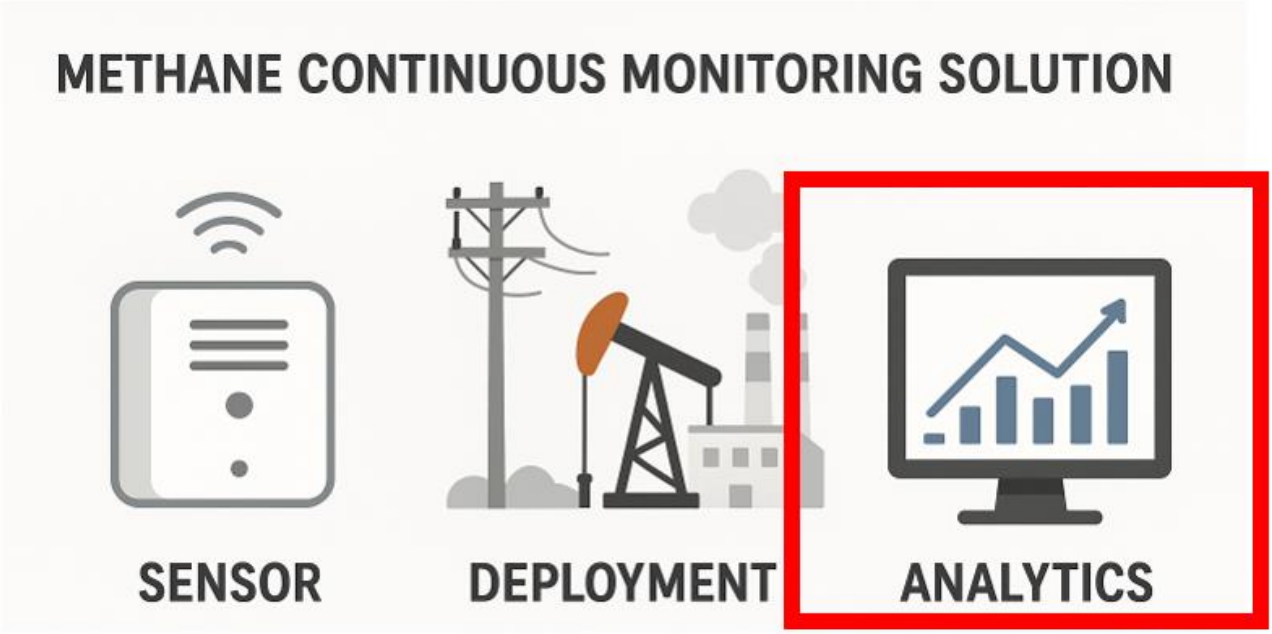

Figure 4. Illustration of a CH_4 continuous monitoring solution comprising three key components: the sensor, its deployment configuration, and the analytics used to convert atmospheric observations into emission rates (e.g., kg CH_4 h^{-1}).

The second study, titled *"A Comparison of Bottom-Up, Measurement-Based and EPA Inventory Methane Emission Estimates for Non–Oil and Gas Sources in the Denver–Julesburg Basin, Colorado"* develops an inventory of non–oil and gas CH_4 emissions in the Denver–Julesburg Basin (39.9–40.7°N, 105.3–104.2°W) using two complementary bottom-up approaches: using U.S. EPA emission factors and measurement-based estimates derived from vehicle-based facility-level measurements. The non–oil and gas sources considered in this study include concentrated animal feeding operations (CAFOs), landfills, wastewater treatment plants, and lakes

or reservoirs. As shown in Figure 2, these sources represent significant contributors to total CH_4 emissions and offer considerable potential for mitigation, despite receiving less regulatory and research attention than oil and gas sources.

Within the CH_4 research community, discrepancies between inventories and measurement-based emission estimates are frequently reported. For example, Song et al. (2023) reported that methane emissions from wastewater treatment facilities were underestimated by approximately 50% in EPA inventories. Similarly, Rutherford et al. (2021) highlighted efforts to bridge the gap between bottom-up and top-down inventories within the oil and gas sector. Vaughn et al. (2018) further suggested that temporal variability plays a major role in explaining discrepancies between top-down and bottom-up CH_4 estimates in natural gas production regions.

The OGMP 2.0 Level 5 reporting framework emphasizes reconciling source-level (bottom-up) and site-level (top-down) measurements conducted by companies. This study seeks to address the persistent challenge of discrepancies between measurement-based and bottom-up CH_4 emission estimates by reducing the temporal bias inherent in survey-based measurements, which are often compared against bottom-up inventories. To illustrate this issue, consider an aerial or satellite survey that measures emissions on a single day out of a year. The emissions observed during this brief window are then extrapolated to represent all potential sources across the region for the entire year. These annualized estimates are subsequently compared to EPA inventories or reporting programs that rely on annual averages. Such extrapolations are based on an essential ergodic assumption, that emissions from a single system observed over time are equivalent to emissions from many systems observed simultaneously (i.e., variation in time equals variation in space).

However, for the ergodic assumption to hold, the emission distribution during the observation window must remain constant throughout the year. This would require that all system failure modes, environmental influences, operational conditions, and regulatory changes affecting emissions are adequately represented within that single measurement period, a condition that is rarely met in practice. In summary, this study addresses this limitation by employing a measurement-based approach that seeks to minimize temporal variability through 12 months of survey observations. It further provides a weighted extrapolation method to scale snapshot measurements both annually and spatially (across all facilities), enabling more representative comparisons with bottom-up inventories. Although the present analysis focuses on non–oil and gas sources, the extrapolation framework developed here can also be applied to oil and gas emission sources.

1.4 Research objectives and hypotheses

1.4.1 Objective 1: Evaluating the feasibility of using downwind methods to quantify point source oil and gas emissions using continuously monitoring fence-line sensors

The first objective of this dissertation is to evaluate the overall quantification accuracy of the closed-path eddy covariance (EC), backward Lagrangian stochastic (bLs) model, and the Gaussian plume inverse method (GPIM) in quantifying single-release single-point (i.e., single emission at the site level) and multi-release single-point (i.e., multiple emissions at the site level, but the mast was downwind of a single source) emissions that simulate oil and gas emissions. Specifically, the objective seeks to assess the overall quantification accuracy expressed in terms of the linear regression slope of estimated versus actual emissions and the coefficient of determination (R^2) for the closed-path EC, bLs model, and GPIM methods.

Research hypotheses

H1a (Quantification accuracy):

Each of the closed-path EC, bLs, and GPIM methods will demonstrate strong linear relationships (R^2 close to 1) between estimated and actual emission rates, indicating high quantification accuracy for both single-release single-point and multi-release single-point experiments.

H0a (Null):

Each of the closed-path EC, bLs, and GPIM methods will not demonstrate strong linear relationships (low R^2 or slopes substantially different from 1) between estimated and actual emission rates, indicating low quantification accuracy.

H1b (Emission type consistency):

Each method is expected to maintain comparable quantification accuracy across single-release single-point and multi-release single-point emission scenarios, with regression slopes near unity and consistent R^2 values.

H01b (Null):

Each method's quantification accuracy will vary noticeably between single-release single-point and multi-release single-point emission scenarios.

1.4.2 Objective 2: A comparison of bottom-up, measurement-based and EPA inventory methane emission estimates for non–oil and gas sources in the Denver–Julesburg basin, Colorado

The second objective of this dissertation is to generate a bottom-up inventory of CH_4 emissions in the Denver-Julesburg (DJ) Basin study region using EPA and measurement-based emission factors. Specifically, this study:

a. Generates measurement-based emission factors (EFs) for concentrated animal feeding operations (CAFOs) (dairy cows, cattle, sheep), landfills, wastewater treatment plants, and lakes/reservoirs;
b. Using these EFs, develop a measurement-based inventory for CH_4 from non-oil and gas sources in the DJ Basin;
c. Compare the generated EFs and measurement-based emission inventory with the EPA inventory and other measurement-based studies; and
d. Investigates seasonal variability in EFs for CAFOs, municipal solid waste landfills, wastewater treatment plants, and lakes/reservoirs.

Research hypotheses

H2a (Emission factor estimation):

Measurement-based CH_4 EFs derived for CAFOs, landfills, wastewater treatment plants, and lakes/reservoirs in the DJ Basin will fall within the range of values reported in previous measurement-based studies and inventories, such as those from the EPA.

H02a (Null):

Measurement-based CH_4 emission factors (EFs) derived for CAFOs, landfills, wastewater treatment plants, and lakes/reservoirs will deviate substantially from previously reported or EPA inventory values.

H2b (Seasonal variability):

Measurement-based CH_4 emissions and emission factors from CAFOs, landfills, wastewater treatment plants, and lakes/reservoirs will exhibit consistent, measurable seasonal variability, with higher emissions expected during winter months due to reduced oxidation and enhanced methane accumulation under stable atmospheric conditions.

H02b (Null):

Measurement-based CH_4 emissions and emission factors from CAFOs, landfills, wastewater treatment plants, and lakes/reservoirs will not exhibit significant or consistent seasonal variability across the DJ Basin.

H2c (Inventory comparison):

The measurement-based CH_4 inventory for non–oil and gas sources in the DJ Basin will align reasonably well with the EPA inventory and other recent measurement-based studies, reflecting similar source contributions and emission magnitudes.

H02c (Null):

The measurement-based CH_4 inventory for non–oil and gas sources in the DJ Basin will differ significantly from the EPA inventory and other measurement-based studies in terms of source contributions or total emission magnitudes.

CHAPTER 2: EVALUATING THE FEASIBILITY OF USING DOWNWIND METHODS TO QUANTIFY POINT SOURCE OIL AND GAS EMISSIONS USING CONTINUOUSLY MONITORING FENCE-LINE SENSORS

Mbua, M., Riddick, S. N., Kiplimo, E., Shonkwiler, K. B., Hodshire, A., & Zimmerle, D. (2025). *Evaluating the feasibility of using downwind methods to quantify point source oil and gas emissions using continuously monitoring fence-line sensors*. Atmospheric Measurement Techniques, 18, 5687–5703. https://doi.org/10.5194/amt-18-5687-2025

2.1 Abstract

The dependable reporting of methane (CH_4) emissions from point sources, such as fugitive leaks from oil and gas infrastructure, is important for profit maximization (retaining more hydrocarbons), evaluating climate impacts, assessing CH_4 fees for regulatory programs, and validating CH_4 intensity in differentiated gas programs. Currently, there are disagreements between emissions reported by different quantification techniques for the same sources. It has been suggested that downwind CH_4 quantification methods using CH_4 measurements on the fence-line of production facilities could be used to generate emission estimates from oil and gas operations at the site level, but it is currently unclear how accurate the quantified emissions are. To investigate downwind methods' accuracy, this study uses fence-line simulated data collected during controlled release experiments as input for a non-standard closed-path eddy covariance (EC), the Gaussian plume inverse method (GPIM), and the backward Lagrangian stochastic (bLs) model in a range of atmospheric conditions. This study's EC attempt was unsuccessful due to data collection and instrumentation issues, resulting in invalid results characterized by underestimated emissions, large negative fluxes, and cospectra/ogives that deviated from their ideal shapes. Consequently, the EC results could not be compared with the GPIM or the bLS models. The bLs model demonstrated the highest accuracy for single-release single-point emissions, though it exhibited greater uncertainty than GPIM under multi-release conditions. Across GPIM and bLs models, the most reliable quantification was achieved with 15-minute averaging and a narrow 5° wind-sector range. Although EC was limited in this context, future studies should consider employing a standard EC system and further optimizing GPIM and bLs approaches—particularly for complex multi-source scenarios—to enhance quantification accuracy and reduce uncertainty.

2.2 Introduction

Reducing methane (CH_4) emissions from oil and gas systems is necessary for adhering to regulations and voluntary reporting frameworks such as the Oil & Gas Methane Partnership 2.0 (OGMP 2.0) (UNEP, 2024). The OGMP 2.0 provides a comprehensive measurement-based international reporting framework allowing companies to stay ahead of regulatory compliance requirements, meet investor and market pressure, have an enhanced corporate image, and prevent revenue loss by lowering their emissions. In the US, currently, the amount of CH_4 emitted from US oil and gas production are compiled by the US Environmental Protection Agency (EPA) under Subpart W. Typically, companies use a bottom-up inventory approach where emission factors (CH_4 emissions per equipment e.g., separator or emissions per event e.g., liquid unloading) are multiplied by activity factors (total number of pieces of equipment or events (US EPA, 2023a) to generate emissions. This quantification approach has several shortcomings, including: 1. It separately calculates CH_4 emissions from natural gas and petroleum systems, which practically are not independent systems, and can result in bias based on changes in gas to oil ratios throughout a basin (Riddick et al., 2024a); 2. Some emission factors used are outdated (Riddick et al., 2024c) and others do not account for the temporal and spatial variation in emissions (Riddick and Mauzerall, 2023); 3. Emission factors do not account for the long-tail distributions (Riddick et al., 2024b); 4. Difficulty in obtaining a truly representative sample from a large diverse population to generate emission factors (Allen, 2014); and 5. Possibly unreliable data reported by operators (Chan et al., 2024). Recently, mechanistic models, such as the Mechanistic Air Emissions Simulator (MAES), have been developed to address shortcomings in bottom-up CH_4 reporting (Mollel et al., 2025), but these still depend on direct measurements to inform emission factors.

Top-down methods, including using aircraft such as Bridger Photonics LiDAR (Light Detection and Ranging; 90% detection limit of ~ 2 kg h^{-1}) (Johnson et al., 2021) and satellites such as Carbon Mapper (predicted 90% detection limit of about 100 kg h^{-1}) (Carbon Mapper, 2025) can also be used to infer emissions. However, these survey methods only quantify emissions over a very short period of time (< 10 s) and observations are typically made during the day which can often coincide with maintenance activities that can bias emissions and result in overestimation (Riddick et al., 2024a; Zimmerle et al., 2024). Additionally, different top-down technologies measuring the same source have disagreed in their reported emissions which has called into question the credibility of these methods (Brown et al., 2023; Conrad et al., 2023). As a result, ensuring accuracy in models and technologies used in CH_4 emissions quantification has been a complex issue.

Currently, fence-line methods are used to detect, localize and quantify emissions. This approach uses point sensors fixed to the fence-line of the production site and emissions detected when the measured concentration exceeds a threshold, localized by triangulating multiple detections and quantified using a simple dispersion modelling framework, usually based on a Gaussian plume inverse approach (Bell et al., 2023; Day et al., 2024; Riddick et al., 2022a). Detection and localization of simulated fugitive emissions using this approach have been demonstrated successfully in controlled release studies. For example, Ilonze et al. (2024) reported a 90% probability of detection for emissions between 3.9 and 18.2 kg CH_4 h^{-1} using multiple point sensors and scanning/imaging systems. However, significant uncertainty in quantification remains; their study reported emissions being misestimated by a factor of 0.2 to 42 for releases between 0.1 and 1 kg CH_4 h^{-1}, and by a factor of 0.08 to 18 for emissions above 1 kg CH_4 h^{-1}. While informative, the methods in Ilonze et al. (2024) differ in key ways from those employed

here—specifically, their use of multiple sensors and a distributed monitoring configuration as opposed to the single-instrument, fence-line-based framework used in our study—limiting direct comparison of quantification accuracy. This study will evaluate the quantification accuracy of the closed-path eddy covariance (EC), Gaussian plume inverse model (GPIM), and the backward Lagrangian stochastic model (bLs) for oil and gas point source quantification using a single-instrument deployed at a fence line distance.

Eddy covariance is a vertical flux gradient measurement that measures CH_4 emissions based on the covariance between CH_4 concentrations measured using a fast-response analyzer (> 10 Hz) and vertical wind vector measured by a fast-response sonic anemometer (>10 Hz) (Figure 5; Morin, 2019). It is typically implemented over long homogeneous fetches where eddy mixing scale is a small fraction of the distance from the site providing more predictable vertical transport. Dumortier et al. (2019) used EC to estimate known point source emissions at a cow's muzzle height and reported the model could estimate emissions between 90 and 113% of the true emission. Dumortier et al. (2019) stated the optimal controls for point source quantification and footprint modelling are using running mean, 15-minute averaging periods, not applying the Foken and Wichura (1996) stationarity filter, and using the Kormann and Meixner (2001) footprint function. The study tested the model using an artificial CH_4 source at 0.8 m, programmed to emit when winds were coming from the source direction (± 45º), and when friction velocity (u_*) was above 0.13 m s^{-1}. In the point source testing of Dumortier et al. (2019), they noted that amplitude resolution, skewness and kurtosis tests were disabled as they deleted almost all periods involving the artificial source in the footprint. Rey-Sanchez et al. (2022) studied the accuracy of the Hsieh model (Hsieh et al., 2000), the Kljun model (Kljun et al., 2015) and the K & M model (Kormann and Meixner, 2001) in calculating the footprint of point source hot spots using footprint-weighted

flux maps. The study reported the K & M model to be the most accurate. Polonik et al. (2019) compared five gas analyzers, two open-paths, two enclosed-path and one closed-path analyzer for carbon dioxide EC measurements. The study noted that while open-path sensors minimize spectral attenuation and require smaller spectral correction factors compared to sensors with an inlet tube such as a closed-path sensor, open-path sensors risk data loss in non-ideal conditions like precipitation, fog, dust or dew. The main challenge of applying EC for continuous monitoring of oil and gas sites is instrument limitations (requires deployment of multiple sensors throughout a facility; sensor cost is a factor), statistical tests, and quality controls, all of which could filter out some of the data.

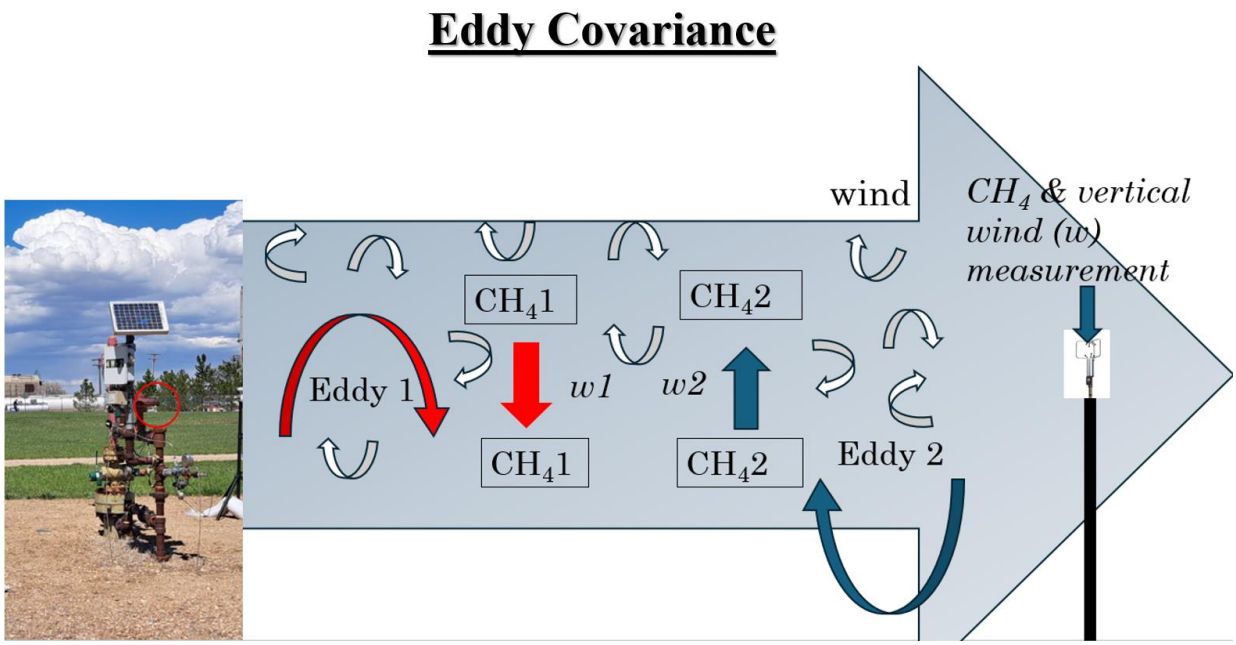

Figure 5: Illustrations of eddy covariance where CH_4 is methane concentrations, and *w* is vertical wind speed.

The GPIM method calculates CH_4 emission rate as a function of mole fraction at a point in space (x, y, z), downwind distance, perpendicular distance (crosswind), mean wind speed and

atmospheric stability (Figure 6 (a); Riddick et al., 2022b). This method has been used to quantify emissions from oil and gas production sites especially for survey solutions (Riddick et al., 2022b). For a single point-source, Riddick et al. (2022b) reported absolute uncertainties of between 40.7 and 60% in a controlled release experiment involving 10 replicate measurements of compressed natural gas (1.5 m release height), with concentrations measured using a mobile vehicle survey. While this differs from continuous fence-line deployment, it offers insight into the inherent uncertainty of the GPIM method in field conditions. Using controlled single point source tests, Foster-Wittig et al. (2015) reported average errors of between -5 to 6%. The limitations of the GPIM method are that it assumes a homogeneous emission source, steady-state flow, and uniform dispersion of gas in an open area free of obstructions (Hutchinson et al., 2017).

The bLs model adapted in WindTrax can simulate the transport of gases from point sources that emit them (Figure 6 (b); Crenna, 2006). The model releases individual particles and follows them along their unique path in air by mimicking random, turbulent motion of the atmosphere. Tagliaferri et al. (2023) investigated the validity of WindTrax in quantifying emissions from complex sources and reported the model to be reliable under neutral conditions, underestimated emission rates during unstable stratification and overestimated emissions during stable conditions. Similarly to the GPIM method, the model assumes free flow of air in the absence of obstructions and uses time-averaged data as input.

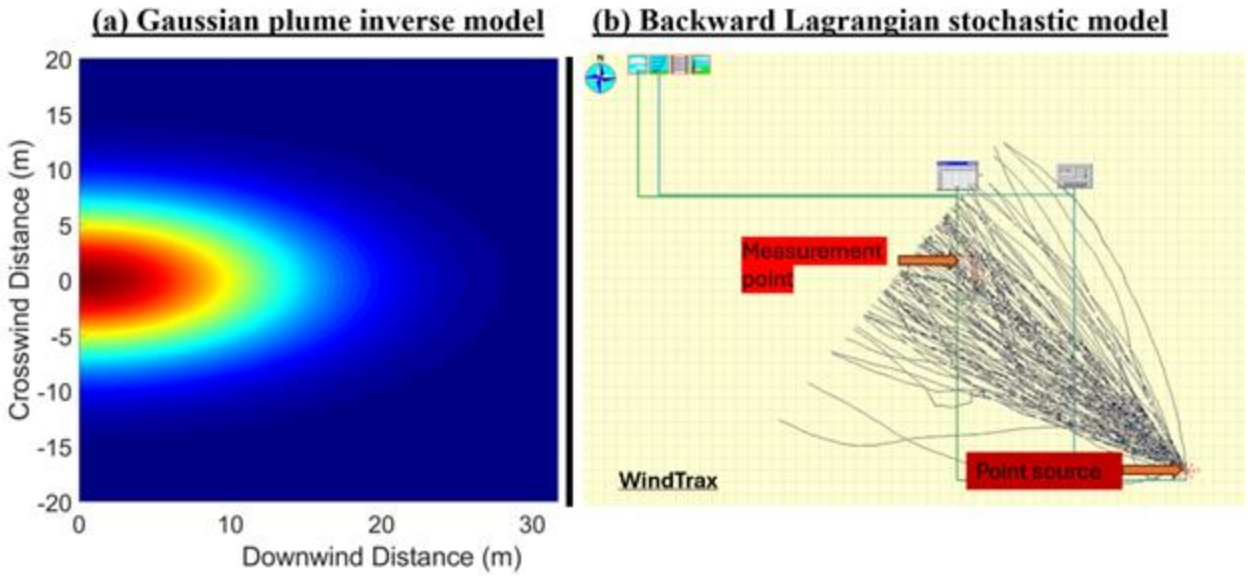

Figure 6. (a) 1 **(a)** A plume that follows a Gaussian plume inverse model, where the emission rate can be inferred from concentrations at different downwind distances and crosswind distances. **(b)** An illustration of how the backward Lagrangian stochastic model traces particles to the source.

Continuous monitoring of CH_4 emissions using fence line sensors requires proper quantification of intermittent and persistent releases from oil and gas during all release (complex emission profiles) and atmospheric conditions (unstable, neutral and stable). Oil and gas emissions are characterized by intermittent, non-uniform, single or multiple point source emissions, varying in leak size, location, height and distance between the source and sensor, and are typically in complex aerodynamic environments (i.e. not flat). An ideal quantification model should always quantify emissions and should capture short and long-lasting emission events. Most models have been validated to work best during neutral conditions for single point sources. However, it is important to test and apply these models during non-neutral conditions as well as these are part of real-world conditions where continuous monitoring is applied. In this study, we evaluate if using a readily available CH_4 cavity ring down analyzer for models' quantification such as the closed-path EC is a feasible solution to quantify point source emissions.

This study aims to inform the feasibility of downwind quantification models in oil and gas settings by investigating which models are likely to work most of the time with instrumentation that is typically available for fence-line deployment. Fence-line sensor deployments involve multiple sensors, continuously running in all conditions and providing emissions data. Using robust releases and environmental conditions, this study aims to investigate the performance of these methods in quantifying emissions for known gas release rates and evaluating uncertainties that could result in incorrect CH_4 reporting. Specifically, the study will evaluate the overall quantification accuracy (linear regression slope of estimated versus actual emissions, and R^2) of closed-path EC, bLs model, and the GPIM method in quantifying single-release single-point and multi-release single-point emissions that simulate oil and gas emissions.

2.3 Methods

2.3.1 Experimental setup

Controlled release experiments were conducted at the Colorado State University's Methane Emissions Technology Evaluation Center (METEC) in Fort Collins, CO (USA, ~ 105 km north of Denver) between February 8, and March 20, 2024. The METEC center is a simulated oil and gas facility that does controlled testing for emissions leak detection and quantification technology development, field demonstration, leak detection protocol and best practices development (Colorado State University, 2025a). The weather conditions during the test period were mostly sunny but precipitation was also observed (32 sunny, 7 snowy, 12 rainy, 7 cloudy and 1 foggy day; Section A1 in the Appendix). Wind speeds were between 0 and 25 m s^{-1} and temperatures ranged between -15 and +19 °C (Section A1 in the Appendix). A stationary mast holding the instrumentation was setup on the North-West corner of METEC to take advantage of the predominant wind direction, avoid the largest aerodynamic obstructions and to simulate the likely

placement of a fence-line instrument (Day et al., 2024; Riddick et al., 2022a). Fence-line sensors are typically placed within the oil and gas perimeter (~30 m). This study collected data for what we considered as close and far away releases; distances between 9 and 94 m.

Methane concentration data for closed-path EC, GPIM and bLs methods were collected through an inlet tubing (3.275 mm inner diameter) at 3 m height, connected to the ABB (Zurich, Switzerland) GLA131 Series Microportable Greenhouse Gas Analyzer (MGGA) set to sample at 10 Hz. The MGGA is a closed-path greenhouse gas analyzer with a ~3.2 L min^{-1} pump flowrate, 10 cm cell length, 2.54 cm cell diameter (~0.23 standard cubic centimeters per minute (sccm) effective volume), and 0.4 s gas flow response time. The inlet tubing was collocated with an R. M. Young (Traverse City, MI, USA) 81000 sonic anemometer which measured micrometeorology at 10 Hz (Figure 7B). The northward, eastward and vertical separation of the inlet tubing from the sonic anemometer was 0, 0, -10 cm, respectively.

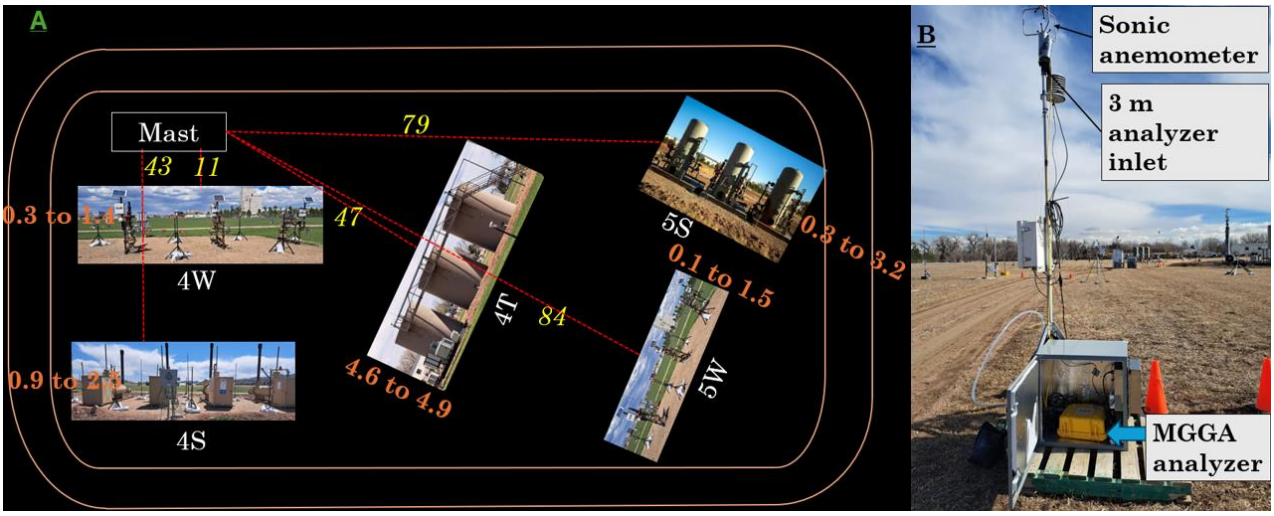

Figure 7: **A**: Map illustration of major pieces of equipment and the measurements points at Colorado State University's Methane Emissions Technology Evaluation Center (METEC) in Fort Collins, CO, USA. Equipment 4S denotes horizontal separators, 4W are well heads, 4T are tanks, 5S are vertical separators and 5W are well heads. **B** is the measurement point for the Microportable Greenhouse Gas Analyzer for closed-path eddy covariance, Gaussian plume inverse model and backward Lagrangian stochastic model quantification. The inlet tubing and the sonic anemometer are at 3 m height. The red dotted lines with yellow numbers show the average distances (meters) between emission equipment and measurement point. The orange numbers show the range of

emission heights (meters) for each equipment. The analyzers were hosted in a temperature-controlled box.

2.3.2 Controlled methane releases

Controlled releases were part of the METEC Spring 2024 Advancing Development of Emissions Detection (ADED) Campaign conducted between February 6 and April 29, 2024 (Colorado State University, 2025b). Natural gas of known CH_4 content was released from above-ground emission points attached to equipment typically present in an oil and gas facility (tanks, separators and well pads). The gas release rates ranged between 0.01 kg h^{-1} and 8.7 kg h^{-1}, and the release durations ranged from 10 seconds to 8 hours, simulating both fugitive and large emission events. The releases were run both during the day and night. The distance from the release points to the measurement points ranged between 9 and 94 m, and emission heights were between 0.1 and 4.9 m (Figure 7A). Emission points simulate the realistic size and locations of typical emissions from components such as the thief hatches, pressure relief valves, flanges, bradenheads, pressure transducers, Kimray valves and vents. The releases included both single-point emissions (single releases) and multi-point emission events (multiple simultaneous releases).

2.3.3 Calculation of roughness length

Surface roughness length (z_0) was calculated from friction velocity (Section A2.1 in the Appendix: Equations A1 and A2) by splitting the high frequency sonic anemometer data into 15-minute tables and filtering for those in neutral conditions, $|L| > 500$ (Section A2.1 in the Appendix: Equation A3). The overall roughness length selected as the median of all the calculated z_0 was 0.1 m (Rey-Sanchez et al., 2022).

2.3.4 Model quantification

2.3.4.1 Eddy covariance

Data pre-processing

Evaluating the MGGA CH_4 data showed that actual sampling was between 4 and 12 Hz (majority of the data collected at approximately 6 Hz), even though the analyzer had been configured to sample at 10 Hz (Section A2.2 in the Appendix). To account for this sampling variability, data were filtered to when sampling was equal to or greater than 8 Hz. Data sampled at frequencies above 8 Hz were down sampled to 8 Hz. The 8 Hz frequency threshold was selected to ensure uniform sampling, enough data for model evaluation as most sampling was at lower frequencies, and to preserve as much temporal resolution as possible given the system limitations. The sonic anemometer meteorological data (horizontal wind vectors (u, v), vertical wind vector (w), temperature (T), and pressure (P)) actual sampling varied between 7 and 9 Hz with the most frequent frequency at 8 Hz (Section A2.2 in the Appendix). As the MGGA gas analyzer and sonic anemometer were not designed to clock synchronously, using the MGGA CH_4 clock time as a reference, meteorological data from the sonic anemometer were matched to the MGGA CH_4 data using linear interpolation to generate concentration-meteorological 8 Hz data. While in an ideal circumstance of a fast pump and short tube length a correct timeseries matching can be achieved through establishing a clear point of maximum covariance when determining the time lag, this is difficult for our system due to a 3 L min^{-1} pump flowrate and a 3 m tubing that caused both attenuation and time lag.

The aggregated concentration-meteorological data were then merged with METEC's release data and metadata, and release event tables created. Release event tables were aggregated tables of concentration, meteorology and release (emission source location, duration and rate)

information for all defined release events at METEC. The concentration-meteorological-release event data were then separated into single-release and multi-release events. Single-release events were when there was a single emission point at the site level, while multi-release events were when there was more than one emission point at the site level. The concentration-meteorological-release event tables were split into 5, 15 and 30-minute release event tables (i.e. there was a continuous release in the duration). Based on the bearing of the emission point to the measurement point and the average wind direction in the duration, the data was further filtered to downwind data, ±10º, ±20º, and ±45º.

Flux calculation

Turbulent fluxes were calculated using the open software EddyPro® version 7 (LI-COR Biosciences, 2021). Acquisition frequency was set at 8 Hz, while file duration and the flux interval were set at 5, 15, and 30 minutes, respectively, depending on the files being processed. Table 1 shows the instruments input to the software.

Table 1. Anemometer and gas analyzer input into EddyPro

Anemometer Information		**Gas Analyzer Information**	
Manufacturer	Young	Manufacturer	Other
Model	81000	Model	Generic closed path
Height	3 m	Tube length	300 cm
Wind data format	u, v, w	Tube inner diameter	3.275 mm
North alignment		Nominal tube flow rate	3.2 L min^{-1}
North offset	0.0	Northward separation	0.00 cm
Northward separation	Reference	Eastward separation	0.00 cm
Eastward separation	Reference	Vertical separation	-10.00 cm
Vertical separation	Reference	Longitudinal path length	10.00 cm
Longitudinal path length		Transversal path length	2.54 cm
Transversal path length		Time response	0.4 s

In raw data processing, axis rotations for tilt correction under wind speed measurement offsets were selected. Under turbulent fluctuations, double rotation and block average detrend methods were used. Covariance maximization with default was used for time lag detection; time lags detection was enabled. Compensation for density fluctuations (Webb-Pearman-Leuning terms) (Webb et al., 1980) was disabled as the MGGA analyzer synchronously reported dry CH_4 and water mole fractions, cell temperature and pressure. Mauder and Foken (2004) (0-1-2 system) were used for quality check. All statistical tests for raw data screening, (Vickers and Mahrt, 1997)– spike count/removal, amplitude resolution, drop-outs, absolute limits, skewness and kurtosis, discontinuities, time lags, angle of attack and steadiness of horizontal wind were selected. The

default values for all these tests were used. Similarly, default settings for spectral analysis and corrections were used. Analytic correction of high-pass filtering effects (Moncrieff et al., 2005) for low frequency range; and correction of low-pass filtering effects (Fratini et al., 2012, in situ analytic and instruments separation; Horst and Lenschow, 2009, only crosswind and vertical) in the high-frequency range were used.

Post-processing

Flux data were flagged "2", low quality, based on Mauder and Foken (2004) (0-1-2) quality system. Cospectral analysis revealed that the EC system in this study smoothed out low-frequency eddies, as the cospectra lacked the ideal shape characterized by a low-frequency rise, a peak region, and a high-frequency decay (Section A2.3.1 in the Appendix). While the slope in the high-frequency region varies around the theoretical −4/3 slope, the cospectral data followed the 1:1 line, indicating consistent spectral shape across sampling periods. We also examined the relationship between CH_4 flux and friction velocity (u_*) to identify a u_* threshold below which flux estimates may be unreliable (Section A2.3.2 in the Appendix). However, no consistent relationship was observed across atmospheric stability classes (unstable, stable, and neutral). CH_4 fluxes varied widely—including both positive and negative values—across the full range of u_* (~0 to 1 m s^{-1}), with no discernible threshold beyond which fluxes stabilized. This indicated that CH_4 fluxes were effectively independent of u_*, and thus, data from all u_* values were retained. Ogive analysis was conducted to assess whether averaging durations of 5, 15, and 30 minutes were sufficient for capturing the full turbulent flux. The resulting ogive curves deviated from the ideal asymptotic shape, particularly at the highest and lowest frequencies (Section A2.3.3 in the Appendix). Notably, the curves did not exhibit a clear plateau near the low-frequency end, where cumulative flux should approach unity. This indicates incomplete flux capture. Furthermore, the similarity in ogive shapes

across different frequencies—mirroring patterns seen in the cospectra—suggests a lack of significant turbulent contributions and the influence of non-turbulent, possibly advective, processes. These results imply that the EC system may not have fully resolved the flux due to either insufficient averaging time, non-stationarity, or instrument-related limitations (Section A2.3.4 in the Appendix). As positive fluxes are generally considered emissions, and negative fluxes depositions, data were further filtered for positive fluxes which were then quantified to emission rates.

Footprint calculation

Eddy covariance footprints were calculated using the Kljun et al. (2015) and the Kormann and Meixner (2001) footprint models. For the Kljun et al. (2015), the freely online MATLAB code of the model was used, while the Kormann and Meixner (2001) was coded in MATLAB. To determine the point source footprint contribution, the study first calculated the area that contributed 90% of the vertical flux; and based on the location (x and y coordinates based on wind direction and distance from source) of the point source, the source was determined if it was within the 90% footprint area. Point source emissions of sources within this region were then calculated based on the approach by Dumortier et al. (2019). This approach assumes all measured flux is equal to flux resulting from a single point source. In case of the mast being downwind of more than one source, more sonic anemometers are needed to solve the two unknown point source fluxes.

2.3.4.2 Gaussian plume inverse method

Data pre-processing

Methane concentration data from the MGGA analyzer and meteorology data from the sonic anemometer were averaged to 1 Hz and aggregated. The aggregated concentration-meteorological data were merged with METEC's release data and metadata, and release event tables created. The

concentration-meteorological-release event data were then separated into single-release and multi-release events. For single-release events, the concentration-meteorological-release event tables were split into 5, 15 and 30-minute release event tables. Based on the bearing of the emission point to the measurement point and the average wind direction in the duration, the data was further filtered to downwind data, ±5º, ±10º and ±20º wind sector ranges. Multi-release events were further classified into multi-release single-point emissions (i.e., there were multiple emissions at the site level, but the mast was downwind of a single source) and multi-release multi-point emissions (i.e. there were multiple emissions at the site level and the mast was downwind of more than one source). This study focuses on single-release single-point and multi-release single-point emissions. For continuous monitoring sensors, background concentration can be determined from CH_4 concentrations measured by a sensor upwind of the emission source, or by sampling when the wind is blowing away from the source. However, for continuous monitoring sensors, using an upwind sensor has the limitation of missing downwind background noise resulting from emissions in the preceding emission event where there is residual CH_4 in air especially during stable conditions, and capturing sensors drift in the downwind sensor. In this study, background CH_4 was calculated as the average of the lowest 5th percentile, 5 minutes before each release started. In cases where this background was greater than the mean CH_4 concentration in the quantifying duration, the minimum CH_4 concentration for that duration was used as the background. Methane enhancement was then calculated as CH_4 concentration minus the background.

Quantification

The GPIM was evaluated under six scenarios (two equations and three different dispersion coefficients generations) using single-release single-point emissions to test when the model works best (Section A2.1 in the Appendix: Equation A7 and A8). Dispersion coefficients were generated

based on (1) high frequency sonic anemometer data at ~ 10 Hz, (2) EPA point-source dispersion coefficients (US EPA, 2013), and (3) 1 Hz sonic anemometer data. The scenario with the slope closest to 1, and highest R^2 across averaging durations, and wind sector ranges was selected and used for multi-release single-point emissions quantification. For single-release tables, the measurement point was downwind of a single source (single-release single-point emission), hence the tables were quantified as they were. However, for multi-release events, the tables were further processed as the GPIM method is designed to quantify a single point source at a time. For multi-release events, the number of emission points in the downwind tables were used to further classify the tables into multi-release single-point emissions (i.e. there were multiple emissions at the site level, but the mast was downwind of a single source), and multi-release multi-point emissions (i.e. there were multiple emissions at the site level and the mast was downwind of more than one emission source). The GPIM method was only used for multi-release single-point emissions.

2.3.4.3 Backward Lagrangian stochastic model

Pre-processed data from the GPIM method was used for bLs quantification. Quantification was done using WindTrax 2.0 (Crenna, 2006; WindTrax 2.0, 2020). For every 5-, 15- and 30-minute duration in the ±5º, ±10º, and ±20º, respectively, inputs included roughness length (z0), Monin-Obukhov length (*L*- Section A2.1 in the Appendix: Equation A3), mean (wind speed, wind direction, concentration, pressure, temperature), background concentration, source height, and distance from the emission point to sensor. WindTrax is also designed to quantify a single point source at a time, and hence, was only used to quantify single-point single emissions and multi-point single emissions.

2.4 Results

2.4.1 Eddy covariance

2.4.1.1 Single-release single-point emissions

For single-release single-point (SRSP) emissions, the closed-path EC underestimated emissions. Using the Kljun et al. (2015) footprint model, the slope of the estimated emissions versus actual emissions linear regression was between -0.03 and 0.54 at 5 minutes, -0.36 and -0.04 at 15 minutes, and 0.03 at 30 minutes, 45 degrees (10 and 20 degrees had insufficient data points) (Figure 8). The adjusted R^2 was between -0.06 and 0.12, indicating no linear relationship between the estimated and actual emission (Figure 8). Using the Kormann and Meixner (2001) footprint model, the slope was between -0.42 and 0.17 at 5 and 15 minutes, respectively, and -0.08 at 30 minutes, 45 degrees. (Section A3.1.1 in the Appendix). Similarly, the adjusted R^2 values were between -0.07 and 0.05. These results indicate that this study's EC system using either the Kljun et al. (2015) or the Kormann and Meixner (2001) footprint models did not reliably quantify emissions for SRSP cases. The low slopes and adjusted R^2 values suggest little to no linear relationship between estimated and actual emissions under the tested conditions (Figure 8; Section A3.1.1 in the Appendix).

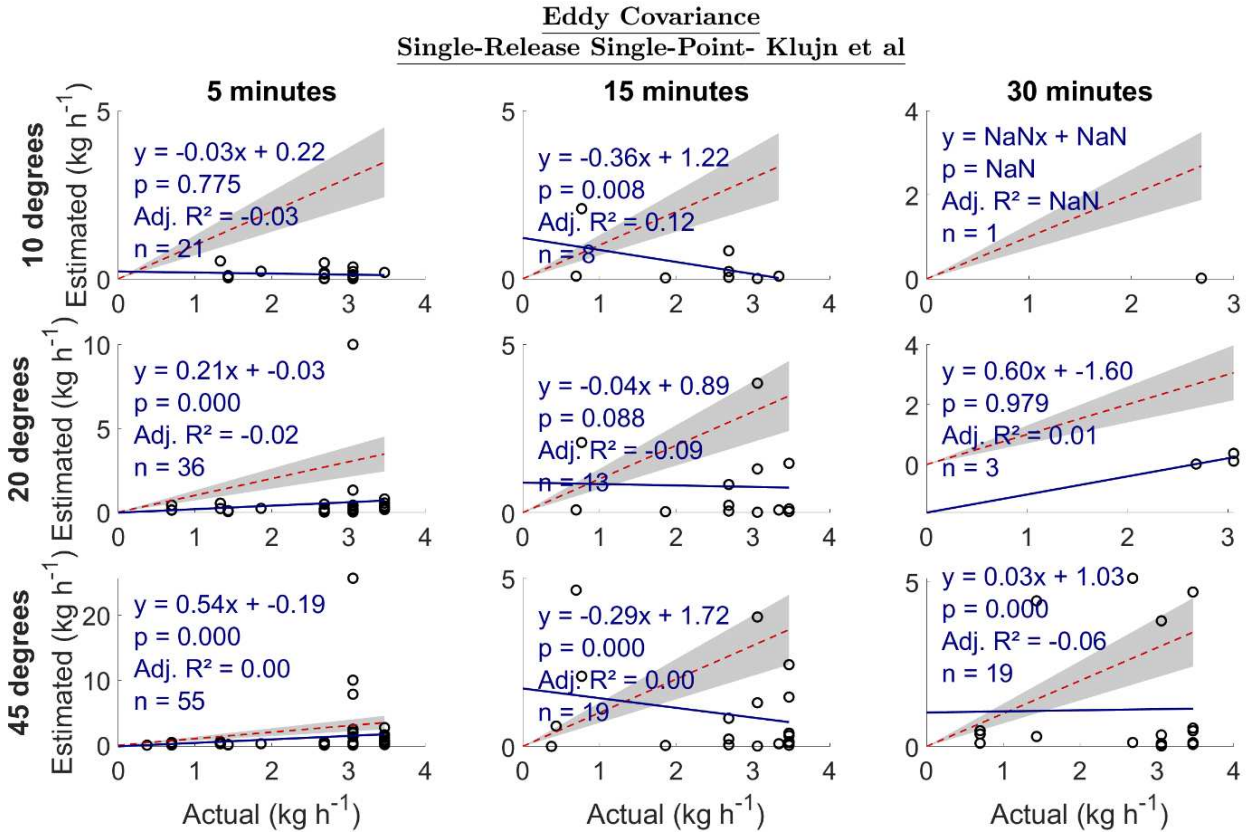

Figure 8. Estimated emission vs actual emission (kg h^{-1}) for single-release single-point emissions. The red dotted line is a 1:1 line based on actual emissions i.e. points below the line are underestimated and above are overestimated emissions. The gray region represents ±30% of the actual emission. Adj. R^2 is the adjusted R^2. The sample size is n.

2.4.1.2 Multi-release single-point emissions

For multi-release single-point (MRSP) emissions, the closed-path EC largely underestimated emissions and did not show good agreement between estimated and actual emissions (Figure 9). Using the Kljun et al. (2015) footprint model, the slope was between -0.51 and 0.18, except for the 5 minutes 45 degrees category that had a slope of 0.61. The adjusted R^2 did not show a linear relationship between estimated and actual emissions with values ranging between -0.02 and 0.00 (Figure 9). Using Kormann and Meixner (2001) footprint model, the slope

was between -0.03 and 1.06, the good agreement of 1.06 was at 30 minutes 45 degrees with an adjusted R^2 of 0.12 (Section A3.1.2 in the Appendix). The rest of the categories had an R^2 of between -0.02 and 0.06. These results suggest that the EC system did not reliably quantify emissions for MRSP cases under most conditions. Only one category (30 minutes, 45 degrees using the Kormann and Meixner (2001) footprint model showed moderate agreement (slope = 1.06, adjusted R^2 = 0.12), but even this explains only a small portion of the variability in actual emissions. Overall, the adjusted R^2 values across scenarios (−0.02 to 0.12) indicate a weak or no linear relationship.

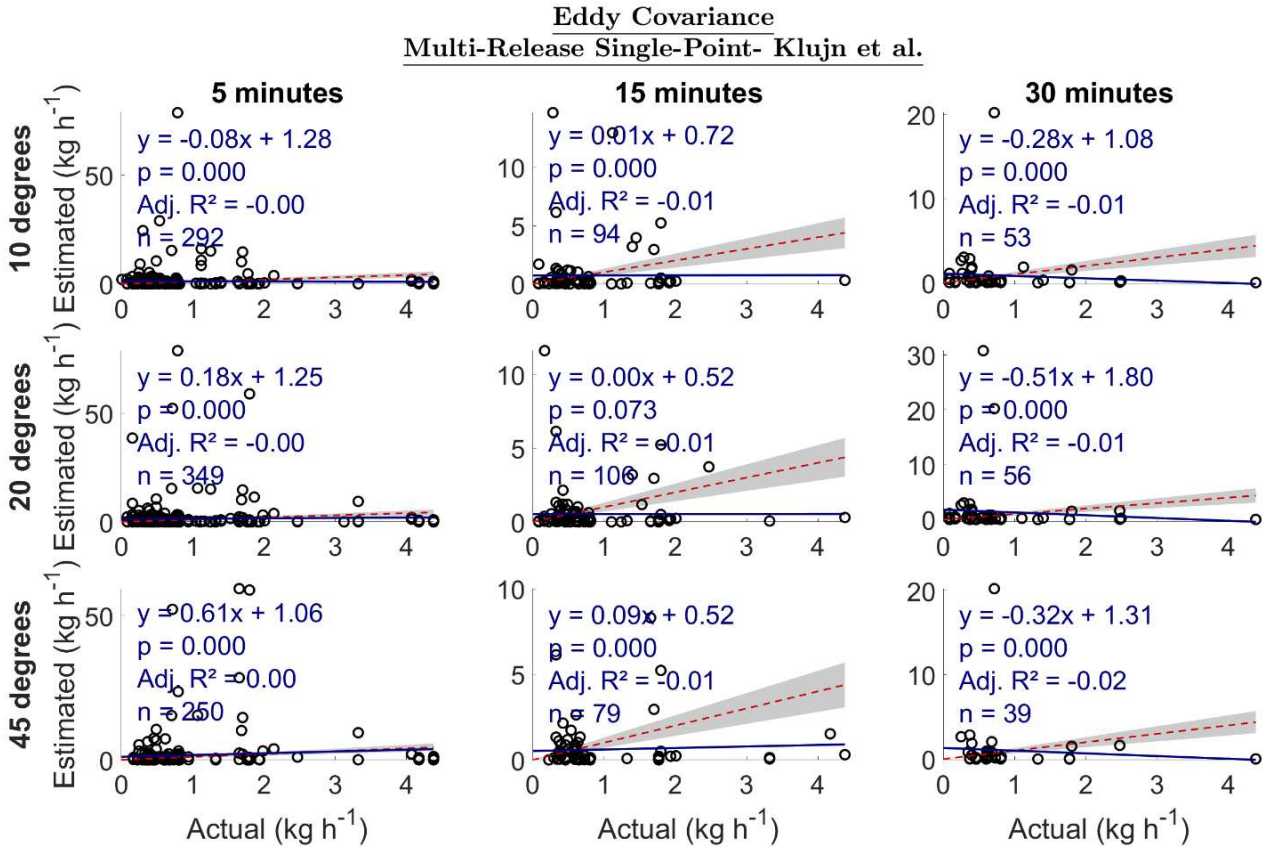

Figure 9. Estimated emission vs actual emission (kg h^{-1}) for multi-release single-point emissions. The red dotted line is a 1:1 line based on actual emissions i.e. points below the line are underestimated and above are overestimated emissions. The gray region represents ±30% of the actual emission. Adj. R^2 is the adjusted R^2. The sample size is n.

2.4.2 Gaussian plume inverse method

2.4.2.1 Single-release single-point emissions

The GPIM sensitivity analysis comparing different equations and dispersion coefficients showed no difference in quantified emissions between Equation A7 and Equation A8. Among the dispersion coefficient sets tested, the US EPA (2013) coefficients resulted in the most consistent performance, with the least variability in slope and the highest overall adjusted R^2 values (Section A3.2 in the Appendix). For this scenario, the slope ranged from 1.65 to 3.92 (excluding the 30-minute, 5-degree case due to insufficient data), and adjusted R^2 values ranged from 0.40 to 0.64 (Figure 10). The 15-minute, 5-degree case had the slope closest to 1 (slope = 1.65, R^2 = 0.40), while the 5-minute, 5-degree case showed the strongest linear relationship overall (slope = 2.42, R^2 = 0.64) (Figure 10). These results suggest that while the GPIM model tends to overestimate emissions (slopes > 1), it provides relatively consistent and stronger linear agreement with actual emissions compared to the closed-path EC system tested above (Section 2.4.1).

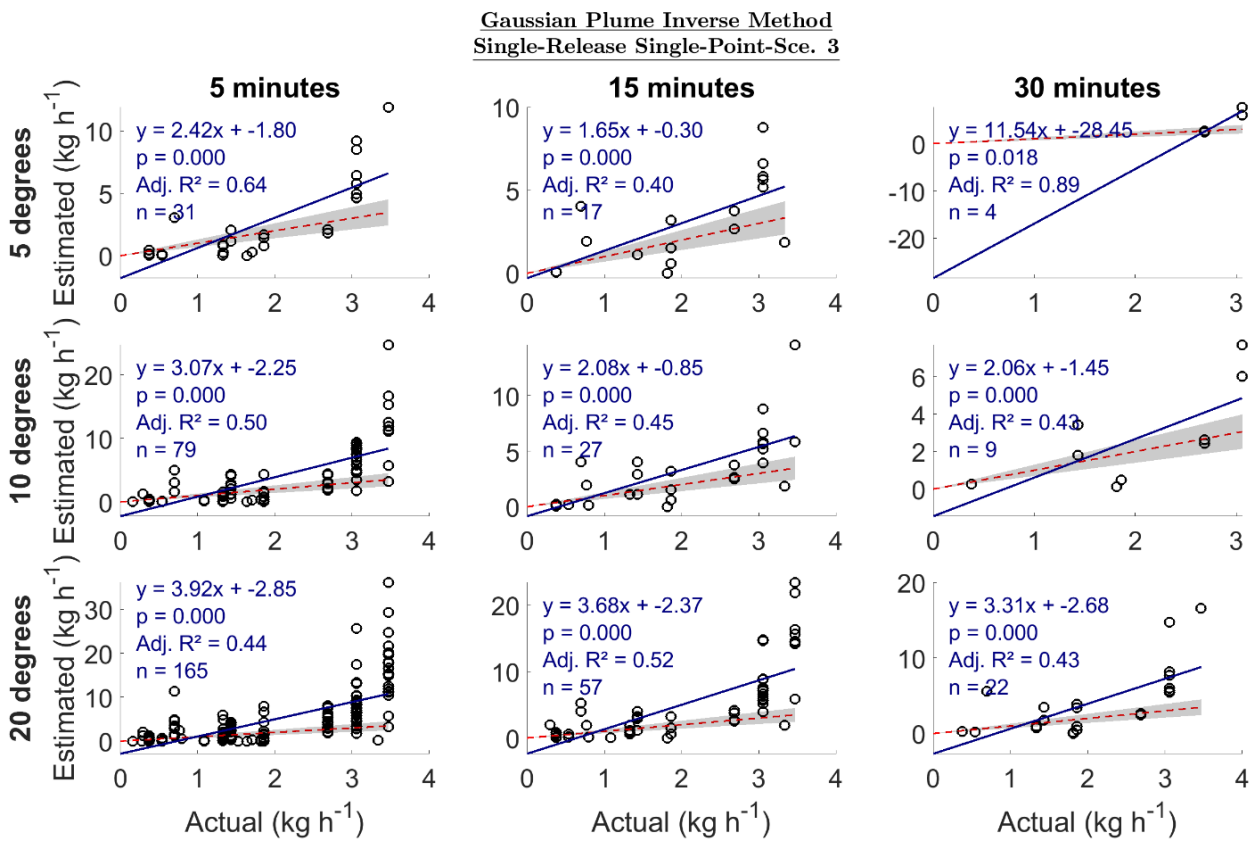

Figure 10. Estimated emission vs actual emission (kg h^{-1}) for single-release single-point emissions. Sce.3 refers to scenario 3 of the sensitivity analysis in Section A3.2 in the Appendix. The red dotted line is a 1:1 line based on actual emissions i.e. points below the line are underestimated and above are overestimated emissions. The gray region represents ±30% of the actual emission. Adj. R^2 is the adjusted R^2. The sample size is n.

2.4.2.2 Multi-release single-point emissions

For MRSP emissions, the GPIM model produced a wide range of slopes, from –43.05 to 1.60 (Figure 11). Excluding the 5-minute 5- and 10 degrees categories, and the 30-minute 10 degrees category, most other cases reported slopes between 0.76 and 1.22, suggesting potential quantification within ~25% of actual emissions. However, the adjusted R^2 values in these cases were close to zero, indicating no consistent linear relationship between estimated and actual emissions (Figure 11). This lack of correlation is likely due to the high variability in GPIM estimates, which reached up to 200 kg h^{-1} for the selected categories, despite actual emissions

being only around ~6 kg h^{-1}. These results indicate that while the GPIM model sometimes produced slope values suggesting close agreement with actual emissions, the lack of linear correlation and large overestimations highlight its limited reliability in quantifying MRSP emissions accurately.

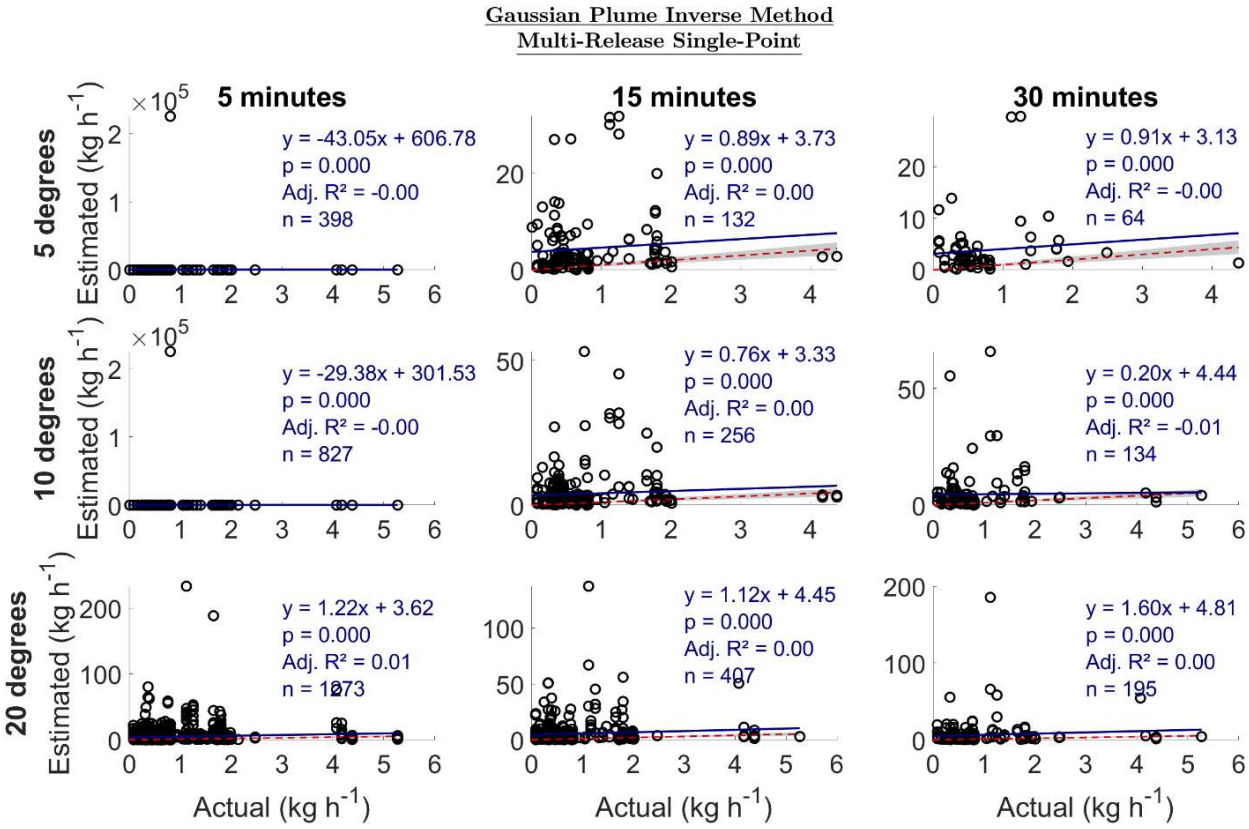

Figure 11. Estimated emission vs actual emission (kg h^{-1}) for multi-release single-point emissions. The red dotted line is a 1:1 line based on actual emissions i.e. points below the line are underestimated and above are overestimated emissions. The gray region represents ±30% of the actual emission. Adj. R^2 is the adjusted R^2. The sample size is n.

2.4.3 Backward Lagrangian stochastic model

2.4.3.1 Single-release single-point emissions

For SRSP emissions, the bLS method generally produced the most accurate slopes (i.e., closest to 1) compared to the EC and GPIM methods (Figure 12). The 15-minute 5- and 10-degrees categories yielded the most accurate estimates, with slopes of 1.05 and 1.10, respectively. The adjusted R^2 ranged from 0.48 to 0.66 for the 5-minute averaging duration, and from 0.40 to 0.48

for the 15-minute duration. At the 30-minute averaging duration, performance improved in the 10- and 20-degrees categories, likely due to increased sample sizes (Figure 12). These results show that bLs is more suitable for quantifying single-release single point emissions.

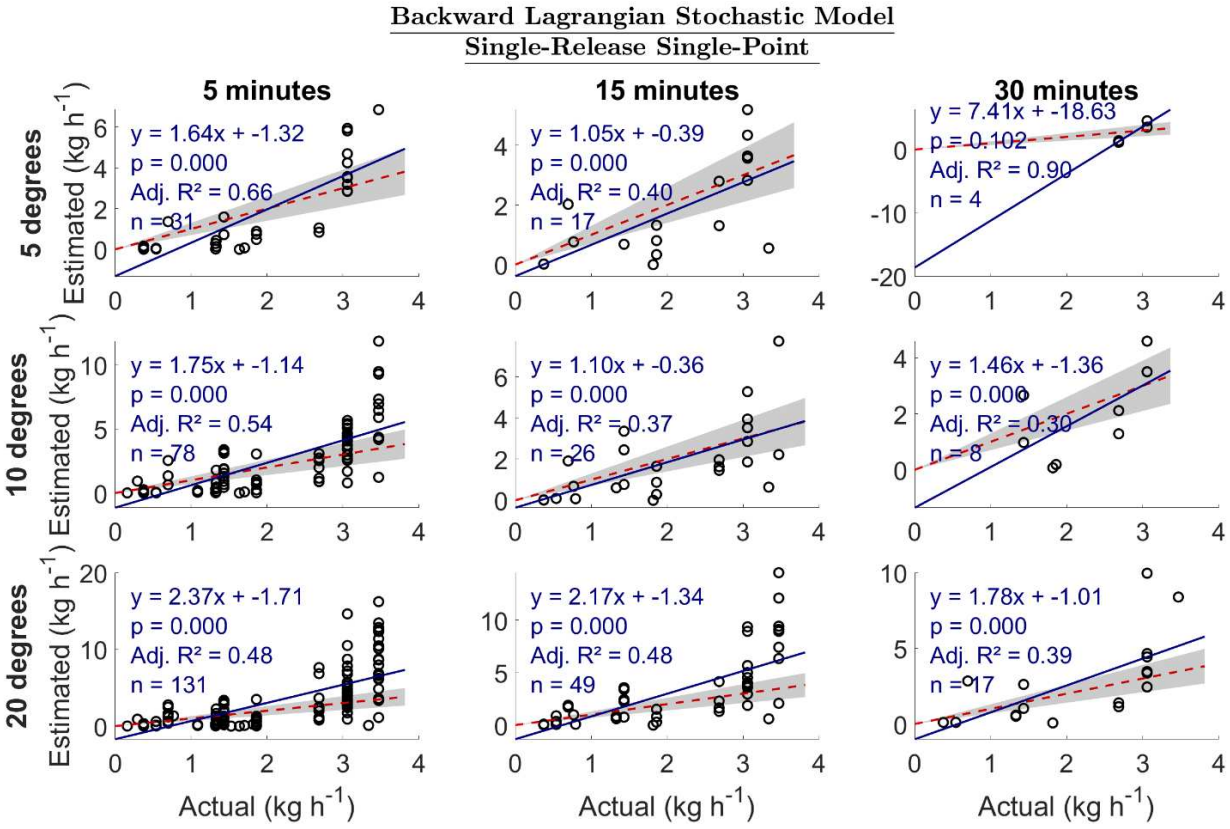

Figure 12. Estimated emission vs actual emission (kg h^{-1}) for single-release single-point emissions. The red dotted line is a 1:1 line based on actual emissions i.e. points below the line are underestimated and above are overestimated emissions. The gray region represents ±30% of the actual emission. Adj. R^2 is the adjusted R^2. The sample size is n.

2.4.3.2 Multi-release single-point emissions

The bLs method had wide uncertainties for MSRP emissions especially in the 5 minutes, 5- and 10-degrees categories (Figure 13). In the other categories, the slopes were between -0.03 and 0.45, and R^2 ~0. Even though the estimated emissions spanned up to >20 kg h^{-1} mostly for actual emissions of up to 6 kg h^{-1}, lots of points were concentrated close to 0. Compared to the GPIM MSRP results, even though both models have an R^2 of ~0, the GPIM had a slope closer to

1 in the 15-munites category than the bLs showing better performance. These results show that the bLs is more suitable for quantifying SRSP emissions than MSRP emissions.

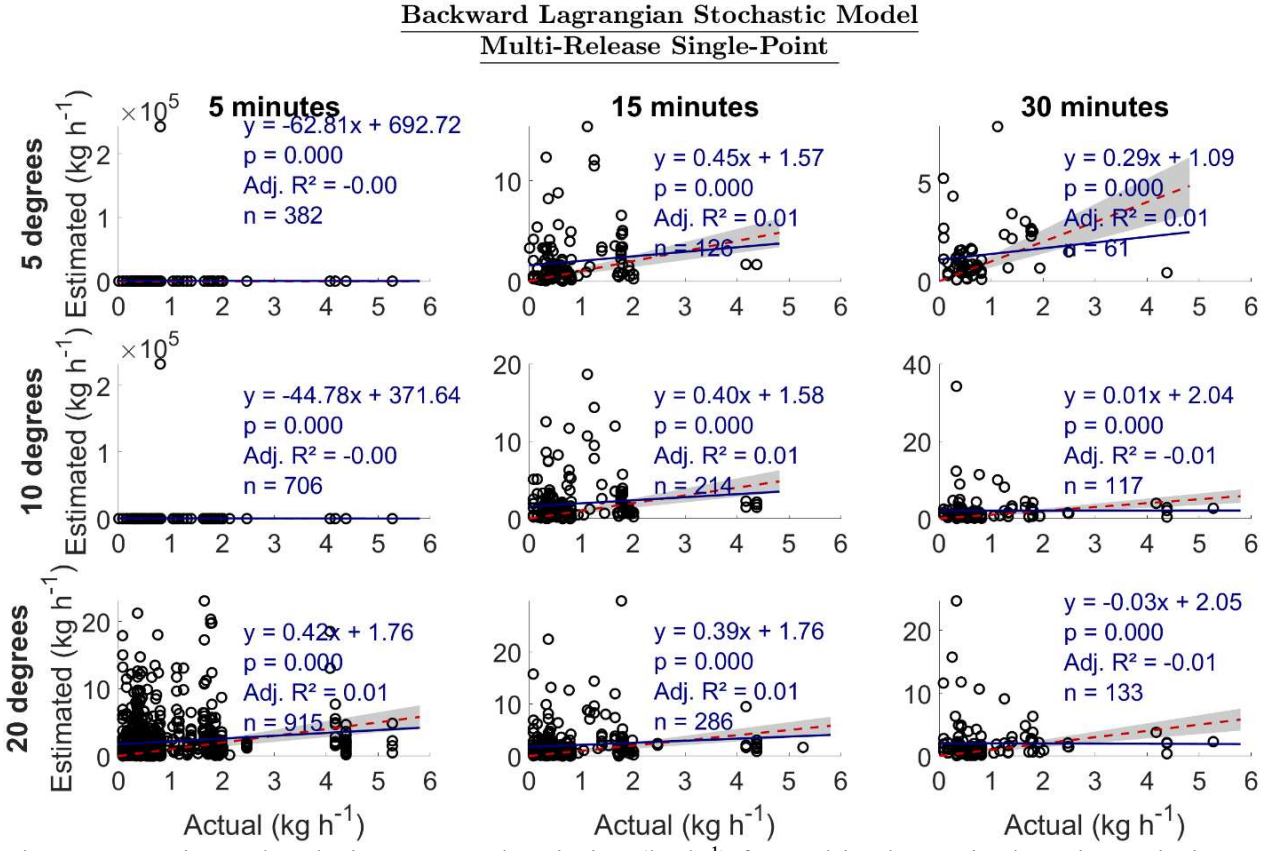

Figure 13. Estimated emission vs actual emission (kg h^{-1}) for multi-release single-point emissions. The red dotted line is a 1:1 line based on actual emissions i.e. points below the line are underestimated and above are overestimated emissions. The gray region represents ±30% of the actual emission. Adj. R^2 is the adjusted R^2. The sample size is n.

2.4.4 Model comparison – subset data

Using a subset of data (SRSP), filtered by 15-minute intervals within a 10-degree wind sector range where each model provided an emission estimate, the bLs model exhibited the best performance, with its linear regression closely aligned with the 1:1 line (Figure 14). The slope of the regression line for the GPIM was 1.6, indicating an overestimation, while the bLs had a slope of 0.95, suggesting high accuracy. In contrast, the EC model produced slopes of 0.08 and 0.10 when using the Kormann and Meixner (2001) and Kljun et al. (2015) footprint parameterizations,

respectively, indicating significant underestimation. When emission estimates were categorized by emission point, the GPIM notably overestimated emissions at locations 4W-22 and 4W-51 (identified in Figure 7), both situated approximately 10 m from the measurement location. The EC model consistently underestimated emissions across all sources, while the bLs (WindTrax) model provided estimates closest to the expected values. The EC model produced negative emission rates associated with negative fluxes during periods of high non-stationarity (Section A2.3.4 in the Appendix). These deviations from stationarity reflect intermittent plume capture, where the EC system alternated between sampling emitting and non-emitting regions. Overall, these findings indicate that for source-receptor distances ranging from approximately 10 to 90 meters, the bLs model demonstrated the highest accuracy in quantifying emissions.

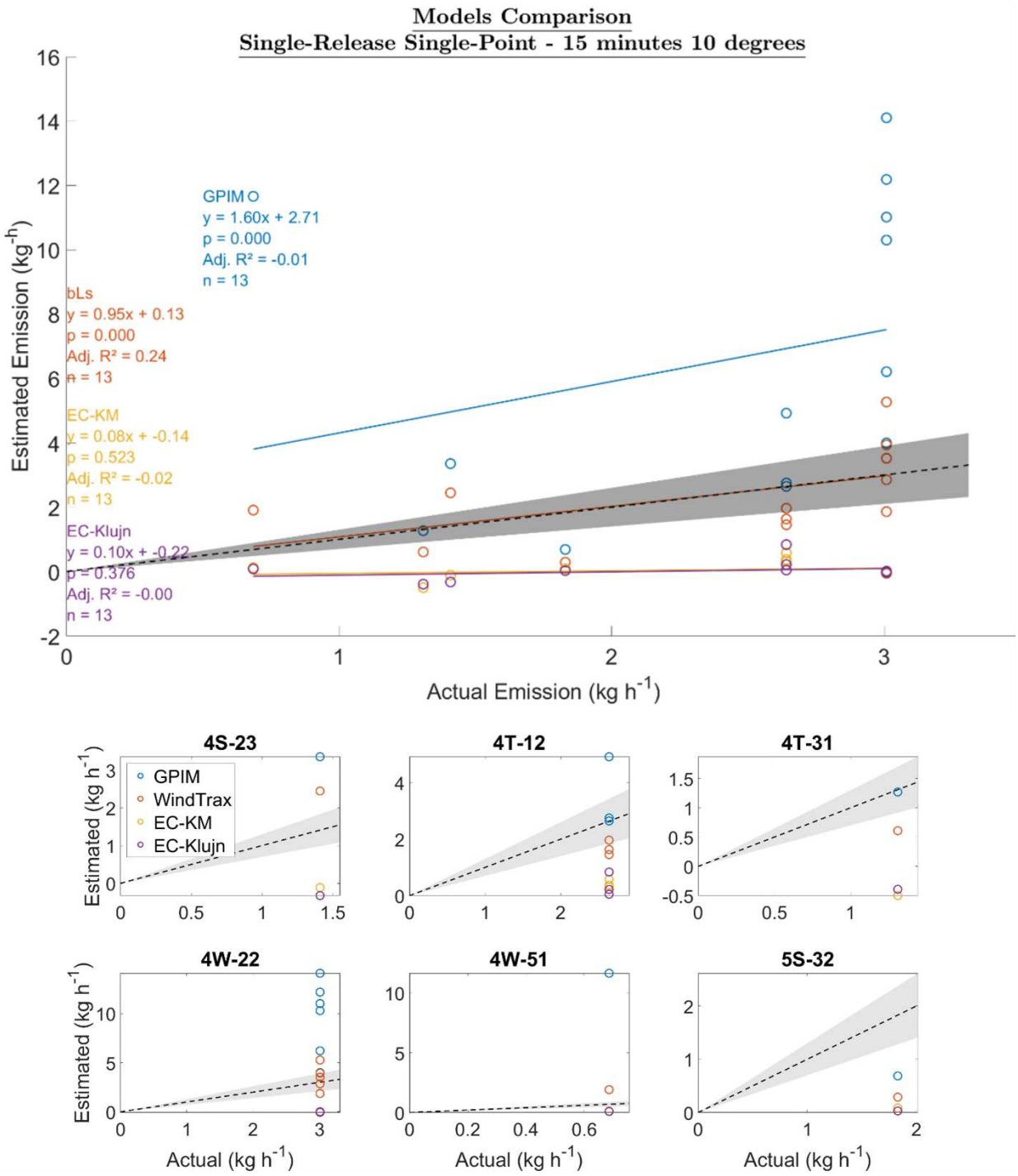

Figure 14. Top plot: Estimated emission vs actual emission (kg h^{-1}) for each model. GPIM is the Gaussian plume inverse model, bLs is the backward Lagrangian stochastic model, EC-KM is eddy covariance with the Kormann and Meixner (2001) footprint, and EC-Kljun is the eddy covariance estimate using the Kljun et al. (2015) footprint. The black dotted line is a 1:1 line based on actual emissions i.e. points below the line are underestimated and above are overestimated emissions. The gray region represents ±30% of the actual emission. Adj. R^2 is the adjusted R^2. The sample size is n. Bottom plot: Estimated emission vs actual emission categorized by Emission Point as

illustrated in Figure 7.

2.4.5 Traceability example

To illustrate how raw data were converted into model-based emission estimates, we present one representative 15-minute interval used in Figure 14. During a controlled release at point 4W-22 (wellhead), located approximately 10.5 m from the mast, the ground-truth release rate was 3 kg CH_4 h^{-1}. Over this interval, the average CH_4 concentration enhancement was 8.3 ppm above the background (determined using the 5th percentile method, see Section 2.3.4.2). The wind direction was 153° (0.3 m crosswind distance), with an average wind speed of 5.8 m s^{-1}. The same interval was processed through the three modeling frameworks:

- The bLs model (WindTrax), using measured concentration, geometry, and meteorological data, estimated 3.5 kg h^{-1}.
- The GPIM model, using Equation A7 and A8 (Section A2.1 in the Appendix) and US EPA (2013) dispersion coefficients, estimated 10.3 kg h^{-1}.
- The EC method using the Kormann and Meixner (2001) footprint) estimated –0.004 kg h^{-1} due to a negative flux under high non-stationarity conditions.

This example illustrates how the bLs model reproduced the true emission most closely, GPIM overestimated, and EC underestimated the emission. More examples of data presented in Figure 13 are available in the Appendix Section 3.3.

2.4.6 Eddy covariance quality assurance and control

Evaluation of the EC data revealed quality assurance and control issues that compromised both the analysis and the conclusions drawn from the EC results. The flux data were flagged as "2" (low quality) according to the 0–1–2 quality classification system of Mauder and Foken (2004), indicating that the data were not suitable for EC analysis. In EC quality assessment, both the qualitative shape of the cospectra and the quantitative slopes of selected portions are examined to determine if the data meet accepted standards. In this study, the cospectra deviated significantly from the ideal shape, indicating problems in data collection and pre-processing. Possible causes include obstructions in the testing area, misalignment between CH_4 and sonic anemometer time series (due to the absence of a reliable method for alignment), slow response time of the gas analyzer, increased lag from the 3 m inlet tubing, and inconsistent sampling frequency. Similarly, ogive analysis—used to evaluate whether the averaging time is sufficient—showed that the ogive curves did not follow the characteristic sigmoidal shape (plateauing at the y-axis and at zero). The ogive shapes were similar across all averaging intervals, none plateaued sufficiently, further indicating data collection issues that invalidate the EC method for this study. For clarity and to guide future studies, Burba (2013) provides examples of ideal cospectra and ogive shapes illustrating how these tools can be used to diagnose instrumentation and data collection problems.

2.5 Discussion

Methane emissions quantification from oil and gas is a complex system comprising of gas emissions from different heights, different locations, encountering aerodynamic obstacles of different sizes, and of varying emissions duration, amongst others. The ability to precisely quantify emissions using data collected by a point sensor, downwind of a source is directly influenced by plume dynamics. The CH_4 plume downwind of a source will change in size and shape in different

atmospheric conditions, in open areas versus areas with obstacles, diurnally, and in different seasons (Casal, 2008). In this study, we evaluated the ability of downwind methods—including a non-standard closed-path EC system, the GPIM, and the bLs model—to quantify emissions from single-release and multi-release point sources. While the field measurements took place under naturally varying meteorological conditions, these were not explicitly stratified or analyzed as experimental factors. Additionally, although on-site infrastructure such as storage tanks was present, their distance from the sampling instruments (~50 m) likely rendered their aerodynamic influence negligible. As such, the analysis focuses on quantification performance under realistic but uncontrolled field scenarios, without attributing model behavior to specific atmospheric or obstacle-related conditions.

2.5.1 Eddy covariance

Eddy covariance was tested using a closed-path analyzer, off-axis integrated cavity output spectroscopy, with a 3.2 L min^{-1} pump flowrate and a 0.4 s gas flow response time. The closed path EC underestimated emissions with a linear regression slope for estimated emissions versus actual emissions of between -0.42 and 0.54 using the Kljun et al. (2015) and the Kormann and Meixner (2001) footprint models, and adjusted R^2 was ~0 (Section 2.4.1). This was a wider uncertainty in estimated emissions than one reported by Dumortier et al. (2019), who estimated emissions at between 90 and 113% of true emission (~1.5 kg day^{-1}) with concentrations between 2 and 3 ppm. Our study tested closed-path EC at emission rates between 0.005 and 8.5 kg h^{-1}. Notably, the results for the non-standard EC system tested this study may not be representative of EC performance in oil and gas as ogive and cospectra analysis indicated that the flux may not have been fully resolved due to non-stationarity, and instrument-related limitations.

Our results were derived from data filtered to include only periods with sampling frequencies ≥8 Hz, which significantly reduced the number of usable emission measurements. Although the instrument was configured to sample at 10 Hz, it did not consistently achieve this rate. This discrepancy may be attributed to instrument-related factors such as the 0.4-second gas flow response time, which could delay analysis of the drawn air sample in the cavity, or the use of a 3 L min^{-1} pump with 3 meters of tubing, which reduced the effective turnover rate. The dataset used for eddy covariance evaluation was predominantly flagged as low quality (flag 2) according to the Mauder and Foken (2004) quality control test, which classifies flux data based on steady-state conditions and the presence of well-developed turbulence (flags 0 = high, 1 = intermediate, 2 = low quality). Many of the low-quality flags were likely driven by wide deviation in vertical wind speed (w) / methane (CH_4) stationarity reflecting intermittent plume capture, where the EC system alternated between sampling emitting and non-emitting regions. The EC model produced negative emission rates associated with negative fluxes during periods of high non-stationarity (Section A2.3.4 in the Appendix).

Despite high non-stationarity that resulted in low data quality issues resulting in EC inaccuracies, this study acknowledges our design limitations. Our study did not have a reliable method for aligning the asynchronous CH_4 and sonic anemometer data streams, which likely introduced substantial timing errors and contributed to uncertainty in the flux calculations. The intake for the closed-path system was positioned approximately 10 cm below the sonic anemometer to protect the inlet tubing from debris and precipitation by mounting it on an aluminum shield facing downward. We recognize that even this small vertical separation can introduce additional errors in flux measurements when using short towers. This design choice was a compromise to ensure instrument protection while maintaining data collection in field conditions.

We acknowledge that the system used in this study was not designed or configured for standard eddy covariance analysis, and that this limitation impacts the interpretation of our results in the context of EC-based flux quantification.

In this study, continuous monitoring was conducted using a single sensor with an inlet deployed at a fence-line distance. This system requires instrumentation capable of measuring a wide concentration range, as emissions from oil and gas sites can vary between 0 and 250 ppm (Section A1 in the Appendix). While continuous monitoring systems, comprising multiple sensors, can offer enhanced spatial coverage and source localization, they also introduce higher costs. The limitations and findings reported here therefore apply specifically to this single-sensor fence-line continuous monitoring approach and may not be representative of all continuous monitoring frameworks. This study acknowledges the limitations of the eddy covariance (EC) setup used, particularly that the ABB MGGA GLA131 Series analyzer is not designed specifically for EC applications. As a result, the conclusions drawn from the EC data are invalid and not comparable to the other tested models.

This study identified data collection and instrumentation issues that future work can address to enable successful EC application. Based on flagged low-quality data, non-ideal cospectra and ogive shapes, and the presence of large negative fluxes, the dataset was deemed unsuitable for EC analysis. The primary causes of the unsuccessful application were: (1) the CH_4 analyzer was not designed for EC measurements, exhibiting slow response time, low pump flow rate, and inconsistent sampling frequency; (2) the 3 m inlet tubing length for the closed-path analyzer caused signal attenuation and increased lag; (3) the sonic anemometer and CH_4 analyzer data were not synchronously logged, preventing accurate time-series alignment; (4) the EC system was installed near obstacles that disrupted smooth eddy formation; and (5) ogive plots suggested

that the maximum 30-minute averaging interval used in this study may have been insufficient. We recommend further EC testing with these issues corrected to properly evaluate its application in continuous oil and gas monitoring.

2.5.2 Gaussian plume inverse method

The GPIM method quantified emissions within a slope of 1.65 to 3.92 and adjusted R^2 of between 0.4 and 0.64 with highest performance at 15-minutes 5-degrees wind sector (slope = 1.65, R^2 =0.4), and 5 minutes 5-degrees (slope = 2.42, R^2 = 0.64) for SRSP emissions (Section 2.4.2). For MSRP emissions, the GPIM showed wide uncertainties even though the slopes for other categories excluding 5-minutes 5-and 10-degrees, and 30-minutes 10-degrees categories, were between 0.74 and 1.60, with R^2 ~0 (Section 2.4.2). The R^2 close to zero showed that there was no linear relationship between the estimated and actual emissions for MSRP conditions. Overall, the GPIM performed well under 15-minutes averaging duration, and 5-degree wind-sector ranges in both SRSP and MSRP categories. The MSRP emission profiles tested in this study were complex challenging the GPIM application as the method is a point-source specific quantification approach and works best in open areas, free of obstacles, and when the background concentration is well defined. For multiple emissions, even when the sensor is nominally downwind of a single source based on the average wind direction, quantification can be complicated by interference from neighboring sources. However, it is important to emphasize that such complexity is not a fundamental limitation of quantification itself, but rather a function of the experimental design and study objectives. For example, plume interference can often be minimized through strategic localization and optimization using multiple sensors—an approach that differs from the single-instrument setup used in this study. This study's design involves defining plumes based on wind sector ranges, as opposed to using multiple sensors to localize sources, and therefore does not

replicate how various continuous monitoring solutions typically operate. The GPIM has previously been reported to quantify emissions within 40.7 and 60% error for a single point-source using controlled release experiments (Riddick et al., 2022b). However, GPIM correct quantification has been suggested to be better for longer distances where the plume is well mixed as seen in Figure 14. This is typically a challenge for fence-line sensors that have to be deployed within the facility boundaries where large downwind distances may not be practical.

2.5.3 Backward Lagrangian stochastic model

The bLs method was the most accurate in quantifying emissions for the SRSP release profiles but had wider uncertainties than the GPIM for MRSP scenarios (Sections 2.4.2.2 and 2.4.3.2). For SRSP emissions, the slopes closest to 1 were during the 15-minutes 5-degrees (slope = 1.05, R^2 = 0.4) and 10-degrees (slope = 1.10, R^2 =0.37). The best R^2 was 5 minutes 5-degrees (slope = 1.64, R^2 = 0.66). However, for MSRP emissions, the slopes were between -0.03 and 0.45 in the best categories with R^2 of ~0. Similarly to the GPIM method, the bLs method used in this study is a point-source specific quantification method that simulates transport of molecules in open area and where the background concentration is defined. In this case, as with the SRSP test scenario, the bLs approach was generally more accurate than the GPIM. However, for MRSP emissions, quantification accuracy was low. This discrepancy may be due to design-related challenges—specifically, interference from neighboring sources and the lack of distinct plume separation in complex flow conditions. Although the measurement point was nominally downwind of a single source, the real-world plume structure may not align with model assumptions. Additionally, the bLs implementation in WindTrax 2.0 is designed for single-source scenarios and applying it in multi-source environments without adaptation can lead to inaccuracies. The GPIM and bLs methods are sensitive to background correction, which in this study was complicated by

temporal overlap between release events and residual CH_4 accumulation, particularly under stable atmospheric conditions. Although this is a controlled-release study, residual methane from prior emissions and the presence of multiple plumes can affect the CH_4 concentration during a candidate event, challenging the assumptions used to define background and isolate a single-source plume using wind-sector-based criteria. These findings highlight the importance of aligning modeling assumptions with the experimental context rather than pointing to a fundamental limitation of the method itself.

2.5.4 Implications

In recent years, there has been growing interest and need for accurate CH_4 quantification from oil and gas sites. This is generally done through survey methods and continuous monitoring using fence-line sensors. Continuous monitoring involves having stationary sensors measuring meteorology and CH_4 mixing ratios, which are then used to infer emission rates. For point sources, downwind methods such as the Gaussian plume inverse method have been widely used, especially for survey quantification. Continuous monitoring is relatively new but fast growing. This study's design replicated a continuous monitoring setup's downwind deployment distance, range of typical emission rates, emissions heights, and meteorological data acquisition.

Oil and gas point sources could either be single emissions or multiple emissions occurring concurrently. In this study's design, cases involving multiple emissions with more than one release point located upwind posed challenges for the specific Gaussian and backward Lagrangian stochastic (bLs) model implementations, which were applied assuming a single active source at a time. While these models can be extended to handle multi-source scenarios, the assumptions used here limited their ability to distinguish individual contributions when plumes overlapped. As a result, interference from neighboring emissions introduced ambiguity in model-observation

alignment, particularly under complex wind conditions. Closed-path eddy covariance was generally unreliable in this study due to data-collection and instrumentation issues associated with using a non-standard EC system. This resulted in invalid EC results that could not be compared with the GPIM and the bLs models. The bLs method was the most accurate for single-release single-point emissions but was less accurate than the GPIM under multi-release conditions. For both GPIM and bLs, 15-minute averaging with a narrow wind-sector (5°) yielded the best performance. While EC results in this study were limited by system constraints, future work is recommended using standard EC instruments and further optimizing GPIM and bLs models—particularly for complex multi-release scenarios—to improve accuracy and reduce uncertainties.

CHAPTER 3: A COMPARISON OF BOTTOM-UP, MEASUREMENT-BASED AND EPA INVENTORY METHANE EMISSION ESTIMATES FOR NON–OIL AND GAS SOURCES IN THE DENVER–JULESBURG BASIN, COLORADO

Mbua, M., Hodshire, A., Riddick, S.N., Kiplimo, E., Santos, A., & Zimmerle, D. (2025). A comparison of bottom-up, measurement-based and EPA inventory methane emission estimates for non–oil and gas sources in the Denver–Julesburg basin, Colorado. *Environmental Science and Technology (In peer review)*.

3.1 Abstract

While oil and gas emissions have historically received the most attention due to regulatory and economic drivers, non-oil and gas sources also contribute substantially to basin- and regional-scale methane (CH_4) fluxes and represent important mitigation opportunities. As part of a broader effort to quantify CH_4 from all sources within the Denver-Julesburg (DJ) basin, this study develops a measurement-based inventory of major non-oil and gas CH_4 sources and reconciles measurement-based and bottom-up EPA estimates. Specifically, a facility-level bottom-up inventory generated using vehicle-mounted instruments was compared to a bottom-up inventory based on EPA emission factors. We focus on emissions from concentrated animal feeding operations (CAFOs), municipal solid waste landfills, wastewater treatment plants, and surface waterbodies (lakes and reservoirs). The applicability of monthly mobile surveys to construct a measurement-based inventory in the DJ basin (39.9–40.7°N, 105.3–104.2°W) is evaluated. Seasonal variability in CH_4 emissions differed across sources, with CAFOs and wastewater treatment plants showing no consistent seasonal pattern, landfills exhibiting higher winter emissions, and lakes and reservoirs displaying higher emissions in warmer seasons. Total annual emissions are estimated at 123 ± 21 Gg y^{-1}, compared to the EPA bottom-up estimate of 119 Gg y^{-1}. The agreement of this study's annualized inventory with the EPA estimate within uncertainty demonstrates that reconciliation between EPA and measurement-based inventories is possible when measurements capture temporal and spatial variability and are appropriately extrapolated to annual scales. Aggregated CH_4 emissions indicate that CAFOs dominate regional emissions, contributing 78% using this study's EFs and 87% using EPA EFs, followed by municipal solid waste landfills (11% in both inventories), while wastewater treatment plants contribute ~1%. This study also demonstrates that spatially distributed measurements conducted multiple times per year

can reduce temporal biases caused by seasonal variation, operational practices, diurnal cycles, and environmental conditions. Overall, the consistency of measurement-based emissions with EPA estimates across most sectors supports the validity of inventory methodologies but underscores the need for temporally resolved measurements to better capture intra-annual variability.

3.2 Introduction

In recent years, there has been growing interest in measuring and mitigating methane (CH_4) emissions due to their significant contribution to climate change (World Bank Group, 2025). Several international initiatives have been established to reduce CH_4, including the Oil and Gas Methane Partnership 2.0 (OGMP 2.0) led by the United Nations Environment Programme (UNEP, 2025), which targets oil and gas sector emissions, as well as programs supported by the Global Methane Hub and the Climate and Clean Air Coalition (CCAC) that extend to agriculture, waste, and energy systems (Global Methane Initiative, 2004). In the United States, the Environmental Protection Agency (EPA) used a bottom-up approach to estimate that most CH_4 emissions originate from natural gas and petroleum systems (28%), enteric fermentation (25%), landfills (16%), manure management (9%), coal mining (6%), flooded land (6%), and other sources (11%) (US EPA, 2025a). While oil and gas emissions have historically received the most attention due to regulatory and economic drivers, non-oil and gas sources collectively contribute more emissions to basin- and regional-scale CH_4 fluxes and represent important opportunities for mitigation.

Livestock (dairy and beef cattle) are major contributors to CH_4 emissions, which are typically categorized as enteric fermentation and manure management. These emissions vary across regions and farms depending on animal type, management practices, nutrition and feed additives, genetic selection, and environmental conditions (Dillon et al., 2021; Place and Mitloehner, 2010). While enteric CH_4 emissions in the United States have remained relatively

stable over the past three decades, manure-related CH_4 emissions increased between 1990 and 2020, driven largely by the expansion of dairy and swine operations (Beck et al., 2023). Multiple methods exist for quantifying enteric CH_4 emissions from ruminants, including respiration chambers, the sulfur hexafluoride (SF_6) tracer technique, automated head-chamber systems, and process-based models (Dillon et al., 2021; Johnson et al., 1994). Research facilities such as Colorado State University's AgNext (Colorado State University, 2025c) are actively developing mitigation strategies to reduce livestock emissions. Approaches include improving feed composition for example, increasing carbohydrate content to lower excess energy conversion to CH_4, and capturing CH_4 produced during anaerobic manure decomposition for energy recovery (Colorado State University, 2025c).

Municipal solid waste landfills are significant sources of CH_4, generated through the anaerobic degradation of buried organic material. Once produced, CH_4 can escape to the atmosphere by diffusing through landfill covers or venting through exposed surfaces. The magnitude of emissions depends on multiple factors, including barometric pressure, topography, landfill design and operation, waste quantity and composition, presence and efficiency of gas capture systems, and whether the landfill is active or closed (Cusworth et al., 2024; Czepiel et al., 2003). Traditionally, landfill CH_4 emissions have been estimated using models based on waste-in-place data, decay rate parametrizations, and assumptions about gas capture efficiency (Barlaz et al., 2009; US EPA, 2008). These approaches require detailed knowledge of landfill-specific material composition and management practices (Cusworth et al., 2024). In recent years, however, a variety of measurement-based approaches have been adopted to improve estimates. These include surface emission monitoring through walking surveys, vehicle-based surveys with tracers and downwind quantification, as well as emerging applications of drone-based measurements,

aerial surveys, and satellites (Abichou et al., 2023; Cusworth et al., 2024; Kormi et al., 2017; Maasakkers et al., 2022; Mønster et al., 2019; Riddick et al., 2017). Dedicated facilities such as the St. Francis University FluxLab Simulation Facility for Landfill Emission Experiments (SIMFLEX) in Canada provide platforms for testing and validating these measurement techniques and models under controlled conditions (FluxLab, 2025).

Wastewater treatment plants (WWTPs) produce CH_4 during collection and treatment processes that involve anaerobic conditions (Song et al., 2023). In the United States, these facilities are considered a relatively minor CH_4 source compared with oil and gas operations, livestock, and landfills (Riddick et al., 2024b; US EPA, 2025a), in part because treatment systems are designed to capture or flare much of the CH_4 generated. The U.S. EPA estimates WWTPs emissions using a bottom-up model that incorporates state population, biochemical oxygen demand (BOD) production, an emission factor of CH_4 per unit BOD, and the fraction of wastewater treated anaerobically (US EPA, 2019). However, direct measurements of CH_4 from wastewater systems remain scarce, and recent studies suggest that emissions may be underestimated in current inventories (Moore et al., 2023). This uncertainty highlights the need for additional measurement-informed assessments of the sector.

Human-made lakes and reservoirs, constructed for purposes such as water storage, hydropower generation, and recreation, can also be sources of CH_4 emissions (US EPA, 2021). Emissions arise from the anaerobic decomposition of organic matter, with algal blooms representing a notable driver. Excess nutrient inputs from agricultural and industrial runoff can stimulate algal growth, and when algae die under oxygen-depleted conditions, methanogenic bacteria thrive, producing CH_4 (US EPA, 2021). In the United States, the EPA is required to account for CH_4 emissions from human-made waterbodies, which are typically quantified by measuring

ebullition and diffusion pathways (Beaulieu et al., 2020; US EPA, 2022a). Beaulieu et al. (2020), for example, surveyed 32 reservoirs spanning agricultural and forested landscapes and found that ebullition was the dominant emission pathway in 75% of cases.

This study contributes to the Site Aerial Basin Emissions Reconciliation (SABER) project, a collaboration among Colorado State University, Pennsylvania State University, the University of Wyoming, and Bridger Photonics, which aims to develop a measurement-informed inventory of CH_4 emissions in the Denver-Julesburg (DJ) Basin, Colorado, and the Upper Green Basin, Wyoming (Colorado State University, 2025d). SABER integrates bottom-up approaches, which scale emissions from individual sources, with top-down approaches, which measure CH_4 over larger scales using satellites, aircraft, towers, drones, or vehicles (Barkley et al., 2023; Jacob et al., 2022; Riddick et al., 2022b; Vaughn et al., 2018).

As part of the SABER study, continuously operating towers were deployed around the DJ Basin, defined here as the region between latitude 39.9 to 40.7 and longitude −105.3 to −104.2. These towers provided basin-level CH_4 flux estimates and attributed oil and gas contributions using methane-to-ethane ratios. Total basin-level emissions were then compared against bottom-up inventories generated by the project's ground and modeling teams. Bottom-up oil and gas emissions were constructed using input data from Bridger Photonics aerial surveys and site-level measurements conducted by CSU and the University of Wyoming, modeled with the Mechanistic Air Emissions Simulator (Colorado State University, 2025e). Non-oil and gas sources including landfills, livestock operations, wastewater treatment plants, and lakes/reservoirs were characterized separately by CSU's ground team through mobile driving surveys conducted from June 2024 to May 2025. This paper focuses on these non-oil and gas sources and their role in reconciling basin-level CH_4 budgets. In this study, the bottom-up approach consists of facility-

level measurements using vehicle-mounted instruments, which provide direct observations of CH_4 emissions without relying on prior inventories. These measurements are compared to a bottom-up inventory generated using EPA and Colorado Department of Public Health and Environment (CDPHE) data (CDPHE, 2025c), along with other source-specific measurements, as described in the Methods section.

Previous studies have estimated non-oil and gas CH_4 emissions in the DJ basin at both regional and facility scales. Pétron et al. (2014) used two days of aircraft-based measurements combined with a mass-balance approach to estimate basin-wide CH_4 emissions. In their study, airborne CH_4 dry air mole fractions were integrated with ground-based wind speed and direction data to quantify total CH_4 fluxes in and out of the region encompassing a 70 km × 85 km region in northeastern Colorado encompassing the highest density of the O&G production activities in the DJ Basin, mostly located in Weld County, north of Denver and east of Boulder and Larimer Counties (Pétron et al., 2014). To estimate non-oil and gas emissions, Pétron et al. (2014) constructed a bottom-up inventory using emission factors (EFs) from the literature, activity data from the state of Colorado (CDPHE, 2025c), and facility-level estimates reported to the EPA's 2012 Greenhouse Gas Reporting Program (US EPA, 2012). These bottom-up inventories indicated that non-oil and gas sources, including agricultural operations, landfills, and wastewater treatment plants, contributed 7.1 ± 1.7 t CH_4 h^{-1} on May 29 and 6.3 ± 1.0 t CH_4 h^{-1} on May 31, 2012. By subtracting these contributions from the total measured flux, the study estimated an average oil and gas contribution of 19.3 ± 6.9 t CH_4 h^{-1}.

Riddick et al. (2022) conducted a driving survey to derive methane EFs for oil and gas facilities, agricultural operations, and waterbodies, using downwind measurements and the WindTrax dispersion model (Crenna, 2006). The study provided EFs for cattle, dairy, and sheep

operations, as well as lakes and reservoirs. Building on this, Riddick et al. (2024) developed a bottom-up inventory of agricultural, waste, and natural emissions using IPCC Tier 1/2 EFs, Colorado-specific EPA Tier 3 EFs, and measurement-informed EFs from their 2022 survey. Annual agricultural emissions ranged from 67–98 Gg CH_4 y^{-1} depending on the EF approach, while waste and wastewater sectors ranged from 0.6–40 Gg CH_4 y^{-1}, and natural water sources contributed an additional 14 Gg CH_4 y^{-1}.

This study quantifies CH_4 emissions from four non–oil and gas source categories: livestock (cattle, dairy, and sheep), municipal solid waste landfills, wastewater treatment plants, and surface waterbodies (lakes and reservoirs). While sector-specific approaches to emissions' estimation exist, this analysis evaluates the applicability of monthly mobile surveys to develop a measurement-based inventory. Snapshot facility-level measurements were collected using a vehicle-based platform equipped with a gas analyzer and meteorological instrumentation. To minimize temporal and spatial bias, facilities were revisited at monthly intervals over a one-year period. These data were used to construct an annual CH_4 emissions inventory for the Denver–Julesburg (DJ) Basin, defined here as the region spanning latitude 39.9–40.7 and longitude −105.3 to −104.2. Specifically, this study (1) generates measurement-based emission factors (EFs) for concentrated animal feeding operations (CAFOs) (dairy cows, cattle, sheep), landfills, wastewater treatment plants, and lakes/reservoirs; (2) uses these EFs to develop a measurement-based inventory for CH_4 from non-oil and gas sources in the DJ Basin; (3) compares the generated EFs and measurement-based emission inventory with the EPA inventory and other measurement-based studies; and (4) investigates seasonal variability in EFs for CAFOs, municipal solid waste landfills, wastewater treatment plants, and lakes/reservoirs.

3.3 Methods

3.3.1 Field survey sites selection

An unpublished 2024 dataset from the Colorado Department of Public Health & Environment (CDPHE, 2025c) was used to identify survey sites within the DJ Basin (lat. 39.9–40.7, long. –105.3 to –104.2) (Figure A22). A preliminary summer 2024 survey covered 125 sites, including CAFOs, landfills, wastewater treatment plants, solid waste sites, and freshwater sources. Monthly survey sites were selected based on confirmed operation, accessibility, observed emissions, and proximity to CSU Methane Emissions Technology Evaluation Center (METEC), which served as the start and end point for daily measurements, resulting in 33 sites: 19 CAFOs (12 dairies, 5 cattle, 2 sheep), 7 landfills, 3 wastewater facilities, and 4 freshwater sources (Table 2). All measurements were conducted from downwind positions due to access limitations.

Table 2: Number of measured facilities relative to the total population

Source	Population Size (Facilities)	Sample Size (Facilities)	% of Population	% of Activity Factor (Section 3.3.5.1)
CAFOs				
Dairy	44	12	27	35
Cattle	30	5	17	37
Sheep	3	2	67	54
Municipal Solid Waste Landfills				
Open	3	5: 2 were outside DJ region	100	100
Closed	4	2	50	86
Wastewater treatment plants	55	3	5	28
Lakes and Reservoirs	175	4	2	7

3.3.2 Field measurements

Methane measurements were collected using the Aeris Strato analyzer (Hayward, CA, USA) connected to a 2 m sampling tube with a 3.275 mm inner diameter. The analyzer operated with a measured pump flow rate of 0.36 L min^{-1} and a sampling frequency of 1 Hz. The tubing inlet was collocated with a 150 WX Airmar (Milford, NH, USA), also sampling at 1 Hz (Figure A23). The Airmar is a mobile weather station that accounts for vehicle motion in calculating wind speed and records wind direction, corrected wind speed, temperature, pressure, humidity, latitude, and longitude.

Measurement height was 3 m during June, August, and October 2024, and 2 m in September and from November onward. This change resulted from switching from a metallic sampling mast to a more stable roof rack configuration. The variation in inlet height is accounted for in the quantification model (Section 3.3.3). Atmospheric stability was determined using the Pasquill–Gifford Stability Classification (PGSC), which requires mean wind speed, cloud cover, and solar insolation as inputs. Cloud cover and insolation were recorded during measurements and supplemented with publicly available data from Weather Underground (Weather Underground, 2025).

3.3.3 Emission quantification

Methane emissions were quantified using WindTrax 2.0 (Crenna, 2006; WindTrax 2.0, 2020), a freely-available backward Lagrangian stochastic (bLS) model applied in the area-source configuration. To calculate model input data for each facility, CH_4 mixing ratios from the gas analyzer were merged with meteorological data from the Airmar sensor at a 1 Hz frequency. Data were filtered to include only periods when the truck was within 1 km of each facility, consistent with the operational limitations of the WindTrax 2.0 quantification model (Riddick et al., 2018). Whenever possible, measurements included both upwind and downwind transects of each facility, capturing emissions from sources in proximity to the site. The background CH_4 mixing ratio was defined as the average of the lowest 5th percentile (Mbua et al., 2025) of the 1 km filtered data. For facility-level quantification, only downwind periods from the facility were retained. Downwind intervals were identified as periods when the sensor remained downwind of the facility for at least 30 seconds (Figure 15). This was determined by generating a polygon around the facility coordinates and selecting 1-second data points where wind direction indicated flow from the region of interest toward the sensor. This filtering approach minimized interference from

adjacent sources. Although this method may be affected by the gas transport time from the source to the sensor, the effect was assumed negligible because the WindTrax model operates under a steady-state framework that uses time-averaged data. The resulting filtered dataset was then averaged for quantification.

Model inputs included homogenous area source configuration site layout using coordinates from Google Maps (Google, 2025), atmospheric stability, mean meteorological variables (wind speed, wind direction, temperature, pressure), mean downwind CH_4 mixing ratios, background mixing ratio, and the average truck location (Figure A24). The homogenous area source configuration in WindTrax assumes the average inputs are representative of the whole facility. The inlet tubing delay to the analyzer was calculated to be 2.8 seconds. However, because the quantification model uses time-averaged rather than time-synchronized CH_4 and meteorological inputs, this delay was assumed negligible. WindTrax was selected due to its demonstrated application in estimating facility-level emissions where sources are spatially diffused. Riddick et al. (2022) applied the WindTrax area-source model with mobile survey data to estimate emissions from agricultural operations, lakes, and reservoirs. Shonkwiler (2018) used WindTrax to quantify CH_4 emissions from a 3.9 ha anaerobic lagoon serving a 1,400-head dairy, and Riddick et al. (2017) applied the model to estimate emissions from a UK landfill.

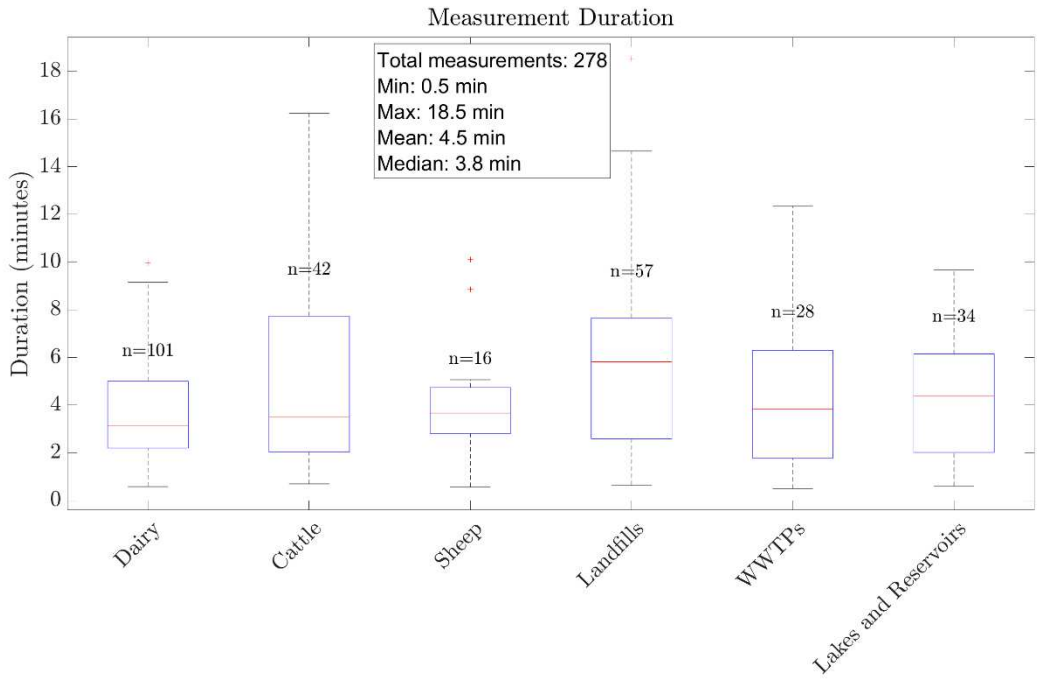

Figure 15. Distribution of CH_4 measurement durations across different source categories. Box plots show the median (center line), interquartile range (IQR, box boundaries), and range (whiskers) of measurement times in minutes. The number of measurements (n) for each category is displayed above the third quartile. Total measurements represent all valid files with duration ≥30 seconds collected during 2024-2025 field campaigns. Measurement durations varied from 0.5 to 18.5 minutes, with an overall mean duration of 4.5 minutes. Box widths are proportional to sample size. WWTPs refers to Wastewater Treatment Plants.

3.3.4 Measurement uncertainty and quality control

Measurement uncertainty was incorporated into quantified emissions by propagating the standard error of key input parameters, including CH_4 mixing ratios, wind speed, wind direction, temperature, pressure, distance from source to sensor, and atmospheric stability (±1 Pasquill–Gifford stability class, PGSC). To evaluate the impact of input variability on modeled emissions, input data were modeled in WindTrax in three cases (Table 3).

Table 3. Modeled uncertainty cases used in WindTrax simulations

Uncertainty case	Description	Input treatment

Case 1 – minimum	Represents lower bound of input variability	Mean (CH_4 mixing ratios, wind speed, wind direction, temperature, pressure, distance) − standard error; mean PGSC − 1 stability class
Case 2 – average	Represents nominal input configuration	Mean (CH_4 mixing ratios, wind speed, wind direction, temperature, pressure, distance); mean PGSC
Case 3 - maximum	Represents upper bound of input variability	Mean (CH_4 mixing ratios, wind speed, wind direction, temperature, pressure, distance) + standard error; mean PGSC + 1 stability class

For quality control, modeled emission rates were excluded if the relative standard deviation of CH_4 (standard deviation/mean) exceeded 30% or if the footprint fraction (fraction of source area covered by touchdowns) was < 0.5%. Touchdowns refer to the locations where back-trajectories from the sensor intersect the ground surface within the defined source polygon, representing the area contributing to the measured concentration. The 0.5% threshold ensures that there are enough touchdowns within the source polygon to provide a reliable estimate of emissions. These filters ensured that only emission rates representative of the source were retained for analysis. After applying filters, 94.1% of CAFOs, 99% of landfills, 99% of WWTPs, and 88% of lakes and reservoirs emission rates were retained for analysis.

3.3.5 Measurement inventory development

3.3.5.1 Emission factors and activity factors

Emission rates (kg h^{-1}) from WindTrax for the three uncertainty cases were divided by activity factors to generate emission factors (EFs). An activity factor is a metric that quantifies the

magnitude of the activity that is responsible for emissions. It links measured emissions to the operational scale. Activity factors were obtained from the following sources: CDPHE (2025) unpublished dataset for CAFOs and WWTPs, the EPA Landfill Methane Outreach Program (LMOP) 2024 data for landfills (US EPA, 2025b), and the Colorado Wetland Information Center for lakes and reservoirs (Colorado State University, 2025f). For CAFOs, the activity factor was the total animal units, defined by CDPHE as the permitted maximum headcount converted to a standardized unit that accounts for differences in animal mass when multiple species are present at a facility (CDPHE, 2025c; Meehan et al., 2018). The category group for CAFOs was based on the primary livestock in the facility. For landfills, the activity factor was the total waste in place (tons), based on the 2022 waste-in-place dataset (US EPA, 2025b). For wastewater treatment plants, the activity factor was the influent flow in million gallons per day (MGD^{-1}), obtained from unpublished CDPHE data (CDPHE, 2025c). For lakes and reservoirs, the activity factor was the surface area (m^2), derived from Google Maps imagery (Google, 2025) and the Colorado Wetland Information Center (Colorado State University, 2025f). To include the effect of activity factor variability on total emissions, and in the absence of explicit variability data, a default uncertainty of ±10% was applied to activity data.

3.3.5.2 Measurement inventory calculation

The EFs from the three uncertainty cases, across all facilities, were aggregated to generate emissions distributions for each source category. Because individual facilities were measured at different times of day, aggregating all EFs within each category—cattle, dairy, and sheep for CAFOs; open and closed landfills; wastewater treatment plants; and lakes and reservoirs—helped reduce temporal bias associated with the timing of measurements. For each category, a total of 1 million Monte Carlo iterations were performed. This large number of iterations ensured stable

estimates, and computational times for this study were not excessive. In each iteration, a bootstrap sample of the aggregated EFs, drawn with replacement, was used to compute a probabilistic estimate of the mean EF. The bootstrap values were binned using logarithmic binning to handle skewed distributions (Milojević, 2010), and the probability of each bin was computed. The Monte Carlo iteration then calculated a weighted average of the binned emission factors using the bin probabilities, generating a distribution of possible mean EFs that reflects the underlying measurement variability. This approach, similar to Lee et al. (2020), is a form of temporal and spatial extrapolation that captures the variability between facilities, extrapolation of snapshot measurements using probability of each emission event, and uncertainty arising from individual measurements, the inventory of activity factors, and temporal and spatial extrapolation. From the resulting Monte Carlo distribution, the mean and 95% confidence intervals (2.5th and 97.5th percentiles) were extracted, providing robust estimates of EFs for each source category. To generate annual estimates, EFs were multiplied by activity factors and 8760 hours.

3.3.5.3 Comparison to existing inventories and measurement studies

Concentrated animal feeding operations (CAFOs)

This study's CAFOs EFs and inventory estimates differ fundamentally from existing bottom-up inventories. Our approach measures facility-level emissions, which inherently integrate both enteric fermentation and manure management contributions within the facility footprint. In contrast, the EPA (US EPA, 2025c) methodologies allocate emissions separately to enteric and manure pathways for each livestock category. Another key distinction lies in how livestock populations are represented: while bottom-up inventories apply species-specific EFs (e.g., dairy versus beef cattle), our study normalizes emissions using animal units (AUs) derived from CDPHE's permitted headcount data. This approach accounts for mixed-species facilities by

standardizing emissions across livestock mass, with facilities categorized by their primary livestock type (CDPHE, 2025c; Meehan et al., 2018). Although this prevents direct one-to-one comparisons with species-specific inventory values, it captures the real-world, net emissions of entire facilities. This integrated perspective reflects both interspecies variability and management practices (e.g., manure handling, feed composition, housing design), factors that are difficult to incorporate into species-specific bottom-up methods. As such, the animal unit-based approach provides a complementary, measurement-informed perspective on agricultural CH_4 sources.

In this study, we compared our CAFOs EFs to EPA EFs from the 2022 Colorado State inventory tool (US EPA, 2025c) and a previous measurement study in the same DJ region (Riddick et al., 2022b). Because our measurement data were normalized by animal units, we represented 'Dairy' primary livestock using the dairy cow EF, 'Cattle' primary livestock using the beef cattle EF, and 'Sheep' using the "sheep on feed" EF from the State Inventory tool. For enteric fermentation emissions, we used the 2022 default EF, and for manure management emissions, we divided the provided total CH_4 emissions by the total number of animals in the tool. We then summed up enteric and manure management EFs to generate a single EF in comparison with our study. Emission factors reported by Riddick et al. (2022) were measured at the facility level and already normalized by animal units, so they were used directly.

Municipal solid waste landfills

Municipal solid waste landfills were compared against the annual emissions that each facility reported to the EPA through the 2023 Greenhouse Gas Reporting Program (GHGRP; US EPA, 2023) using the Facility Level Information on Greenhouse Gases Tool (FLIGHT). These emissions are reported under Subpart HH and are calculated using two methods: Equation HH-6, which estimates CH_4 emissions based on modeled CH_4 generation rates and other site-specific

factors; and Equation HH-8, which estimates emissions based on the measured quantity of CH_4 recovered for destruction along with an assumed landfill gas collection efficiency (Electronic Greenhouse Gas Reporting Tool, n.d.). For this analysis, facilities were categorized as either "Open" or "Closed," and both the measured data from this study and the reported annual emissions were aggregated within each category. Reported CH_4 emissions were converted from CO_2-equivalent values using a global warming potential (GWP) of 28 (US EPA, 2016).

Wastewater treatment plants

Wastewater treatment plant emissions were compared to the measurement-based study by Song et al. (2023). The EFs initially calculated in units of kg CH_4 h^{-1} per million gallons per day (MGD) of influent were converted to grams per cubic meter (g m^{-3}) of wastewater to standardize emissions relative to wastewater volume. This was done by multiplying the EF by 1000 to convert kilograms to grams and then dividing by the equivalent flow in cubic meters per hour for 1 MGD (157.7254 m^3 h^{-1}). Song et al. (2023) reported an average EF of 12.5 (7.9–17.2) g CH_4 m^{-3} for plants with anaerobic digesters and 12.9 (7.5–18.2) g CH_4 m^{-3} for plants without anaerobic digesters. Because our study did not disaggregate EFs by digester type, and the two Song et al. (2023) categories EFs are almost similar, we take the simple average of those values to obtain 12.7 (7.7–17.7) g CH_4 m^{-3}. EPA's wastewater methodology calculates emissions from influent flow, biogas generation, and the destruction efficiency of devices that burn biogas (US EPA, 2022b), information we did not have for our sites. Song et al. (2023) reports that their measurement-based EFs are approximately twice the EPA values; using that relationship we therefore estimate an EPA-based EF of 6.4 (3.9–8.9) g CH_4 m^{-3} for comparison.

Lakes and reservoirs

Methane emissions from lakes and reservoirs were evaluated against EFs reported by the Intergovernmental Panel on Climate Change (IPCC) in the U.S. EPA *Inventory of Greenhouse Gas Emissions and Sinks* (US EPA, 2022b) and those derived by Riddick et al. (2022). The IPCC distinguishes between Reservoirs and Other Constructed Waterbodies (Freshwater Ponds). As the study area spans both *Cool Temperate* and *Warm Temperate Dry* climate zones as defined in the U.S. EPA *Inventory of Greenhouse Gas Emissions and Sinks* (US EPA, 2022b) Reservoir section, we applied surface EFs from both categories. The Colorado Wetland Inventory (Colorado State University, 2025f) used in this study to generate total surface area does not resolve the relative proportions of lakes versus reservoirs. As a result, we generated a Monte Carlo distribution of aggregated EFs using equal weights of 0.054 MT CH_4 ha^{-1} yr^{-1} (*Cool Temperate Reservoir*), 0.0803 MT CH_4 ha^{-1} yr^{-1} (*Warm Temperate Dry Reservoir*), and 0.183 MT CH_4 ha^{-1} yr^{-1} (*Freshwater Ponds*). For comparison with measurement-based estimates, we applied the EF reported by Riddick et al. (2022) of 0.015 g CH_4 m^{-2} h^{-1}.

3.4 Results

3.4.1 Concentrated animal feeding operations

This study's emission factors (EFs) and inventory estimates aligned with those from the EPA's 2022 Colorado State Inventory Tool (US EPA, 2025c) within uncertainty, particularly for dairy farms where the average annual emissions were identical. The annualized measured EFs in this study were 0.023 kg CH_4 h^{-1} per dairy unit, 0.010 kg CH_4 h^{-1} per cattle unit, and 0.001 kg CH_4 h^{-1} per sheep unit (Figure 16). For comparison, the EPA EFs were 0.023 kg CH_4 h^{-1} per dairy head, 0.012 kg CH_4 h^{-1} per cattle head, and 0.001 kg CH_4 h^{-1} per sheep head, while Riddick et al. (2022)

reported 0.031 kg CH_4 h^{-1} per dairy head, 0.005 kg CH_4 h^{-1} per cattle head, and 0.001 kg CH_4 h^{-1} per sheep head.

Seasonally, no consistent pattern was observed, though dairy showed the highest EFs in winter and summer (0.03 kg CH_4 h^{-1} per dairy unit) and the lowest in fall (0.02 kg CH_4 h^{-1} per dairy unit). Compared with Riddick et al. (2022), which used a similar approach during summer 2021, this study's summer dairy EF (0.03 kg CH_4 h^{-1} per dairy unit) was identical, while the summer cattle EF (0.009 kg CH_4 h^{-1} per cattle unit) was higher than Riddick et al. (2022)'s value (0.005 kg CH_4 h^{-1}). For sheep, this study reported a summer EF of 0.002 kg CH_4 h^{-1} per sheep head, slightly higher than Riddick et al. (2022)'s 0.001 kg CH_4 h^{-1} per sheep head (Figure 16).

Unlike Riddick et al. (2022) which derived EFs from summer-only measurements, this study captured data throughout the year, resulting in a more temporally comprehensive dataset aligned with the EPA's annualized EFs. The corresponding annualized emission estimates were 59 Gg CH_4 for dairy, 36 Gg CH_4 for cattle, and 0.4 Gg CH_4 for sheep, compared with EPA's 58 Gg, 44 Gg, and 0.3 Gg, respectively. Using Riddick et al. (2022)'s EFs, estimated emissions were 78 Gg CH_4 for dairy, 20 Gg CH_4 for cattle, and 0.3 Gg CH_4 for sheep (Figure 16).

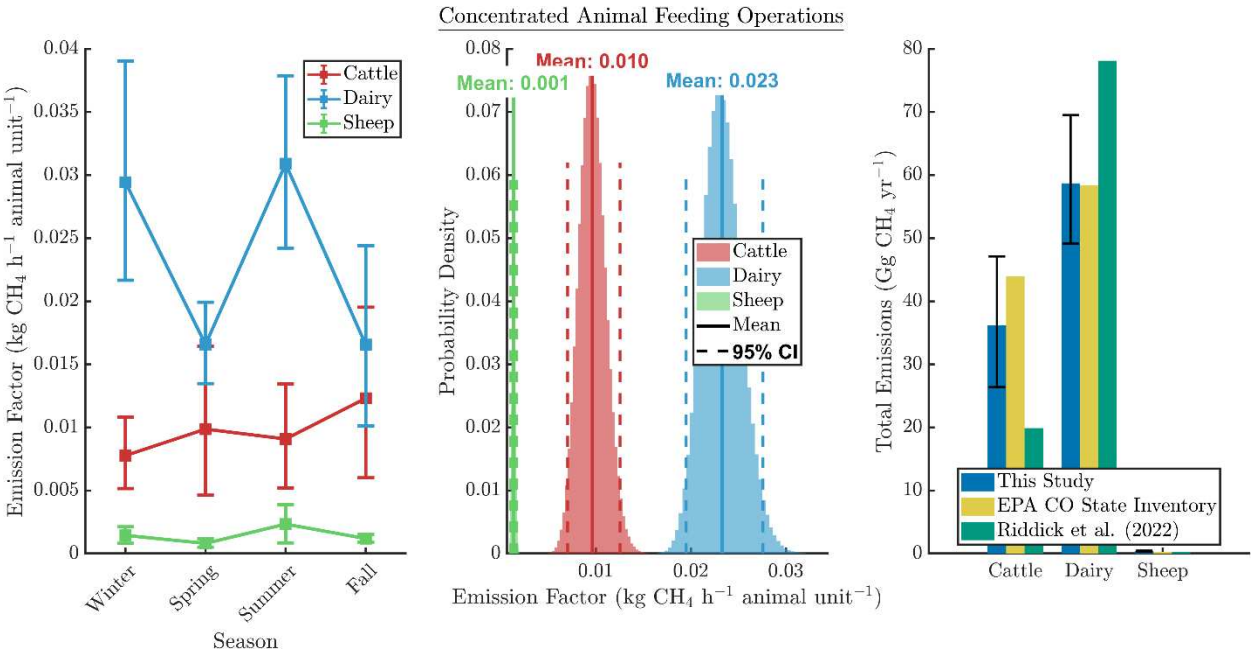

Figure 16. Left Plot: A plot showing the average emission factors for each season based on Monte Carlo simulations. Middle Plot: Probability distribution plots showing the annualized emission factor distribution based on Monte Carlo simulations. Right plot: A bar plot showing annualized CH_4 estimates of CAFOs based on this study's measurements, the EPA inventory of Colorado and Riddick et al. (2022) measurement study.

3.4.2 Municipal solid waste landfills

This study's annualized landfill emissions were consistent with EPA estimates within uncertainty, at 13 Gg CH_4 for open landfills and 1 Gg CH_4 for closed landfills (Figure 17). At the individual facility level, reported emissions differed slightly from those calculated using measured data; however, when aggregated across all facilities in the study area, the measured emissions closely aligned with EPA's reported values. This finding demonstrates that aggregated measurement-based data can provide representative emission estimates at regional or basin scales.

The EFs derived in this study were 0.005 g CH_4 h^{-1} ton^{-1} waste for closed landfills and 0.033 g CH_4 h^{-1} ton^{-1} waste for open landfills. Open landfills exhibited substantially greater variability in EFs compared to closed sites. This variability likely reflects differences in ongoing waste deposition, daily and intermediate cover practices, gas collection system efficiency, and other site-specific operational conditions. In contrast, closed landfills tend to show more uniform emissions due to stabilized waste and consistent management practices. The measured dataset included four landfills, whereas EPA's reported data covered three. One closed landfill did not report emissions to the EPA for valid reasons (US EPA, 2023b) however, its contribution to total emissions, based on measured data, was minimal (Figure 17).

Seasonal analysis showed that EFs for both open and closed landfills were highest in winter and lowest in summer, even though winter included the largest number of measurements. For open landfills, the seasonal EFs were 0.051, 0.018, 0.012, and 0.022 g CH_4 h^{-1} ton^{-1} waste for winter, spring, summer, and fall, respectively. For closed landfills, the corresponding EFs were 0.007, 0.0002, and 0.007 g CH_4 h^{-1} ton^{-1} waste for winter, spring, and fall, respectively; no valid summer measurements were available (Figure 17).

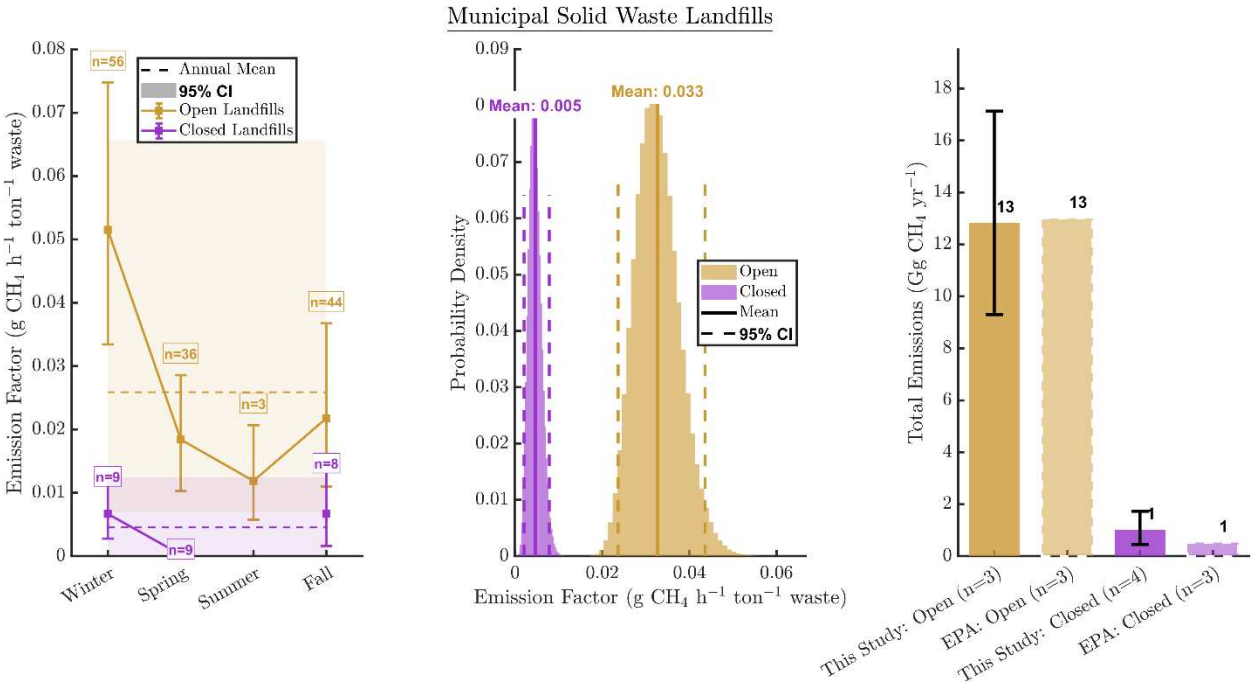

Figure 17. Left Plot: A plot showing the average emission factors for each season based on Monte Carlo simulations. Middle Plot: Probability distribution plots showing the annualized emission factor distribution based on Monte Carlo simulations. Right plot: A bar plot showing annualized CH_4 estimates of municipal solid waste landfills based on this study's measurements.

3.4.3 Wastewater treatment plants

This study's annualized methane emissions from wastewater treatment plants (WWTPs) were consistent with EPA estimates within uncertainty (Figure 18). The estimated average annual emissions were 1.3 Gg CH_4, compared with 1.6 Gg CH_4 based on EPA-equivalent emission factors and 3.1 Gg CH_4 using Song et al. (2023)'s EFs. These results mirror the pattern observed for landfills and CAFOs, where the annual emissions derived in this study also aligned closely with EPA's calculation-based estimates within uncertainty. The average wastewater treatment EF estimated in this study was 5.3 g CH_4 m^{-3}, representing CH_4 emitted per cubic meter of wastewater treated. No clear seasonal pattern was observed. Seasonal EFs were 5.3, 6.7, and 2.5 g CH_4 m^{-3} for winter, spring, and fall, respectively; no valid summer measurements were available (Figure 18).

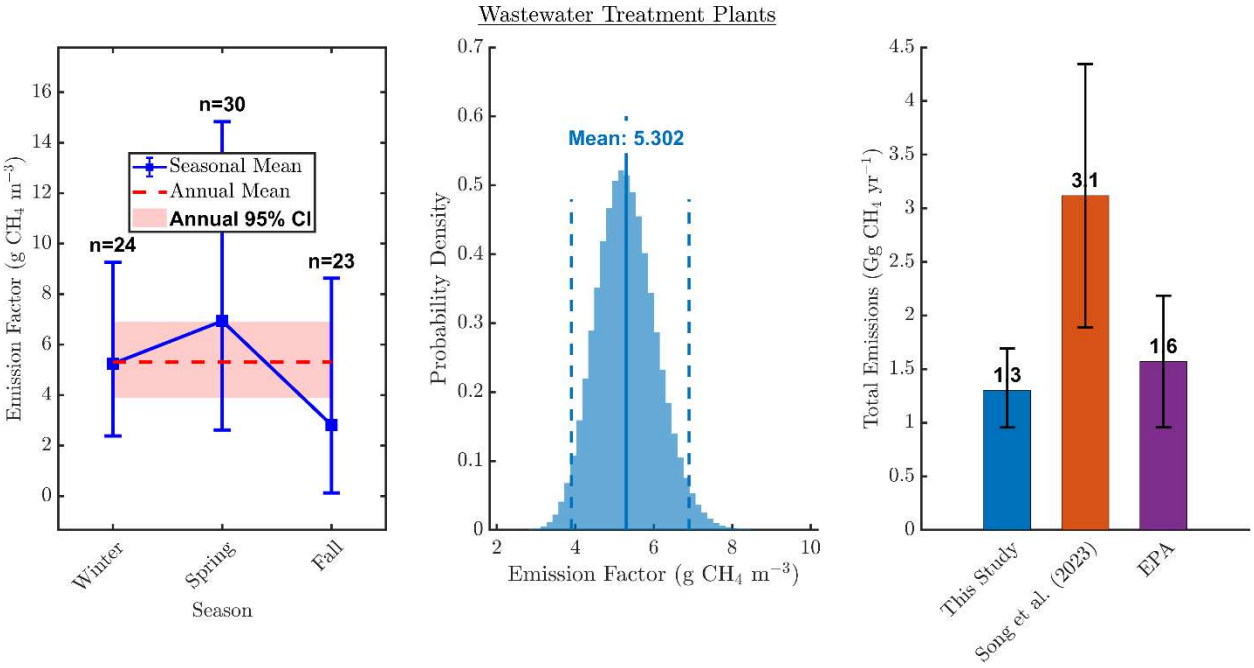

Figure 18. Left Plot: A plot showing the average emission factors for each season based on Monte Carlo simulations. Middle Plot: Probability distribution plots showing the annualized emission factor distribution based on Monte Carlo simulations. Right plot: A bar plot showing annualized CH_4 estimates of wastewater treatment plants based on this study's measurements.

3.4.4 Lakes and reservoirs

This study's annualized CH_4 emissions from lakes and reservoirs were higher than those calculated using IPCC EFs (US EPA, 2022b) but lower than those estimated using Riddick et al. (2022)'s EF (Figure 19). Although Riddick et al. (2022)'s measurements were conducted during summer, their relatively high EF, consistent with this study's findings, suggests that IPCC EFs may underestimate CH_4 emissions from lakes and reservoirs. The seasonal EFs estimated in this study were 0.006, 0.012, and 0.013 g CH_4 m^{-2} h^{-1} for winter, spring, and fall, respectively; no valid summer measurements were available. The lowest EF occurred in winter. This seasonal pattern is consistent with previous studies; for example, Skwierawski (2024) reported seasonal averages of 3.2, 12.1, 20.6, and 14.9 mg CH_4 m^{-2} d^{-1} for winter, spring, summer, and autumn, respectively, based on four years of measurements at Lake Kortowskie, Poland. The average annual emissions estimated in this study were 12.7 Gg CH_4, compared with 1.5 Gg CH_4 based on IPCC EFs and 18.1 Gg CH_4 using Riddick et al. (2022)'s (Figure 19). These results emphasize the importance of continuous, year-round measurement campaigns that capture both temporal (seasonal) and spatial variability to refine emission factor estimates and improve the accuracy of regional methane inventories.

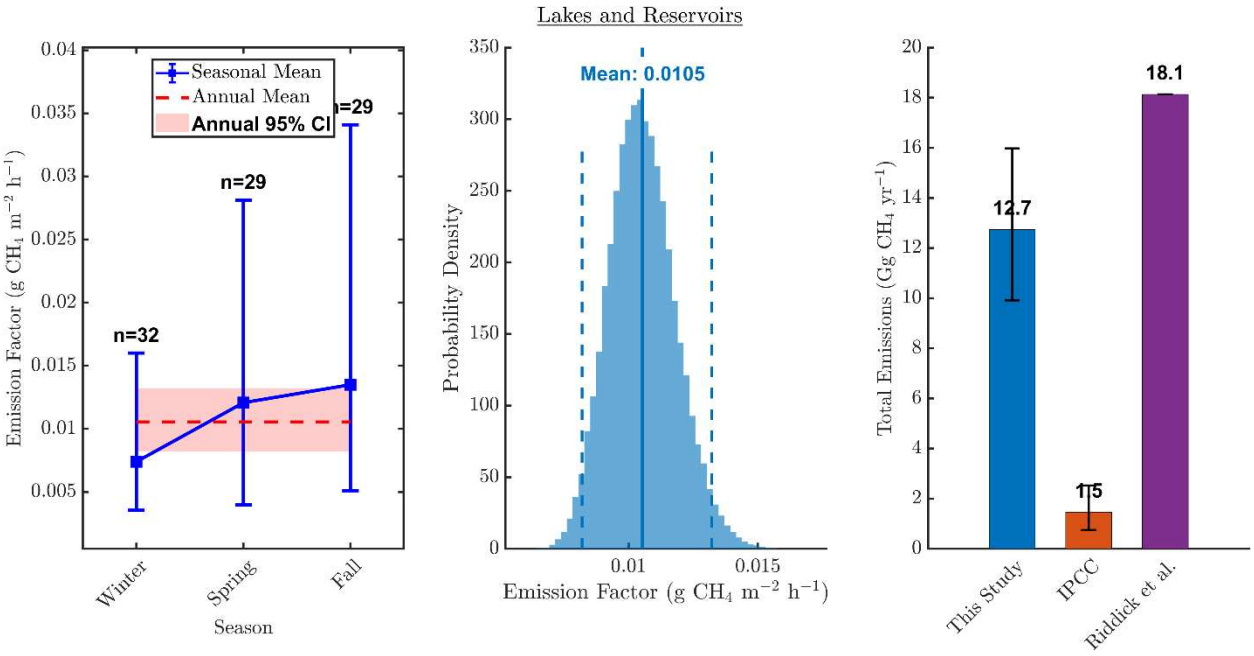

Figure 19. Left Plot: A plot showing the average emission factors for each season based on Monte Carlo simulations. Middle Plot: Probability distribution plots showing the annualized emission factor distribution based on Monte Carlo simulations. Right plot: A bar plot showing annualized CH_4 estimates of lakes and reservoirs based on this study's measurements, IPCC emission factors (Riddick et al., 2022b) measurement study.

3.4.5 Non-OG inventory and reconciliation

We estimate total annual emissions of 123 ± 21 Gg y^{-1}, compared to the EPA estimate of 119 Gg y^{-1} (Figure 20). This study's annualized inventory agrees with the EPA-calculated bottom-up inventory within uncertainty, demonstrating that reconciliation between bottom-up inventories and measurement-based approaches is possible when measurements adequately capture temporal and spatial variability and are appropriately extrapolated to annual emissions. Aggregated CH_4 emissions from CAFOs, municipal solid waste landfills, wastewater treatment plants, and lakes/reservoirs indicate that CAFOs are the dominant source of CH_4 in the DJ region, contributing 78% using this study's EFs and 87% using EPA EFs (Figure 20). Municipal solid waste landfills contribute 11% based on both this study and EPA's EFs, while wastewater treatment plants represent the smallest source at 1% (Figure 20).

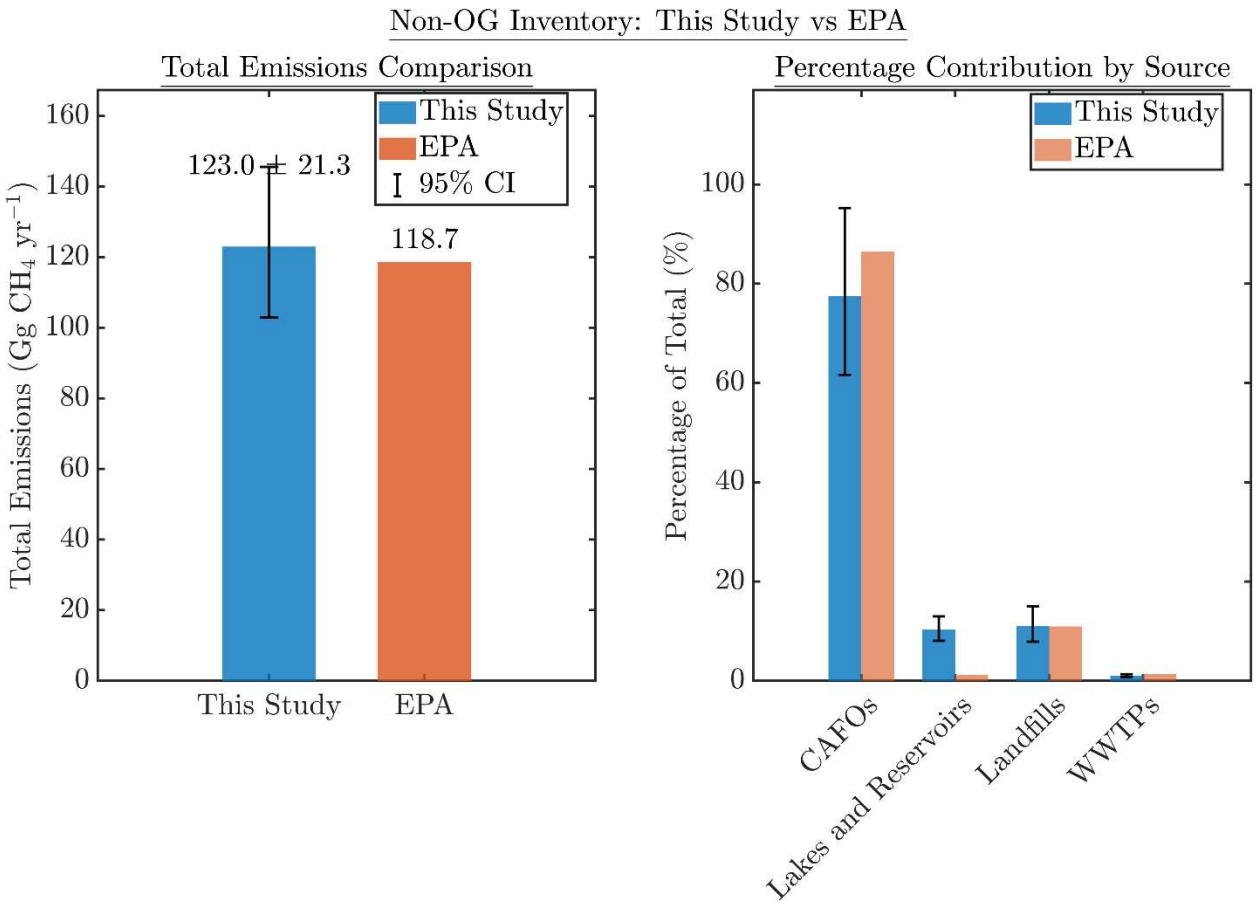

Figure 20. Left: Annualized total CH_4 emissions from this study compared emission estimate calculated using EPA emission factors. Right: Annualized emissions by percentage contribution from each source category. EPA error bars are not shown because some source categories lacked reported uncertainty, preventing aggregation of overall uncertainty.

3.5 Discussion

This study demonstrates that measurement-based methane emission factors (EFs) and annualized emission estimates across major anthropogenic and natural sectors in Colorado's portion of the DJ Basin generally agree with EPA inventory estimates within uncertainty, while revealing key sector-specific differences. The alignment between measured and inventory-derived emissions for CAFOs, landfills, and wastewater treatment plants (WWTPs) suggests that EPA methodologies provide reasonable regional estimates when averaged across multiple facilities.

However, the observed variability between facilities highlights the importance of incorporating direct measurements to refine emission factors and reduce uncertainty.

3.5.1 Concentrated animal feeding operations (CAFOs)

For CAFOs, the measured CH_4 EFs were consistent with EPA inventory values within uncertainty, indicating good agreement between measurement-based and inventory-derived estimates. The absence of a strong seasonal pattern suggests that representative measurements taken at any time of year can yield reliable annual emission estimates. The close alignment between this study's annual emissions (59, 36, and 0.4 Gg CH_4 for dairy, cattle, and sheep, respectively) and EPA estimates (58 Gg, 44 Gg, and 0.3 Gg CH_4 for dairy, cattle, and sheep, respectively) underscores the robustness of the EPA framework while validating the utility of year-round, ground-based measurement campaigns for characterizing agricultural CH_4 emissions.

EPA's EFs for enteric fermentation and manure management, as implemented in the State Inventory Tool (SIT), are derived from the same methodological framework as the National Greenhouse Gas Inventory (GHGI) but are downscaled to the state level. The EPA employs a process-based Tier 2 (IPCC, 2006a) energy balance model, rather than relying on empirical constants. Each emission factor represents the annual CH_4 output per animal, estimated from feed intake, digestion characteristics, and energy requirements (US EPA, 2023c). For enteric fermentation, the Cattle Enteric Fermentation Model (CEFM), a lifecycle model, accounts for animal demographics (age, sex, and weight), physiological status (growth, lactation, or pregnancy), and diet composition (forage-to-grain ratio, feed digestibility, and regional feed types) to determine the CH_4 conversion rate. For manure management, emissions are calculated from the volatile solids excretion rate, the maximum CH_4-producing capacity (B_0) of the manure, and the

CH_4 conversion factor (MCF), which reflects the proportion of manure handled in various management systems and state-specific climatic conditions (US EPA, 2023c).

The agreement between this study's measurement-based estimates and EPA's modeled factors confirms that EPA's bottom-up, process-driven approach effectively captures the dominant drivers of CH_4 generation in Colorado livestock systems, providing confidence in the accuracy and transferability of both measurement and inventory approaches.

3.5.2 Municipal solid waste landfills

For landfills, measurement-derived emissions (13 Gg CH_4 for open and 1 Gg CH_4 for closed sites) closely matched EPA-reported values. However, substantial variability in EFs among open landfills indicates that operational factors such as cover integrity, waste age, and gas collection efficiency strongly influence CH_4 release. The higher winter EFs, observed despite greater sampling frequency, suggest that cold-season meteorological conditions may enhance CH_4 accumulation or inhibit oxidation within landfill covers.

The U.S. EPA estimates CH_4 emissions from municipal solid waste landfills using a first-order decay (FOD) model consistent with the (IPCC, 2006b) framework but adapted for U.S. conditions in the Greenhouse Gas Inventory and Greenhouse Gas Reporting Program (40 CFR Part 98, Subpart HH) (US EPA, 2025d). In this process-based model, CH_4 generation depends on the mass of waste deposited each year and key parameters characterizing waste decomposition dynamics. These include the quantity of waste disposed (W_x), the degradable organic carbon (DOC) content, the fraction of DOC dissimilated (DOC_F), the CH_4 correction factor (MCF) accounting for aerobic versus anaerobic conditions, the CH_4 fraction (F) of landfill gas, and the decay rate constant (k), which varies with climate and waste composition. For landfills equipped with gas collection and control systems, additional parameters such as collection efficiency (CE),

destruction efficiency (DE), and oxidation factor (OX) are applied to account for CH_4 captured, destroyed, or oxidized within cover soils. Together, these inputs simulate CH_4 generation and recovery over time, yielding annual emission estimates that reflect both degradation kinetics and management practices. The close agreement between measurement-based and EPA-modeled emissions indicates that EPA's bottom-up, process-based emission factors are robust and representative of real-world landfill conditions.

3.5.3 Wastewater treatment plants

For wastewater treatment plants, measured EFs (5.3 g CH_4 m^{-3}) and annualized emissions (1.3 Gg CH_4) closely matched EPA estimates (1.6 Gg CH_4) but were lower than those derived using Song et al. (2023). The absence of clear seasonal patterns supports the use of consistent annual emission factors for inventory applications in temperate regions. EPA calculates CH_4 emissions from municipal and industrial wastewater using a process-based approach adapted from the (IPCC, 2006b) guidelines, in which emissions are determined from the biochemical oxygen demand (BOD) removed during treatment, the methane-producing potential of the organic matter (B_0), and the CH_4 correction factor (MCF) accounting for the fraction of BOD decomposed anaerobically (US EPA, 2025d). Additional CH_4 generation from sludge management including storage, dewatering, and land application is calculated based on volatile solids content, decay characteristics, and site-specific correction factors. The close agreement between measurement-based and EPA-modeled emissions demonstrates that the EPA EFs are robust and representative of real-world WWTP operations.

3.5.4 Lakes and reservoirs

Measured CH_4 emissions from lakes and reservoirs in this study (12.7 Gg CH_4 yr^{-1}) were substantially higher than estimates derived from IPCC default emission factors (1.5 Gg CH_4; US

EPA, 2022a) but lower than those based on Riddick et al. (2022) (18.1 Gg CH_4), reflecting the influence of regional environmental conditions on CH_4 production. The IPCC framework distinguishes between reservoirs and freshwater ponds, and in this study, a Monte Carlo approach was used to aggregate EFs across these categories due to uncertainty in the relative proportions of lakes versus reservoirs. The close alignment of seasonal EFs with expected patterns, lowest in winter (0.006 g CH_4 m^{-2} h^{-1}) and higher in spring–fall (0.012–0.013 g CH_4 m^{-2} h^{-1}) underscores the role of temperature, organic carbon availability, and thermal stratification in controlling CH_4 flux. The comparison with Riddick et al. (2022) further highlights that IPCC default factors likely underestimate emissions in semi-arid regions. Together, these findings demonstrate that measurement-based, region-specific emission factors are critical for improving the accuracy of CH_4 inventories from surface waters, and that year-round monitoring is necessary to capture temporal variability that may be missed when relying solely on global default factors.

3.6 Implications

In recent years, several studies have reported disagreements between measurement-based and bottom-up CH_4 emission inventories from both oil and gas and non-oil and gas sources. Most measurement-based studies rely on the ergodic assumption, in which sampling many sources at a given time is considered equivalent to observing a single source over an extended period to annualize emissions. This assumption implies that all emission events are captured during the snapshot measurement and that the emission distribution remains constant throughout the year. However, understanding how variability at the time of measurement compares to the full population over the year is critical when annualizing snapshot measurements and comparing them to bottom-up inventories. Bottom-up approaches, in contrast, employ detailed engineering calculations or source-level measurements based on scientific principles to predict emission

behavior throughout the year. If snapshot measurements are not correctly interpreted in terms of occurrence and frequency, extrapolated emissions can be inaccurate, leading to discrepancies with bottom-up estimates.

This study demonstrates that measuring a spatially distributed sample across different times of the year can mitigate temporal biases caused by seasonal variation, operational and management differences, diurnal variability, and uncertainties in measurement and quantification methods, particularly those influenced by environmental conditions. This variability is reflected in the wide distribution of Monte Carlo simulated emission factors shown in the results. Furthermore, this approach is especially valuable when access to all facilities for source attribution is limited. By sampling many facilities at multiple times, variability in emissions is minimized and normalized, resulting in more robust regional estimates. Finally, this study provides a weighted emission factor methodology for extrapolating snapshot measurements to annual emission estimates. This method, based on weighted probabilities, ensures that average emission factors from Monte Carlo simulations account for both the few large emission events that could otherwise skew estimates and the numerous smaller emissions that are often underestimated in averages.

Overall, the consistency of measurement-based emissions with EPA estimates across most sectors supports the validity of inventory methodologies but underscores the need for temporally resolved measurements to better capture intra-annual variability. Sectors such as lakes and reservoirs, which are more sensitive to temperature and biogeochemical processes, may require region-specific EFs to improve inventory accuracy. These findings collectively demonstrate the value of integrated measurement–inventory frameworks, where snapshot measurement-based and bottom-up approaches are combined to reduce uncertainty and enhance the spatial and temporal representativeness of methane estimates. Such integration is critical for improving greenhouse gas

inventories and informing state and federal policy decisions under evolving methane monitoring and reporting programs.

CHAPTER 4: CONCLUSION

5.1 Research objectives and hypotheses

5.1.1 Objective 1: Evaluating the feasibility of using downwind methods to quantify point source oil and gas emissions using continuously monitoring fence-line sensors

This objective aimed to assess the quantification accuracy of the closed-path eddy covariance (EC), Gaussian plume inverse method (GPIM), and backward Lagrangian stochastic (bLs) models in controlled-release experiments simulating oil and gas emissions.

The closed-path EC system failed to provide valid flux estimates due to instrument and configuration limitations, including non-synchronous data logging, low sampling frequency, and a slow analyzer response. *Consequently, research hypotheses H1a and H1b for EC were rejected, as the system did not demonstrate a strong linear relationship ($R^2 \approx 0$) or consistent accuracy across emission types.*

For the GPIM, quantification accuracy varied widely with wind-sector and averaging configurations. The method showed moderate performance for single-release single-point (SRSP) tests (slopes between 1.65 and 3.92; R^2 up to 0.64) but poor correlations for multi-release single-point (MRSP) tests ($R^2 \approx 0$). *This partial performance indicates that research hypothesis H1a was not fully supported, though GPIM can be effective under optimal averaging (15-min, 5°) and open terrain. H1b was not supported since performance consistency across emission types was not maintained.*

The bLs model demonstrated the highest overall quantification accuracy among the tested methods. For SRSP conditions, bLs results approached unity slopes (1.05–1.10) and moderate R^2 values (0.37–0.66), meeting the expected linearity between estimated and true emissions.

However, performance degraded substantially under MRSP scenarios ($R^2 \approx 0$), reflecting the method's sensitivity to multi-source interference and complex flow. *Therefore, research hypothesis H1a was supported for SRSP conditions but rejected for MRSP, and H1b was not supported since performance consistency across emission types was not maintained.*

In summary, the bLs and GPIM methods are feasible for quantifying emissions from isolated point sources, particularly under steady winds and defined background conditions, while EC was unsuitable in the configuration tested. The findings highlight that method feasibility depends strongly on the experimental design, source complexity, and data quality assurance.

5.1.2 Objective 2: A comparison of bottom-up, measurement-based and EPA inventory methane emission estimates for non–oil and gas sources in the Denver–Julesburg basin, Colorado

This objective aimed to develop and compare a measurement-based CH_4 inventory for concentrated animal feeding operations (CAFOs), municipal solid waste (MSW) landfills, wastewater treatment plants (WWTPs), and lakes/reservoirs in the DJ Basin using both EPA and empirically derived emission factors (EFs), while assessing seasonal variability and consistency with existing inventories.

Measurement-based EFs for CAFOs, MSW landfills, and WWTPs agreed closely with EPA inventory values within uncertainty, confirming that EPA's bottom-up, process-based approach effectively represents CH_4 generation in these sectors. For CAFOs, the close correspondence between measured and EPA-estimated emissions (e.g., 59 vs. 58 Gg CH_4 yr^{-1} for dairy operations) validated the representativeness of both methodologies. Similarly, landfill emissions (13 Gg open, 1 Gg closed) and WWTP emissions (1.3 Gg vs. 1.6 Gg CH_4 yr^{-1}) were consistent with EPA estimates. In contrast, measured lake and reservoir emissions (12.7 Gg CH_4 yr^{-1}) exceeded IPCC default factors but aligned with regional studies, reflecting climatic and ecosystem variability in semi-arid environments. *Therefore, research hypothesis H2a was supported confirming that measurement-based EFs generally fall within the expected range of previous inventories.*

Seasonal analyses revealed source-specific variability. Landfills exhibited higher winter emissions consistent with reduced CH_4 oxidation, while lakes and reservoirs showed enhanced fluxes in warmer seasons due to temperature-driven stratification and microbial activity. Conversely, CAFOs and WWTPs displayed minimal or no seasonal dependence, suggesting stable emissions throughout the year. *Therefore, research hypothesis H2b was partially supported, and*

H02b was partially rejected, as seasonal variability was evident for landfills and lakes/reservoirs but not for CAFOs or WWTPs.

The resulting measurement-based inventory estimated total annual CH_4 emissions of 123 ± 21 Gg yr^{-1}, compared with 119 Gg yr^{-1} from the EPA inventory agreement within uncertainty that demonstrates reconciliation between measurement-based and bottom-up approaches when spatial and temporal variability are adequately represented. CAFOs were the dominant source category, contributing 78 % (this study) and 87 % (EPA) of total emissions, followed by landfills (11 %) and WWTPs (1 %). *Therefore, research hypothesis H2c was supported, and H02c was rejected, confirming that the measurement-based inventory aligns closely with EPA estimates in both magnitude and relative source contributions.*

In summary, Objective 2 demonstrated that measurement-based and EPA bottom-up inventories are largely consistent across major non-oil and gas CH_4 sources in the DJ Basin. While lakes and reservoirs exhibit higher region-specific emissions, and some sources show seasonal patterns, overall agreement within uncertainty supports the validity of both measurement-based and inventory methodologies for regional methane assessments.

5.2 Application of systems engineering to methane emissions

This dissertation applied systems engineering principles to methane emissions research by treating quantification, modeling, and inventory comparison as interconnected subsystems within a broader methane management framework. Objective 1 evaluated the feasibility of downwind quantification methods for oil and gas point sources, revealing that each modeling approach—EC, GPIM, and bLs—offered distinct advantages under specific atmospheric and operational conditions. This demonstrated that quantification accuracy depends not only on individual model performance but also on the integration of sensor placement, atmospheric data, and model assumptions—key systems engineering considerations for system reliability and optimization.

Objective 2 extended this systems view (i.e., understanding emissions collectively) to non–oil and gas sources by developing a measurement-based CH_4 inventory for CAFOs, landfills, wastewater treatment plants, and lakes/reservoirs in the DJ Basin. Comparing these results with EPA and empirical emission factors revealed that both emissions and emission factors vary across source types and seasons, reflecting inherent system complexity and dynamic behavior. The analysis highlighted the importance of harmonizing bottom-up and measurement-based data streams to improve regional and national methane budgets.

Together, these objectives demonstrate that methane quantification and mitigation are best addressed through a system-of-systems approach, in which diverse subsystems—oil and gas, waste, wastewater, and natural environments—are integrated through consistent data standards, model interoperability, and coordinated validation frameworks (e.g., OGMP reconciliation processes). This integrative perspective enables cross-domain learning, where validated approaches in one subsystem inform improvements in another, accelerating global progress toward methane reduction.

5.3 Research Contributions

1. **A comprehensive comparison of methods to quantify methane emissions using a controlled release oil and gas quantification study** – This research developed and published a systematic comparison of eddy covariance (EC), backward Lagrangian stochastic (bLs) modeling, and Gaussian plume inversion (GPIM) for quantifying methane emissions from oil and gas operations. By testing these methods under controlled-release single- and multi-point scenarios, the study identified the relative strengths and limitations of each approach, providing practical guidance on method selection and deployment in complex emission environments.
2. **Improved and evidence-based guidance on practical methane quantification** – Through a direct evaluation of multiple model's accuracy and application in controlled oil and gas settings, this research produced scientifically validated methodologies for estimating methane emissions at fence-line distances. The study highlighted the conditions under which each method performs optimally, demonstrated the impact of instrumentation and environmental factors on measurement uncertainty, and illustrated the trade-offs between temporal averaging, spatial coverage (wind sector), and operational complexity. These insights provide operators and researchers with practical guidance to improve monitoring strategies and reduce uncertainty in emission estimates.
3. **A field-data-based measurement methane inventory** – This research developed a detailed field-based measurement campaign to generate spatially and temporally resolved emission factors and methane inventories for concentrated animal feeding operations (CAFOs), municipal solid waste landfills, wastewater treatment plants, and freshwater sources in the Denver-Julesburg Basin. New emission factors derived from these measurements were applied to develop a measurement-based basin-level inventory, which was then compared to the EPA

inventory. The results identified CAFOs as the dominant non–oil and gas methane source, quantified sector-specific contributions, and highlighted seasonal and facility-level variability. This contribution provides both a benchmark for regional methane emissions and a methodological framework for extending measurement-based inventories to other sectors and regions.

4. **A field-based methodology for scaling snapshot measurements to annual scales for inventory comparisons** – This study presents a weighted emission factor methodology for extrapolating snapshot methane measurements to annual emission estimates. The method employs weighted probabilities within Monte Carlo simulations to ensure that the resulting average emission factors capture both high magnitude but infrequent emission events and numerous smaller releases that are typically underrepresented in unweighted averages. While the present analysis focuses on non–oil and gas sources, the extrapolation framework developed here is generalizable and can also be applied to oil and gas emission sources.

CHAPTER 5: RECOMMENDATIONS AND FUTURE WORK

This study faced two primary limitations that provide direction for future research and methodological improvement.

For Objective 1, the closed-path eddy covariance (EC) system failed to provide valid flux estimates due to instrumentation and configuration issues. In addition, the study design relied on a single sensor to evaluate model performance, whereas real-world continuous monitoring networks typically employ multiple sensors distributed around a site. Future work should therefore evaluate model performance under multi-sensor configurations and explore the use of optimization algorithms to improve quantification accuracy in complex oil and gas environments. Continuous monitoring systems remain highly valuable due to their ability to generate temporally resolved data across many sites, which—if quantification accuracy improves—could support both rapid leak detection and repair (LDAR) programs and site-level emission inventories. They also enable relatively fast reporting of equipment failures or abnormal emission events, enhancing operational response between inspection cycles. While most current systems have yet to achieve this capability, continuous monitoring technologies can capture short-duration and intermittent emissions that periodic surveys often miss, providing insights into temporal emission patterns, and linking observed emissions to operational or meteorological factors. If fully realized, these capabilities could improve the accuracy and representativeness of site- or basin-level inventories by reducing reliance on assumed temporal profiles and enabling more direct temporal scaling of emissions. Furthermore, continuous monitoring could support independent verification and transparent reporting of emissions, facilitate automated compliance tracking, and generate datasets suitable for integration with advanced analytics or predictive maintenance tools. Collectively, these

potential capabilities would reduce dependence on aerial or aircraft-based surveys that lack temporal resolution and often require assumptions that increase inventory uncertainty.

For Objective 2, the main limitation was the lack of direct facility access, which restricted detailed process-level characterization. For methane mitigation, the ultimate goal is to localize and reduce or eliminate emission sources. The non–oil and gas sector, however, remains less advanced than the oil and gas industry in source attribution and quantification, though both sectors continue to progress toward effective mitigation. Current EPA inventory equations appear broadly representative, yet this study demonstrated that measurement-based methods, particularly those incorporating weighted emission factors, can complement these inventories and track reduction progress without the need to develop entirely new tools. The weighted emission factor framework developed in this study enables the extrapolation of snapshot or campaign-based measurements to annual scales, addressing the imbalance between infrequent large emission events and numerous smaller, persistent sources that can bias simple averages. By integrating probabilistic weighting within Monte Carlo simulations, the approach provides more representative sector-level emission factors and helps to reconcile discrepancies between bottom-up inventories and measurement-based estimates.

The backward Lagrangian stochastic (bLs) model, used in both objectives, provides a flexible foundation—offering point-source configurations suitable for oil and gas sites and area-source configurations applicable to landfills, agricultural systems, and natural environments. When combined with weighted emission factors, such models can be adapted to reflect the temporal and spatial variability inherent in different source types, improving inventory fidelity and supporting targeted mitigation strategies. Future studies applying these and similar tools, calibrated for sector-

specific conditions, could significantly enhance methane quantification and accelerate progress toward verifiable emission reductions.

Finally, as emphasized in the integration between systems engineering and methane emissions, achieving meaningful reductions in the global atmospheric methane growth rate (currently ~21 Tg CH_4 yr^{-1}) requires integration across technologies, datasets, and teams. Methane monitoring remains costly—through platforms such as satellites, aerial surveys, continuous monitors, and advanced analytics—but effective reduction demands systematic tracking of progress across all sources and regions. While significant advances have been made in oil and gas mitigation, especially in North America, future efforts must assess the global value of expanding focus toward other methane sources and under-monitored regions. A coordinated, systems-based framework that integrates measurements, inventories, and reduction initiatives across domains is essential for achieving measurable and sustained global methane reduction.

REFERENCES

Abichou, T., Bel Hadj Ali, N., Amankwah, S., Green, R., Howarth, E.S., 2023. Using Ground- and Drone-Based Surface Emission Monitoring (SEM) Data to Locate and Infer Landfill Methane Emissions. Methane 2, 440–451. https://doi.org/10.3390/methane2040030

adaorah, 2024. Boeing Dreamliner Case Study: Impact of Poor Supply Chain Visibility and Collaboration. Multus Competentia Ltd. URL https://multuscompetentia.com/boeing-dreamliner-case-study-impact-of-poor-supply-chain-visibility-and-collaboration/ (accessed 9.19.25).

Allen, D.T., 2014. Methane emissions from natural gas production and use: reconciling bottom-up and top-down measurements. Curr. Opin. Chem. Eng. 5, 78–83. https://doi.org/10.1016/j.coche.2014.05.004

Barkley, Z., Davis, K., Miles, N., Richardson, S., Deng, A., Hmiel, B., Lyon, D., Lauvaux, T., 2023. Quantification of oil and gas methane emissions in the Delaware and Marcellus basins using a network of continuous tower-based measurements. Atmospheric Chem. Phys. 23, 6127–6144. https://doi.org/10.5194/acp-23-6127-2023

Barlaz, M.A., Chanton, J.P., Green, R.B., 2009. Controls on Landfill Gas Collection Efficiency: Instantaneous and Lifetime Performance. J. Air Waste Manag. Assoc. 59, 1399–1404. https://doi.org/10.3155/1047-3289.59.12.1399

Beaulieu, J.J., Waldo, S., Balz, D.A., Barnett, W., Hall, A., Platz, M.C., White, K.M., 2020. Methane and Carbon Dioxide Emissions From Reservoirs: Controls and Upscaling. J. Geophys. Res. Biogeosciences 125, e2019JG005474. https://doi.org/10.1029/2019JG005474

Beck, M.R., Thompson, L.R., Rowntree, J.E., Thompson, T.N., Koziel, J.A., Place, S.E., Stackhouse-Lawson, K.R., 2023. U.S. manure methane emissions represent a greater contributor to implied climate warming than enteric methane emissions using the global warming potential* methodology. Front. Sustain. Food Syst. 7, 1209541. https://doi.org/10.3389/fsufs.2023.1209541

Bell, C., Ilonze, C., Duggan, A., Zimmerle, D., 2023. Performance of Continuous Emission Monitoring Solutions under a Single-Blind Controlled Testing Protocol. Environ. Sci. Technol. 57, 5794–5805. https://doi.org/10.1021/acs.est.2c09235

Brown, J.A., Harrison, M.R., Rufael, T., Roman-White, S.A., Ross, G.B., George, F.C., Zimmerle, D., 2023. Informing Methane Emissions Inventories Using Facility Aerial Measurements at Midstream Natural Gas Facilities. Environ. Sci. Technol. 57, 14539–14547. https://doi.org/10.1021/acs.est.3c01321

Burba, G., 2013. Eddy Covariance Method for Scientific, Industrial, Agricultural, and Regulatory Applications. Li-COR Biogeosciences, Lincoln, NE.

Carbon Mapper, 2025. Carbon Mapper - Science & Technology [WWW Document]. URL https://carbonmapper.org/work/science (accessed 2.18.25).

Casal, J., 2008. Chapter 6 Atmospheric dispersion of toxic or flammable clouds, in: Industrial Safety Series. Elsevier, pp. 195–248. https://doi.org/10.1016/S0921-9110(08)80008-0

CDPHE, 2025a. Colorado takes action to further reduce methane emissions from oil and gas operations | Colorado Department of Public Health and Environment [WWW Document]. URL https://cdphe.colorado.gov/press-release/colorado-takes-action-to-further-reduce-methane-emissions-from-oil-and-gas-operations (accessed 10.15.25).

CDPHE, 2025b. Oil and Natural Gas Annual Emission Inventory Reporting | Colorado Department of Public Health and Environment [WWW Document]. URL https://cdphe.colorado.gov/ongaeir (accessed 10.15.25).

CDPHE, 2025c. Home | Colorado Department of Public Health and Environment [WWW Document]. URL https://cdphe.colorado.gov/ (accessed 3.5.25).

Chan, E., Vogel, F., Smyth, S., Barrigar, O., Ishizawa, M., Kim, J., Neish, M., Chan, D., Worthy, D.E.J., 2024. Hybrid bottom-up and top-down framework resolves discrepancies in Canada's oil and gas methane inventories. Commun. Earth Environ. 5, 566. https://doi.org/10.1038/s43247-024-01728-6

Colorado State University, 2025a. METEC | Colorado State University [WWW Document]. URL https://metec.colostate.edu/ (accessed 2.18.25).

Colorado State University, 2025b. Advancing Development of Emissions Detection (ADED).

Colorado State University, 2025c. Methane | AgNext | Colorado State University [WWW Document]. URL https://agnext.colostate.edu/methane/ (accessed 9.4.25).

Colorado State University, 2025d. Site-Aerial-Basin Emissions Reconciliation (SABER) [WWW Document]. URL https://metec.colostate.edu/site-aerial-basin-emissions-reconciliation-saber/

Colorado State University, 2025e. Using Prototypical Sites to Model Methane Emissions in Colorado's Denver-Julesburg Basin Using the Mechanistic Air Emissions Simulator (MAES) [WWW Document].

Colorado State University, 2025f. Colorado Wetland Inventory [WWW Document]. URL https://csurams.maps.arcgis.com/apps/webappviewer/index.html?id=a8e43760cb934a5084e89e46922580cc (accessed 9.8.25).

Conrad, B.M., Tyner, D.R., Johnson, M.R., 2023. Robust probabilities of detection and quantification uncertainty for aerial methane detection: Examples for three airborne technologies. Remote Sens. Environ. 288, 113499. https://doi.org/10.1016/j.rse.2023.113499

Crenna, B., 2006. An introduction to WindTrax.

Cusworth, D.H., Duren, R.M., Ayasse, A.K., Jiorle, R., Howell, K., Aubrey, A., Green, R.O., Eastwood, M.L., Chapman, J.W., Thorpe, A.K., Heckler, J., Asner, G.P., Smith, M.L., Thoma, E., Krause, M.J., Heins, D., Thorneloe, S., 2024. Quantifying methane emissions from United States landfills. Science 383, 1499–1504. https://doi.org/10.1126/science.adi7735

Czepiel, P.M., Shorter, J.H., Mosher, B., Allwine, E., McManus, J.B., Harriss, R.C., Kolb, C.E., Lamb, B.K., 2003. The influence of atmospheric pressure on landfill methane emissions. Waste Manag. 23, 593–598. https://doi.org/10.1016/S0956-053X(03)00103-X

Day, R.E., Emerson, E., Bell, C., Zimmerle, D., 2024. Point Sensor Networks Struggle to Detect and Quantify Short Controlled Releases at Oil and Gas Sites. Sensors 24, 2419. https://doi.org/10.3390/s24082419

Dillon, J.A., Stackhouse-Lawson, K.R., Thoma, G.J., Gunter, S.A., Rotz, C.A., Kebreab, E., Riley, D.G., Tedeschi, L.O., Villalba, J., Mitloehner, F., Hristov, A.N., Archibeque, S.L., Ritten, J.P., Mueller, N.D., 2021. Current state of enteric methane and the carbon footprint of beef and dairy cattle in the United States. Anim. Front. 11, 57–68. https://doi.org/10.1093/af/vfab043

Dumortier, P., Aubinet, M., Lebeau, F., Naiken, A., Heinesch, B., 2019. Point source emission estimation using eddy covariance: Validation using an artificial source experiment. Agric. For. Meteorol. 266–267, 148–156. https://doi.org/10.1016/j.agrformet.2018.12.012

EPA, O., 2023. Subpart W – Petroleum and Natural Gas Systems [WWW Document]. URL https://www.epa.gov/ghgreporting/subpart-w-petroleum-and-natural-gas-systems (accessed 10.23.23).

EU, 2024. Reducing methane emissions in the energy sector | EUR-Lex [WWW Document]. URL https://eur-lex.europa.eu/EN/legal-content/summary/reducing-methane-emissions-in-the-energy-sector.html (accessed 10.15.25).

FluxLab, 2025. Landfills – FluxLab. URL https://fluxlab.ca/landfill/ (accessed 9.5.25).

Foken, Th., Wichura, B., 1996. Tools for quality assessment of surface-based flux measurements. Agric. For. Meteorol. 78, 83–105. https://doi.org/10.1016/0168-1923(95)02248-1

Foster-Wittig, T.A., Thoma, E.D., Albertson, J.D., 2015. Estimation of point source fugitive emission rates from a single sensor time series: A conditionally-sampled Gaussian plume reconstruction. Atmos. Environ. 115, 101–109. https://doi.org/10.1016/j.atmosenv.2015.05.042

Fratini, G., Ibrom, A., Arriga, N., Burba, G., Papale, D., 2012. Relative humidity effects on water vapour fluxes measured with closed-path eddy-covariance systems with short sampling lines. Agric. For. Meteorol. 165, 53–63. https://doi.org/10.1016/j.agrformet.2012.05.018

Global Methane Initiative, 2004. GMI Strategic Partners for International Collaboration | Global Methane Initiative [WWW Document]. URL

https://www.globalmethane.org/(S(4sfyfl5j3nlrzhlat2c0nmac))/collaboration/index.aspx (accessed 9.4.25).

Google, 2025. Google Maps [WWW Document]. Google Maps. URL https://www.google.com/maps (accessed 9.8.25).

Herrick, J., 2019. Oil and gas regulators to decide whether to make maps of flow lines public. Colo. Indep. URL https://www.coloradoindependent.com/2019/11/20/oil-gas-regulators-flowlines-map/ (accessed 10.15.25).

Horst, T.W., Lenschow, D.H., 2009. Attenuation of Scalar Fluxes Measured with Spatially-displaced Sensors. Bound.-Layer Meteorol. 130, 275–300. https://doi.org/10.1007/s10546-008-9348-0

Hsieh, C.-I., Katul, G., Chi, T., 2000. An approximate analytical model for footprint estimation of scalar fluxes in thermally stratified atmospheric flows. Adv. Water Resour. 23, 765–772. https://doi.org/10.1016/S0309-1708(99)00042-1

Hutchinson, M., Oh, H., Chen, W.-H., 2017. A review of source term estimation methods for atmospheric dispersion events using static or mobile sensors. Inf. Fusion 36, 130–148. https://doi.org/10.1016/j.inffus.2016.11.010

Ilonze, C., Emerson, E., Duggan, A., Zimmerle, D., 2024. Assessing the Progress of the Performance of Continuous Monitoring Solutions under a Single-Blind Controlled Testing Protocol. Environ. Sci. Technol. 58, 10941–10955. https://doi.org/10.1021/acs.est.3c08511

INCOSE, 2025. Systems Engineering Definition [WWW Document]. INCOSE. URL https://www.incose.org/about-systems-engineering/system-and-se-definitions/systems-engineering-definition (accessed 10.27.25).

IPCC, 2006a. Chapter 10: Emissions from Livestock and Manure Management. In 2006 IPCC Guidelines for National Greenhouse Gas Inventories, Volume 4: Agriculture, Forestry and Other Land Use. [WWW Document]. URL https://www.ipcc-nggip.iges.or.jp/public/2006gl/pdf/4_Volume4/V4_10_Ch10_Livestock.pdf

IPCC, 2006b. Chapter 2: Waste Generation, Composition and Management Data. In 2006 IPCC Guidelines for National Greenhouse Gas Inventories – Volume 5: Waste. [WWW Document]. URL https://www.ipcc-nggip.iges.or.jp/public/2006gl/pdf/5_Volume5/V5_2_Ch2_Waste_Data.pdf

Jacob, D.J., Varon, D.J., Cusworth, D.H., Dennison, P.E., Frankenberg, C., Gautam, R., Guanter, L., Kelley, J., McKeever, J., Ott, L.E., Poulter, B., Qu, Z., Thorpe, A.K., Worden, J.R., Duren, R.M., 2022. Quantifying methane emissions from the global scale down to point sources using satellite observations of atmospheric methane. Atmospheric Chem. Phys. 22, 9617–9646. https://doi.org/10.5194/acp-22-9617-2022

Johnson, Kristen., Huyler, Mark., Westberg, Hal., Lamb, Brian., Zimmerman, Pat., 1994. Measurement of methane emissions from ruminant livestock using a sulfur hexafluoride tracer technique. Environ. Sci. Technol. 28, 359–362. https://doi.org/10.1021/es00051a025

Johnson, M.R., Tyner, D.R., Szekeres, A.J., 2021. Blinded evaluation of airborne methane source detection using Bridger Photonics LiDAR. Remote Sens. Environ. 259, 112418. https://doi.org/10.1016/j.rse.2021.112418

Kljun, N., Calanca, P., Rotach, M.W., Schmid, H.P., 2015. A simple two-dimensional parameterisation for Flux Footprint Prediction (FFP). Geosci. Model Dev. 8, 3695–3713. https://doi.org/10.5194/gmd-8-3695-2015

Kormann, R., Meixner, F.X., 2001. An Analytical Footprint Model For Non-Neutral Stratification. Bound.-Layer Meteorol. 99, 207–224. https://doi.org/10.1023/A:1018991015119

Kormi, T., Bel Hadj Ali, N., Abichou, T., Green, R., 2017. Estimation of landfill methane emissions using stochastic search methods. Atmospheric Pollut. Res. 8, 597–605. https://doi.org/10.1016/j.apr.2016.12.020

Lee, K.M., Lee, M.H., Lee, J.S., Lee, J.Y., 2020. Uncertainty Analysis of Greenhouse Gas (GHG) Emissions Simulated by the Parametric Monte Carlo Simulation and Nonparametric Bootstrap Method. Energies 13, 4965. https://doi.org/10.3390/en13184965

LI-COR Biosciences, 2021. EddyPro 7 | Software Downloads [WWW Document]. URL https://www.licor.com/support/EddyPro/software.html (accessed 1.30.25).

Maasakkers, J.D., Varon, D.J., Elfarsdóttir, A., McKeever, J., Jervis, D., Mahapatra, G., Pandey, S., Lorente, A., Borsdorff, T., Foorthuis, L.R., Schuit, B.J., Tol, P., Van Kempen, T.A., Van Hees, R., Aben, I., 2022. Using satellites to uncover large methane emissions from landfills. Sci. Adv. 8, eabn9683. https://doi.org/10.1126/sciadv.abn9683

Mauder, M., Foken, T., 2004. Documentation and Instruction Manual of the Eddy Covariance Software Package TK2.

Mbua, M., Riddick, S.N., Kiplimo, E., Shonkwiler, K.B., Hodshire, A., Zimmerle, D., 2025. Evaluating the feasibility of using downwind methods to quantify point source oil and gas emissions using continuously monitoring fence-line sensors. Atmospheric Meas. Tech. 18, 5687–5703. https://doi.org/10.5194/amt-18-5687-2025

Meehan, M., Sedivec, K.K., Printz, J., Brummer, F., 2018. Determining Carrying Capacity and Stocking Rates [WWW Document]. Nat. Resour. Conserv. Serv. URL https://www.nrcs.usda.gov/sites/default/files/2022-10/Determining%20Carry%20Capacity%20and%20Stocking%20Rates%20_ND.pdf

Milojević, S., 2010. Power law distributions in information science: Making the case for logarithmic binning. J. Am. Soc. Inf. Sci. Technol. 61, 2417–2425. https://doi.org/10.1002/asi.21426

Mollel, W., Zimmerle, D., Santos, A., Hodshire, A., 2025. Using Prototypical Oil and Gas Sites to Model Methane Emissions in Colorado's Denver-Julesburg Basin Using a Mechanistic Emission Estimation Tool. ACS EST Air 2, 723–735. https://doi.org/10.1021/acsestair.4c00168

Moncrieff, J., Clement, R., Finnigan, J., Meyers, T., 2005. Averaging, Detrending, and Filtering of Eddy Covariance Time Series, in: Lee, X., Massman, W., Law, B. (Eds.), Handbook of Micrometeorology, Atmospheric and Oceanographic Sciences Library. Kluwer Academic Publishers, Dordrecht, pp. 7–31. https://doi.org/10.1007/1-4020-2265-4_2

Mønster, J., Kjeldsen, P., Scheutz, C., 2019. Methodologies for measuring fugitive methane emissions from landfills – A review. Waste Manag. 87, 835–859. https://doi.org/10.1016/j.wasman.2018.12.047

Moore, D.P., Li, N.P., Wendt, L.P., Castañeda, S.R., Falinski, M.M., Zhu, J.-J., Song, C., Ren, Z.J., Zondlo, M.A., 2023. Underestimation of Sector-Wide Methane Emissions from United States Wastewater Treatment. Environ. Sci. Technol. 57, 4082–4090. https://doi.org/10.1021/acs.est.2c05373

Morin, T.H., 2019. Advances in the Eddy Covariance Approach to CH 4 Monitoring Over Two and a Half Decades. J. Geophys. Res. Biogeosciences 124, 453–460. https://doi.org/10.1029/2018JG004796

Mudavadi, C., Nafisi, J., Pakdeekasem, P., Pornsatit, C., Chiamsiri, V., 2011. Boeing 787 Financial Approach. Eng. Technol. Manag. Stud. Proj.

Niazi, A., Dai, J.S., Balabani, S., Seneviratne, L., 2006. Product Cost Estimation: Technique Classification and Methodology Review. J. Manuf. Sci. Eng. 128, 563–575. https://doi.org/10.1115/1.2137750

Pétron, G., Karion, A., Sweeney, C., Miller, B.R., Montzka, S.A., Frost, G.J., Trainer, M., Tans, P., Andrews, A., Kofler, J., Helmig, D., Guenther, D., Dlugokencky, E., Lang, P., Newberger, T., Wolter, S., Hall, B., Novelli, P., Brewer, A., Conley, S., Hardesty, M., Banta, R., White, A., Noone, D., Wolfe, D., Schnell, R., 2014. A new look at methane and nonmethane hydrocarbon emissions from oil and natural gas operations in the Colorado Denver-Julesburg Basin. J. Geophys. Res. Atmospheres 119, 6836–6852. https://doi.org/10.1002/2013JD021272

Place, S.E., Mitloehner, F.M., 2010. Invited review: Contemporary environmental issues: A review of the dairy industry's role in climate change and air quality and the potential of mitigation through improved production efficiency. J. Dairy Sci. 93, 3407–3416. https://doi.org/10.3168/jds.2009-2719

Polonik, P., Chan, W.S., Billesbach, D.P., Burba, G., Li, J., Nottrott, A., Bogoev, I., Conrad, B., Biraud, S.C., 2019. Comparison of gas analyzers for eddy covariance: Effects of analyzer type and spectral corrections on fluxes. Agric. For. Meteorol. 272–273, 128–142. https://doi.org/10.1016/j.agrformet.2019.02.010

Rey-Sanchez, C., Arias-Ortiz, A., Kasak, K., Chu, H., Szutu, D., Verfaillie, J., Baldocchi, D., 2022. Detecting Hot Spots of Methane Flux Using Footprint-Weighted Flux Maps. J. Geophys. Res. Biogeosciences 127, e2022JG006977. https://doi.org/10.1029/2022JG006977

Riddick, S.N., Ancona, R., Cheptonui, F., Bell, C.S., Duggan, A., Bennett, K.E., Zimmerle, D.J., 2022a. A cautionary report of calculating methane emissions using low-cost fence-line sensors. Elem. Sci. Anthr. 10, 00021. https://doi.org/10.1525/elementa.2022.00021

Riddick, S.N., Cheptonui, F., Yuan, K., Mbua, M., Day, R., Vaughn, T.L., Duggan, A., Bennett, K.E., Zimmerle, D.J., 2022b. Estimating Regional Methane Emission Factors from Energy and Agricultural Sector Sources Using a Portable Measurement System: Case Study of the Denver–Julesburg Basin. Sensors 22, 7410. https://doi.org/10.3390/s22197410

Riddick, S.N., Connors, S., Robinson, A.D., Manning, A.J., Jones, P.S.D., Lowry, D., Nisbet, E., Skelton, R.L., Allen, G., Pitt, J., Harris, N.R.P., 2017. Estimating the size of a methane emission point source at different scales: from local to landscape. Atmospheric Chem. Phys. 17, 7839–7851. https://doi.org/10.5194/acp-17-7839-2017

Riddick, S.N., Hancock, B.R., Robinson, A.D., Connors, S., Davies, S., Allen, G., Pitt, J., Harris, N.R.P., 2018. Development of a low-maintenance measurement approach to continuously estimate methane emissions: A case study. Waste Manag. 73, 210–219. https://doi.org/10.1016/j.wasman.2016.12.006

Riddick, S.N., Mauzerall, D.L., 2023. Likely substantial underestimation of reported methane emissions from United Kingdom upstream oil and gas activities. Energy Environ. Sci. 16, 295–304. https://doi.org/10.1039/D2EE03072A

Riddick, S.N., Mbua, M., Anand, A., Kiplimo, E., Santos, A., Upreti, A., Zimmerle, D.J., 2024a. Estimating Total Methane Emissions from the Denver-Julesburg Basin Using Bottom-Up Approaches. Gases 4, 236–252. https://doi.org/10.3390/gases4030014

Riddick, S.N., Mbua, M., Anand, A., Kiplimo, E., Santos, A., Upreti, A., Zimmerle, D.J., 2024b. Estimating Total Methane Emissions from the Denver-Julesburg Basin Using Bottom-Up Approaches. Gases 4, 236–252. https://doi.org/10.3390/gases4030014

Riddick, S.N., Mbua, M., Santos, A., Hartzell, W., Zimmerle, D.J., 2024c. Potential Underestimate in Reported Bottom-up Methane Emissions from Oil and Gas Operations in the Delaware Basin. Atmosphere 15, 202. https://doi.org/10.3390/atmos15020202

Rutherford, J.S., Sherwin, E.D., Ravikumar, A.P., Heath, G.A., Englander, J., Cooley, D., Lyon, D., Omara, M., Langfitt, Q., Brandt, A.R., 2021. Closing the methane gap in US oil and natural gas production emissions inventories. Nat. Commun. 12, 4715. https://doi.org/10.1038/s41467-021-25017-4

Saunois, M., Martinez, A., Poulter, B., Zhang, Z., Raymond, P.A., Regnier, P., Canadell, J.G., Jackson, R.B., Patra, P.K., Bousquet, P., Ciais, P., Dlugokencky, E.J., Lan, X., Allen, G.H., Bastviken, D., Beerling, D.J., Belikov, D.A., Blake, D.R., Castaldi, S., Crippa, M., Deemer, B.R., Dennison, F., Etiope, G., Gedney, N., Höglund-Isaksson, L., Holgerson, M.A., Hopcroft, P.O., Hugelius, G., Ito, A., Jain, A.K., Janardanan, R., Johnson, M.S., Kleinen, T., Krummel, P.B., Lauerwald, R., Li, T., Liu, X., McDonald, K.C., Melton, J.R., Mühle, J., Müller, J., Murguia-Flores, F., Niwa, Y., Noce, S., Pan, S., Parker, R.J., Peng, C., Ramonet, M., Riley, W.J., Rocher-Ros, G., Rosentreter, J.A., Sasakawa, M., Segers, A., Smith, S.J., Stanley, E.H., Thanwerdas, J., Tian, H., Tsuruta, A., Tubiello, F.N., Weber, T.S., Van Der Werf, G.R., Worthy, D.E.J., Xi, Y., Yoshida, Y., Zhang, W.,

Zheng, B., Zhu, Qing, Zhu, Qiuan, Zhuang, Q., 2025. Global Methane Budget 2000–2020. Earth Syst. Sci. Data 17, 1873–1958. https://doi.org/10.5194/essd-17-1873-2025

Shonkwiler, K., 2018. Micrometeorological studies of a beef feedlot, dairy, and grassland: measurements of ammonia, methane, and energy balance closure. Colorado State University.

Skwierawski, A., 2024. Seasonal and annual variability of methane emissions to the atmosphere from the surface of a eutrophic lake located in the temperate zone (Lake Kortowskie, Poland). https://doi.org/10.5194/egusphere-2024-1786

Song, C., Zhu, J.-J., Willis, J.L., Moore, D.P., Zondlo, M.A., Ren, Z.J., 2023. Methane Emissions from Municipal Wastewater Collection and Treatment Systems. Environ. Sci. Technol. 57, 2248–2261. https://doi.org/10.1021/acs.est.2c04388

Stull, R.B., 1988. An Introduction to Boundary Layer Meteorology, 1988 edition. ed, Atmospheric and Oceanographic Sciences Library. Springer Nature, Dordrecht. https://doi.org/10.1007/978-94-009-3027-8

Tagliaferri, F., Invernizzi, M., Capra, F., Sironi, S., 2023. Validation study of WindTrax reverse dispersion model coupled with a sensitivity analysis of model-specific settings. Environ. Res. 222, 115401. https://doi.org/10.1016/j.envres.2023.115401

UNEP, 2025. A solution to the methane challenge | The Oil & Gas Methane Partnership 2.0 [WWW Document]. URL https://www.ogmpartnership.org/solution-methane-challenge (accessed 9.4.25).

UNEP, 2024. Homepage | The Oil & Gas Methane Partnership 2.0.

US EPA, 2025a. Methane Emissions [WWW Document]. URL https://www.epa.gov/ghgemissions/methane-emissions (accessed 9.4.25).

US EPA, 2025b. LMOP Landfill and Project Database [WWW Document]. URL https://www.epa.gov/lmop/lmop-landfill-and-project-database (accessed 9.8.25).

US EPA, 2025c. Download the State Inventory and Projection Tool [WWW Document]. URL https://www.epa.gov/statelocalenergy/download-state-inventory-and-projection-tool (accessed 9.10.25).

US EPA, 2025d. 40 CFR Part 98 Subpart HH -- Municipal Solid Waste Landfills [WWW Document]. URL https://www.ecfr.gov/current/title-40/part-98/subpart-HH (accessed 10.28.25).

US EPA, 2023a. Natural Gas and Petroleum Systems in the GHG Inventory: Additional Information on the 1990-2021 GHG Inventory (published April 2023) (Reports and Assessments).

US EPA, 2023b. EPA Facility Level GHG Emissions Data [WWW Document]. URL https://ghgdata.epa.gov/ghgp/main.do (accessed 9.12.25).

US EPA, 2023c. Inventory of U.S. Greenhouse Gas Emissions and Sinks: 1990 – 2021 — Annex 3: Additional source or sink categories, Part B (EPA 430-R-23-003) [WWW Document]. URL https://www.epa.gov/system/files/documents/2023-04/US-GHG-Inventory-2023-Annex-3-Additional-Source-or-Sink-Categories-Part-B.pdf

US EPA, 2022a. Research on Emissions from U.S. Reservoirs [WWW Document]. URL https://www.epa.gov/air-research/research-emissions-us-reservoirs (accessed 9.5.25).

US EPA, 2022b. Inventory of U.S. Greenhouse Gas Emissions and Sinks: 1990-2020.

US EPA, 2021. New Monitoring Method Improves Ability to Measure Methane Emissions from Reservoirs [WWW Document]. URL https://www.epa.gov/sciencematters/new-

monitoring-method-improves-ability-measure-methane-emissions-reservoirs (accessed 9.5.25).

US EPA, 2019. USER'S GUIDE FOR ESTIMATING METHANE AND NITROUS OXIDE EMISSIONS FROM WASTEWATER USING THE STATE INVENTORY TOOL.

US EPA, 2016. Importance of Methane [WWW Document]. URL https://www.epa.gov/gmi/importance-methane (accessed 10.15.25).

US EPA, 2013. Standard Operating Procedure for Analysis of US EPA Geospatial Measurement of Air Pollution Remote Emission Quantification by Direct Assessment (GMAP-REQDA) Method Data for Methane Emission Rate Quantification using the Point Source Gaussian Method.

US EPA, 2012. GHGRP 2012: Reported Data [WWW Document]. URL https://19january2017snapshot.epa.gov/ghgreporting/ghgrp-2012-reported-data (accessed 10.27.25).

US EPA, 2008. Document Display | NEPIS | US EPA [WWW Document]. URL https://nepis.epa.gov/Exe/ZyNET.exe/P1002UVK.TXT?ZyActionD=ZyDocument&Client=EPA&Index=2006+Thru+2010&Docs=&Query=&Time=&EndTime=&SearchMethod=1&TocRestrict=n&Toc=&TocEntry=&QField=&QFieldYear=&QFieldMonth=&QFieldDay=&IntQFieldOp=0&ExtQFieldOp=0&XmlQuery=&File=D%3A%5Czyfiles%5CIndex%20Data%5C06thru10%5CTxt%5C00000006%5CP1002UVK.txt&User=ANONYMOUS&Password=anonymous&SortMethod=h%7C-&MaximumDocuments=1&FuzzyDegree=0&ImageQuality=r75g8/r75g8/x150y150g16/i425&Display=hpfr&DefSeekPage=x&SearchBack=ZyActionL&Back=ZyActionS&Bac

kDesc=Results%20page&MaximumPages=1&ZyEntry=1&SeekPage=x&ZyPURL# (accessed 9.5.25).

Vaughn, T.L., Bell, C.S., Pickering, C.K., Schwietzke, S., Heath, G.A., Pétron, G., Zimmerle, D.J., Schnell, R.C., Nummedal, D., 2018. Temporal variability largely explains top-down/bottom-up difference in methane emission estimates from a natural gas production region. Proc. Natl. Acad. Sci. 115, 11712–11717. https://doi.org/10.1073/pnas.1805687115

Vickers, D., Mahrt, L., 1997. Quality Control and Flux Sampling Problems for Tower and Aircraft Data. J. Atmospheric Ocean. Technol. 14, 512–526. https://doi.org/10.1175/1520-0426(1997)014<0512:QCAFSP>2.0.CO;2

Weather Underground, 2025. Local Weather Forecast, News and Conditions | Weather Underground [WWW Document]. URL https://www.wunderground.com/ (accessed 9.8.25).

Webb, E.K., Pearman, G.I., Leuning, R., 1980. Correction of flux measurements for density effects due to heat and water vapour transfer. Q. J. R. Meteorol. Soc. 106, 85–100. https://doi.org/10.1002/qj.49710644707

WindTrax 2.0, 2020. thunder beach scientific.

World Bank Group, 2025. How can we reduce methane emissions? [WWW Document]. World Bank. URL https://www.worldbank.org/en/programs/gasflaringreduction/methane-explained (accessed 10.27.25).

Zimmerle, D., Dileep, S., Quinn, C., 2024. Unaddressed Uncertainties When Scaling Regional Aircraft Emission Surveys to Basin Emission Estimates. Environ. Sci. Technol. 58, 6575–6585. https://doi.org/10.1021/acs.est.3c08972

APPENDIX

A1: Atmospheric Conditions during the Test Period

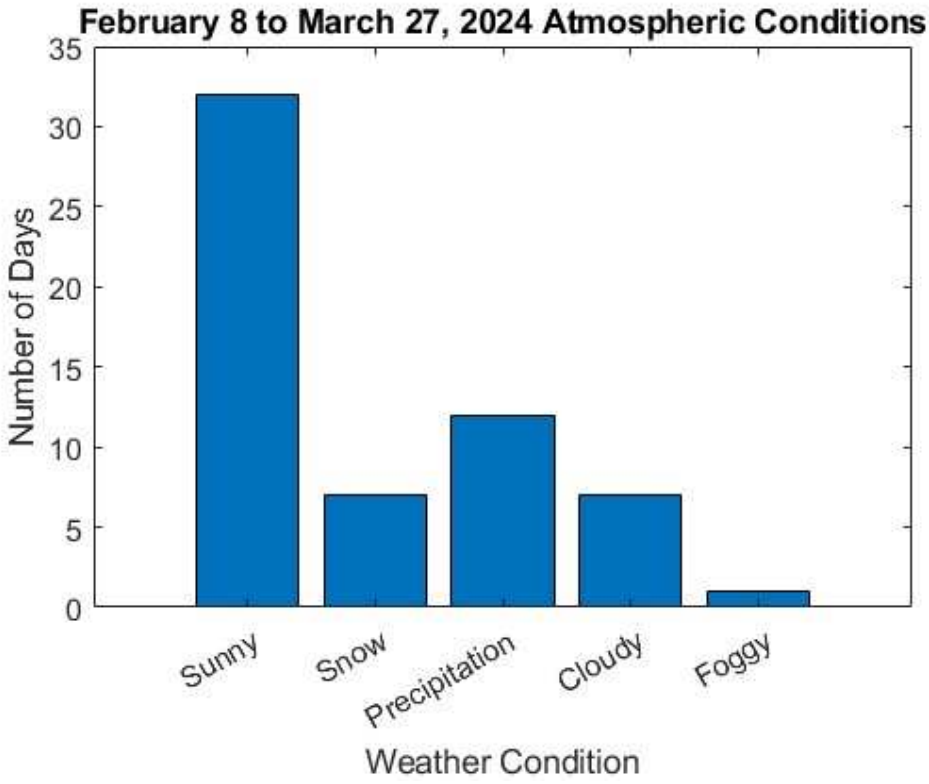

Figure A1. A bar plot of weather conditions during the test period

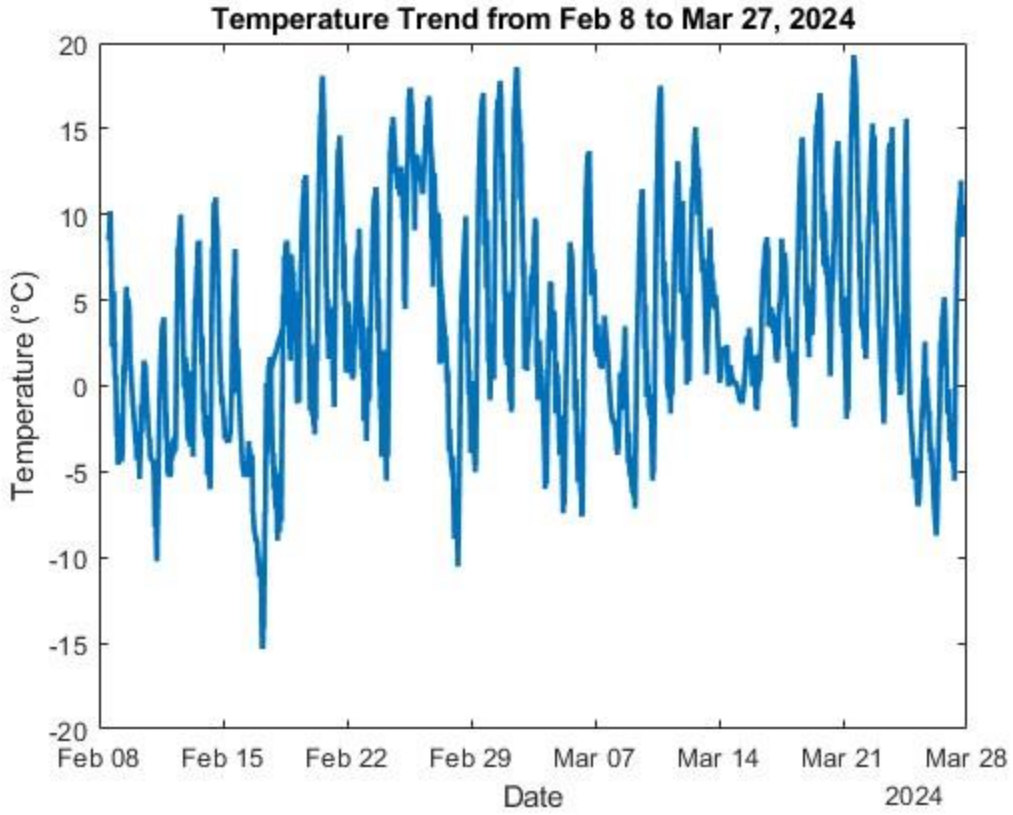

Figure A2. A plot of temperature during the test period

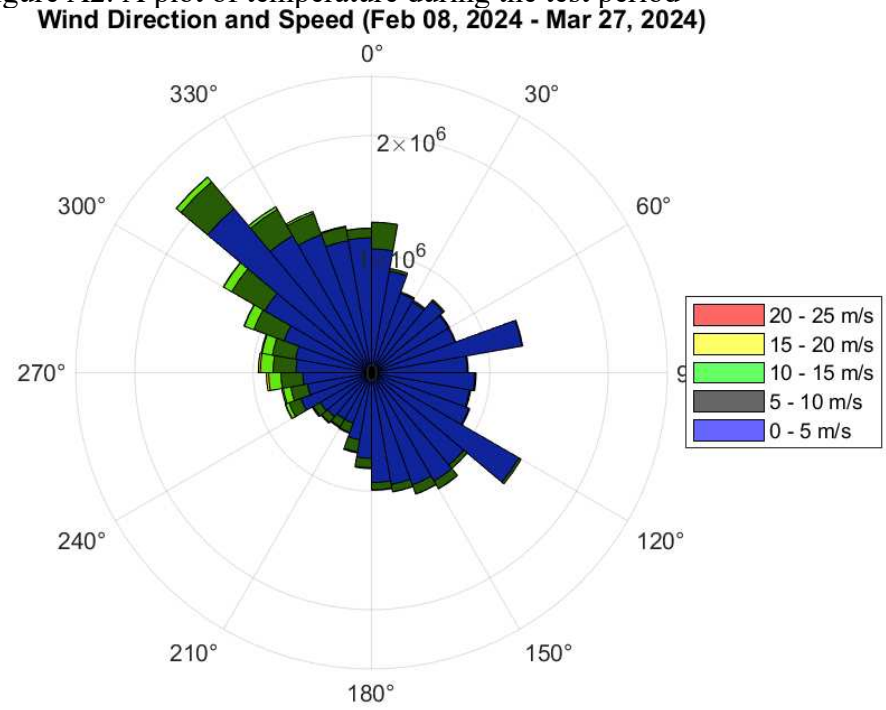

Figure A3. A wind rose plot of wind direction and wind speed during the test period

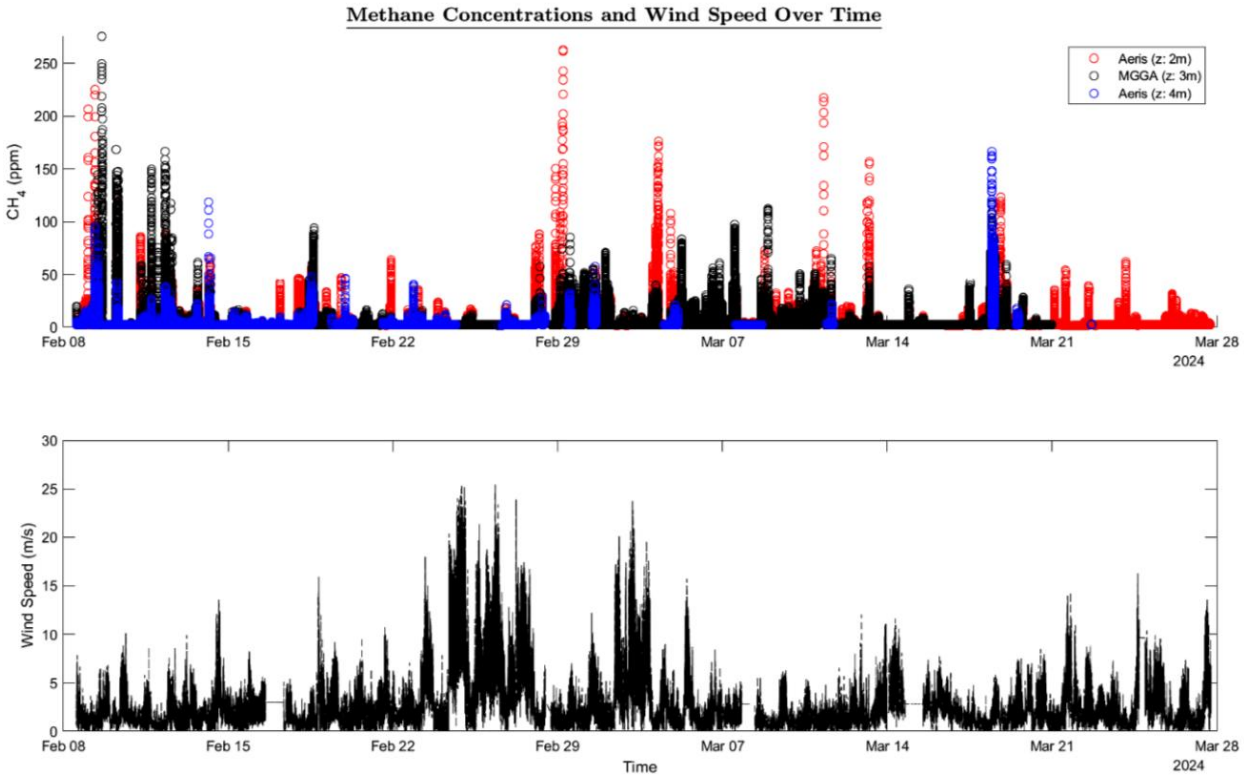

Figure A4. Top plot: A time series plot of CH_4 concentrations during the test period. Bottom plot: A time series of wind speed during the test period

A2.1: Equations

$$\boldsymbol{z0 = z * \exp\left(-\frac{0.4U}{u_*}\right)} \quad \text{(A1)}$$

$$\boldsymbol{u_* = \left[\left(\overline{u'w'}\right)^2 + \left(\overline{v'w'}\right)^2\right]^{1/4}} \quad \text{(A2)}$$

Where z0 = roughness length (m)

z = measurement height (m)

U = mean wind speed (m/s)

u_* = surface friction velocity (m/s)

u and v = horizontal wind speeds (m/s)

w = vertical wind speed (m/s)

L was calculated from the surface friction velocity (u_*, m s^{-1}), mean potential temperature (Θ, K), von Kármán's constant (*k*, 0.41), gravitational acceleration (*g*, 9.8 m s^{-1}) and the surface (kinematic) turbulent flux of sensible heat w'Θ' (Equation 3) (Kljun et al., 2015; Stull, 1988).

$$L = -\frac{u_*^3 \Theta}{k_v g \overline{w'\Theta'}} \quad \text{(A3)}$$

The wind direction (*WD*) and speed (*WS*) were calculated from the wind vectors u and v, based on the manufacturer's configuration: +*u* values = wind from the east, +*v* values = wind from the north, and +*w* = updraft (Equations 4 and 5).

$$\boldsymbol{WD = \mathbf{mod}(90 - \mathbf{atan2d}(v, u), 360)} \quad \text{(A4)}$$

$$\mathbf{WS} = \sqrt{\mathbf{u^2 + v^2}} \quad \text{(A5)}$$

$$\mathbf{F} = \frac{\mathbf{u_* k_v (c_2 - c_1)}}{\mathbf{In}\left(\frac{\mathbf{z_2}}{\mathbf{z_1}}\right) - \boldsymbol{\Psi}_{\mathbf{c,2}} + \boldsymbol{\Psi}_{\mathbf{c,1}}} \quad \text{(A6)}$$

$$\mathbf{Q} = \frac{\mathbf{mean_{Enh}(x,y,x) * 2\pi\sigma_y\sigma_z U}}{\mathbf{exp\left(-\frac{y^2}{2{\sigma_y}^2}\right) * \left(exp\left(-\frac{(z-H)^2}{2{\sigma_z}^2}\right) + exp\left(-\frac{(z+H)^2}{2{\sigma_z}^2}\right)\right)}} \quad \text{(A7)}$$

$$Q = \frac{mean_{Enh}(x,y,x)*2\pi\sigma_y\sigma_z U}{exp\left(-\frac{y^2}{2{\sigma_y}^2}\right)*\left(exp\left(-\frac{(z-H)^2}{2{\sigma_z}^2}\right)+exp\left(-\frac{(z+H)^2}{2{\sigma_z}^2}\right)+ exp\left(-\frac{(z-2h+H)^2}{2{\sigma_z}^2}\right)+ exp\left(-\frac{(z+2h-H)^2}{2{\sigma_z}^2}\right)+exp\left(-\frac{(z-2h-H)^2}{2{\sigma_z}^2}\right)\right)} \quad \text{(A8)}$$

Where

Q = point source emission rate (kg h^{-1})

$mean_{Enh}$ (x,y,z) = mean CH_4 enhancement at the measurement point (ppm)

σ_y (m) = horizontal dispersion coefficient calculated as $\sigma_v(x/U)$: σ_v is the standard deviation of v wind speed from the sonic anemometer, x is the downwind distance from the point source and U is the mean wind speed

σ_z (m) = vertical dispersion coefficient calculated as $\sigma_w(x/U)$: σ_w is the standard deviation of w wind speed from the sonic anemometer, x is the downwind distance from the point source and U is the mean wind speed

y (m) = mean cross wind distance in the averaged period

z (m) = measurement height

h (m) = height of boundary layer: estimated based on (Kljun et al., 2015)

H (m) = point source height

A2.2: Instrument Sampling Frequency

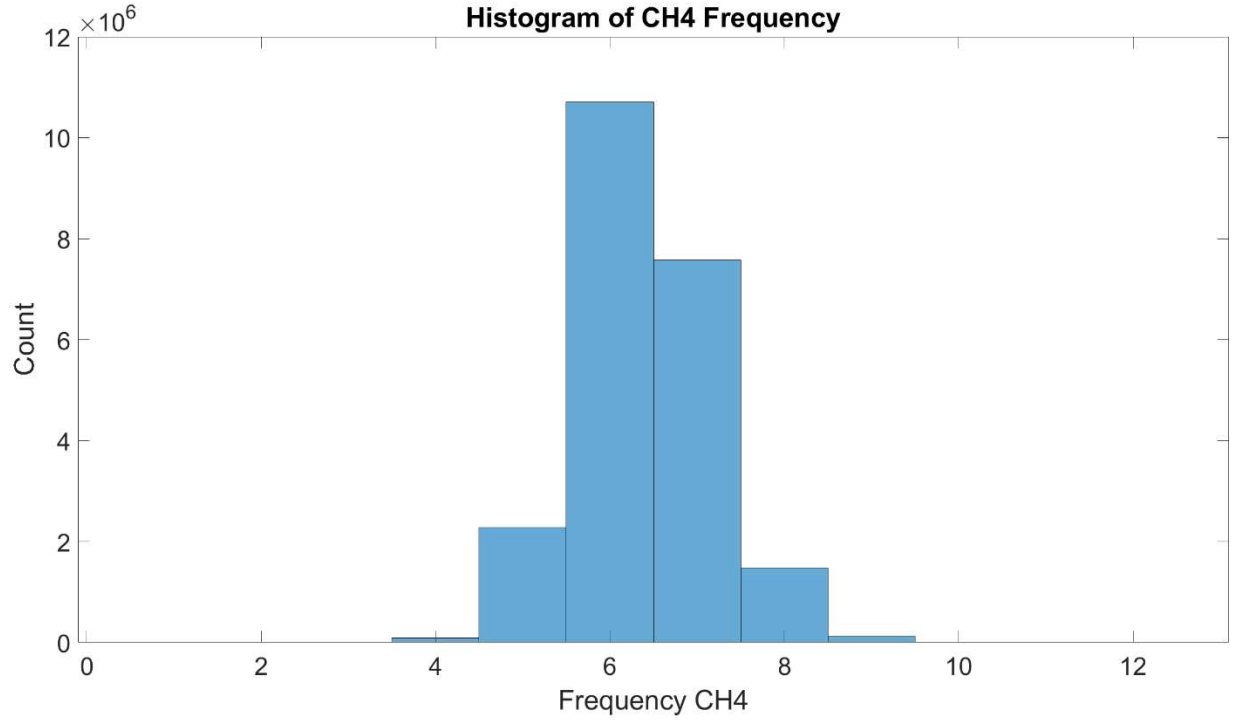

Figure A5. A histogram of CH_4 sampling frequency by the MGGA

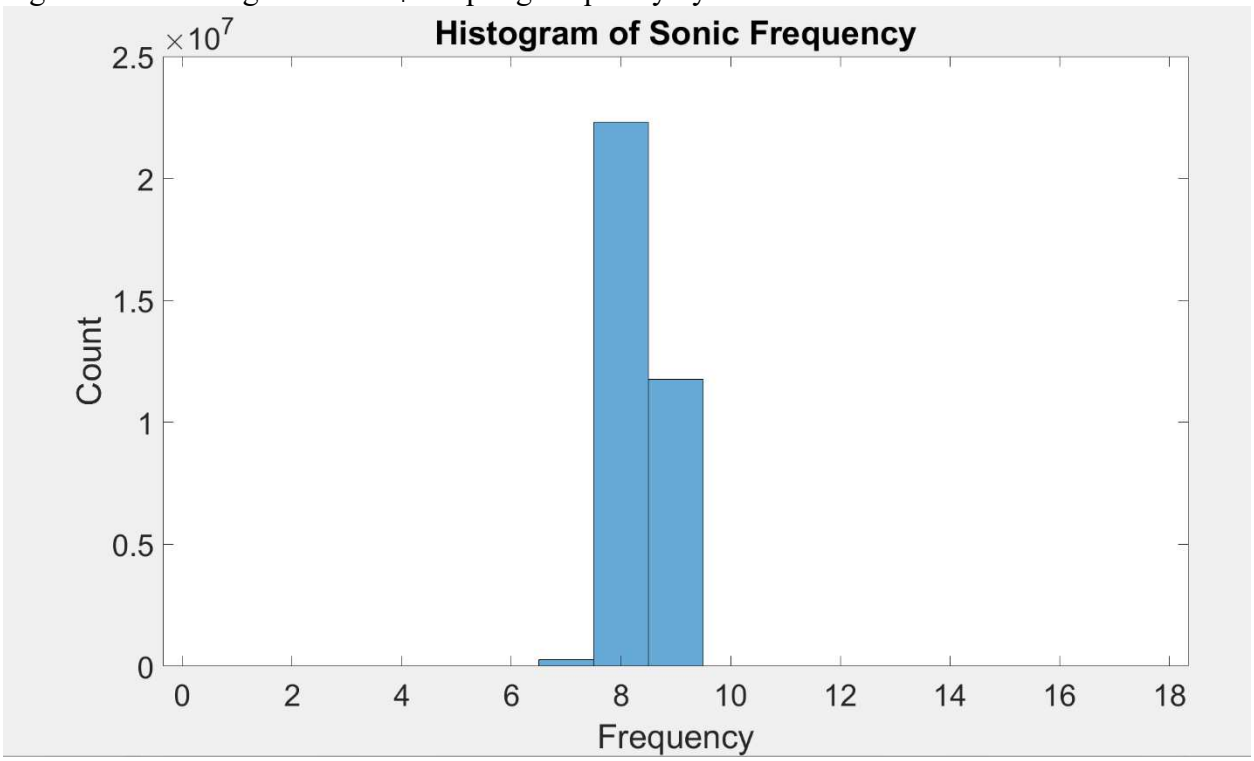

Figure A6. A histogram of sonic anemometer sampling frequency

A2.3 Cospectra/ogive/u*/stationarity

A2.3.1 Cospectra Analysis

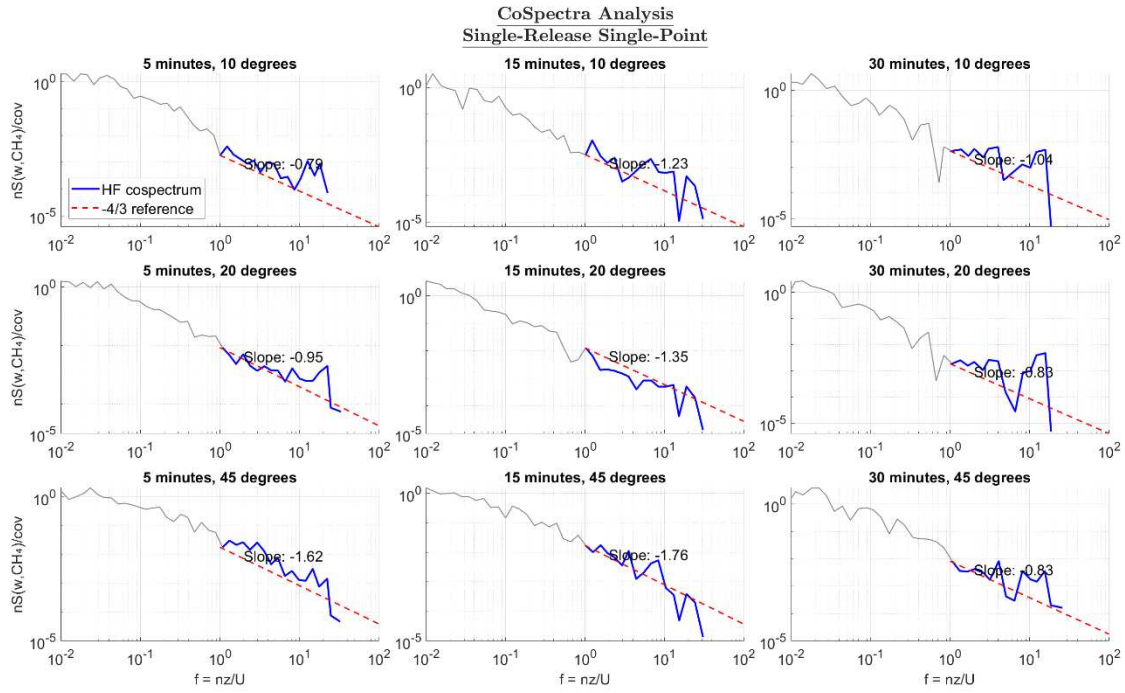

Figure A7. CoSpectra analysis for the eddy covariance fluxes for single release single point emissions

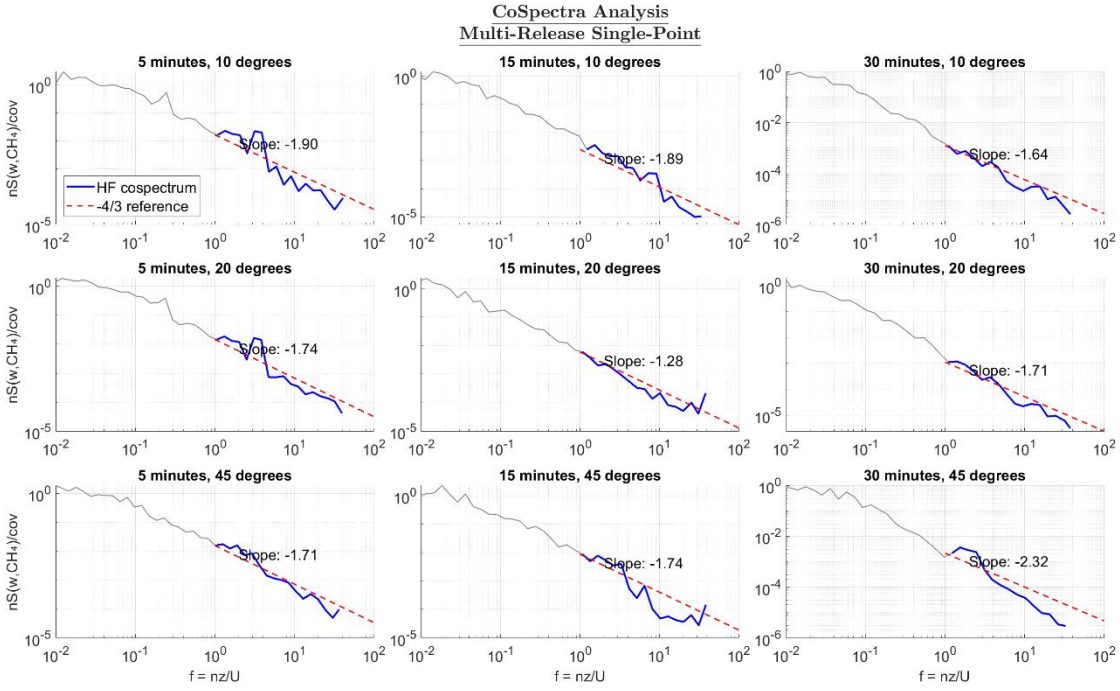

Figure A8. CoSpectra analysis for the eddy covariance fluxes for multi release single point emissions

A2.3.2 CH_4 Flux vs u*

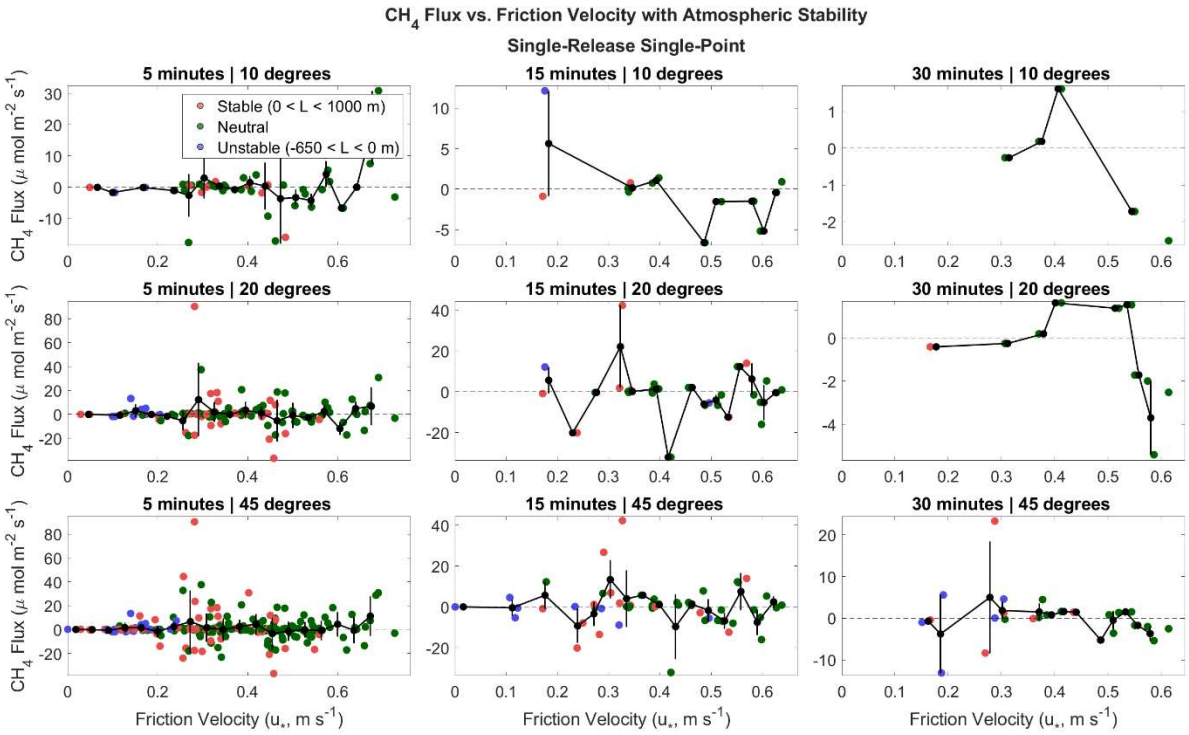

Figure A9. A plot of CH_4 flux vs friction velocity for the eddy covariance fluxes for single release single point emissions

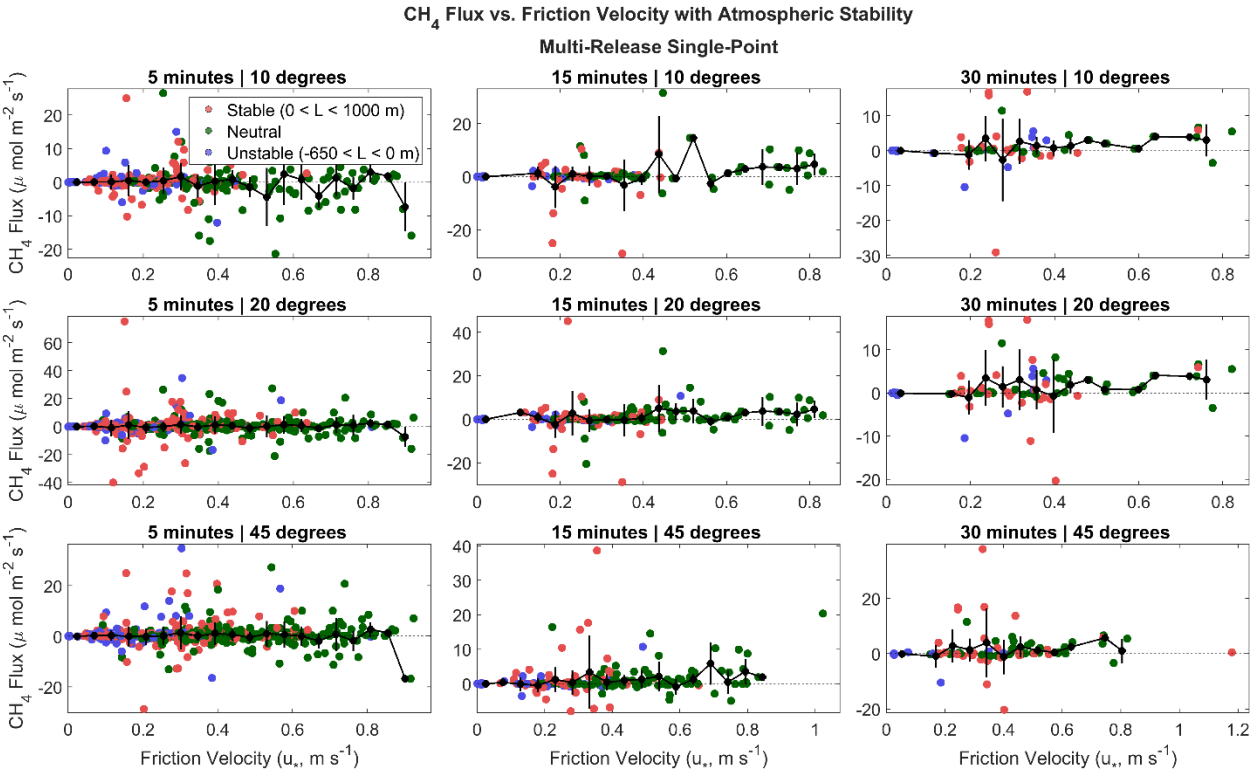

Figure A10. A plot of CH_4 flux vs friction velocity for the eddy covariance fluxes for multi release single point emissions

A2.3.3 Ogive Analysis

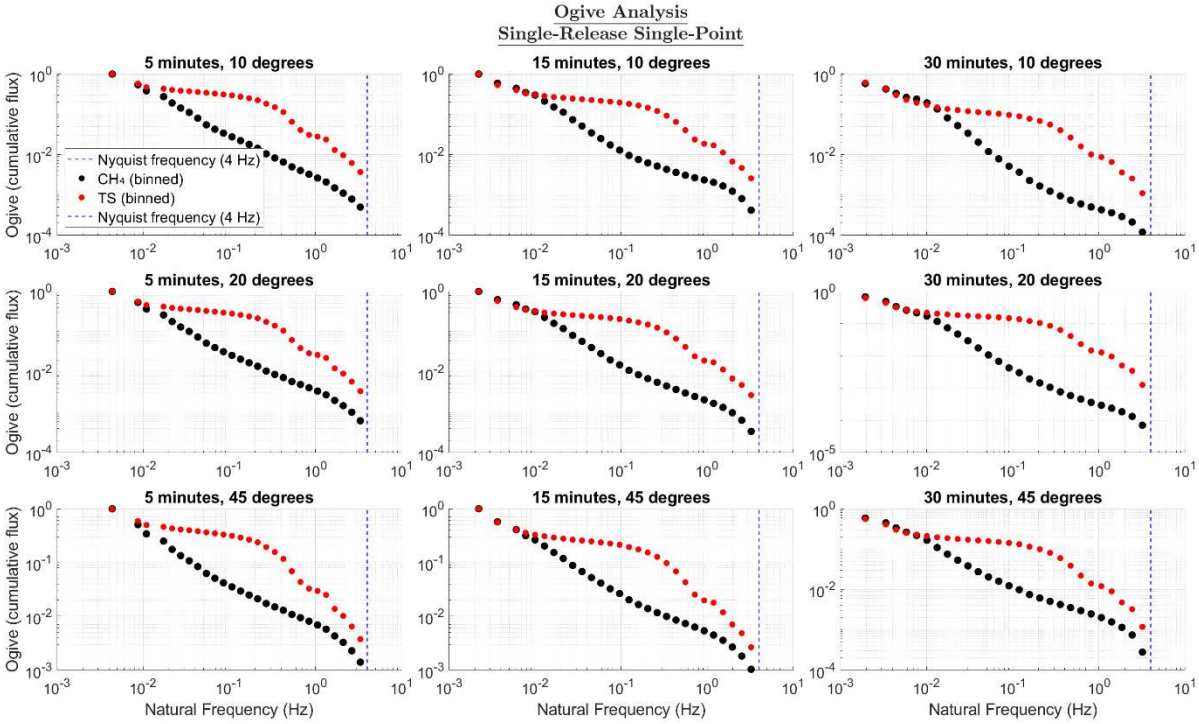

Figure A11. Ogive analysis for the eddy covariance fluxes for single release single point emissions

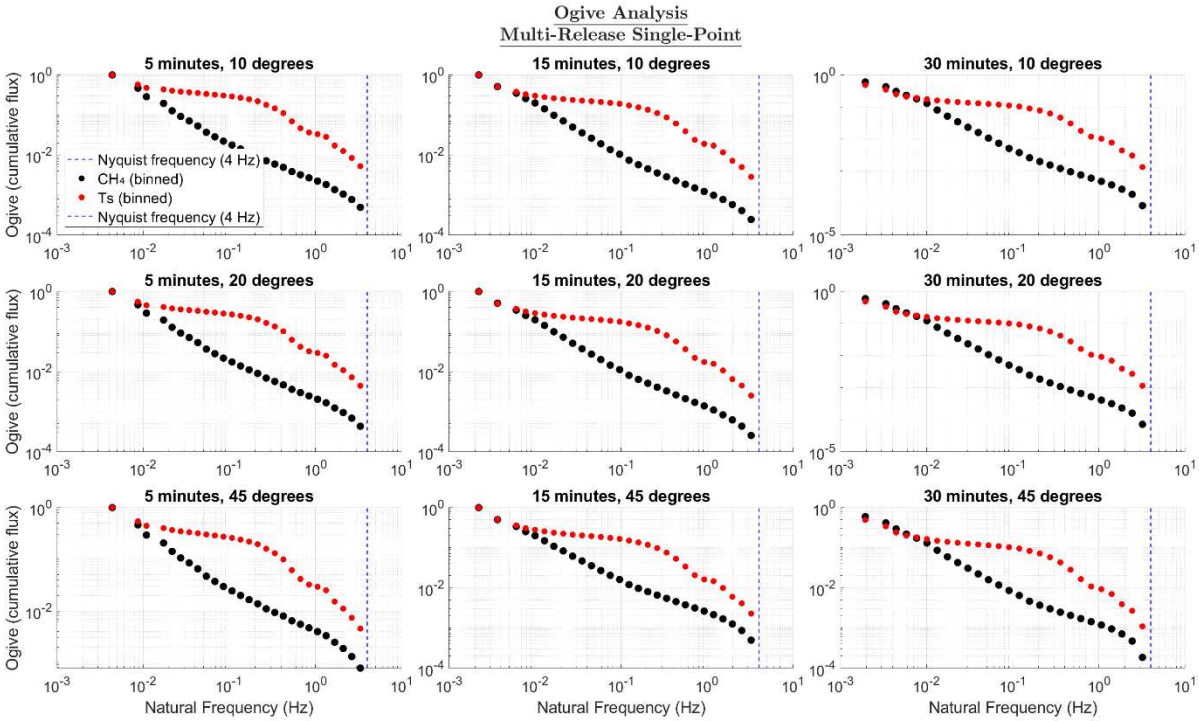

Figure A12. Ogive analysis for the eddy covariance fluxes for Multi release single point emissions

S2.3.4 Stationarity Plot

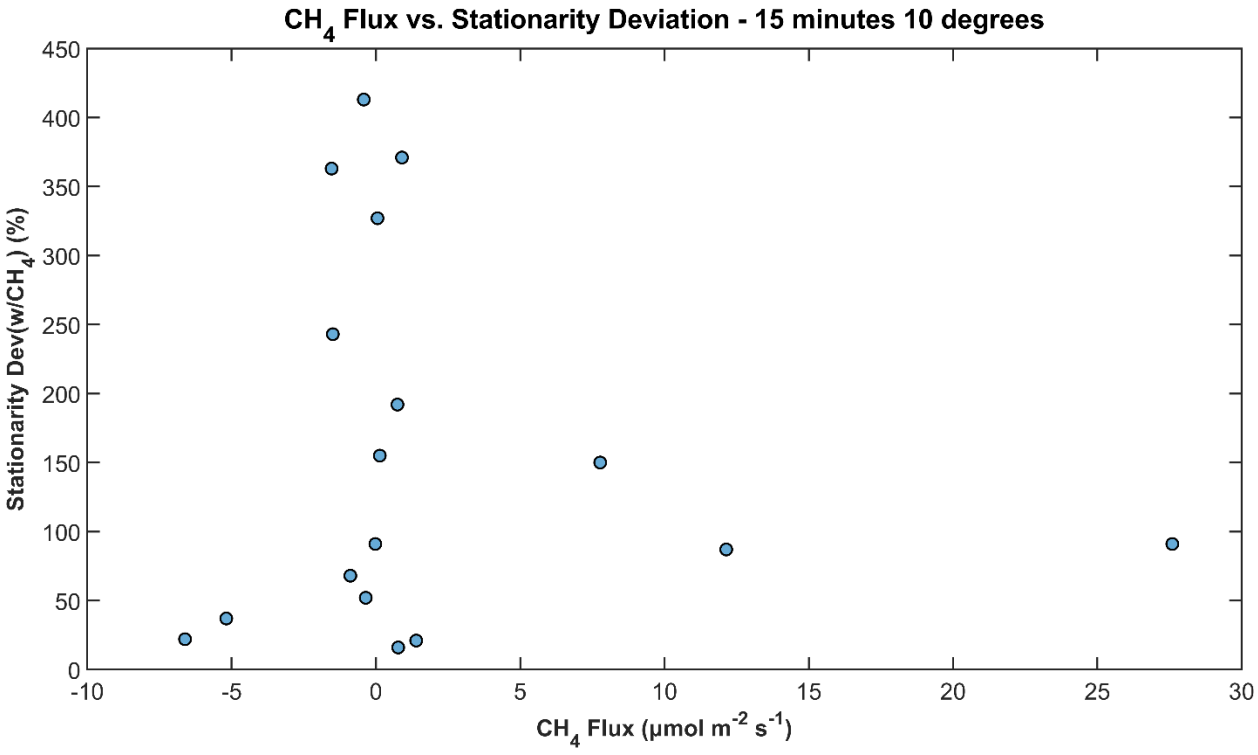

Figure A13. A sample plot of CH_4 flux vs stationarity deviation for the eddy covariance fluxes-15 minutes 10 degrees wind sector

A3: Results

A3.1 Eddy Covariance

A3.1.1 Single Release Single Point

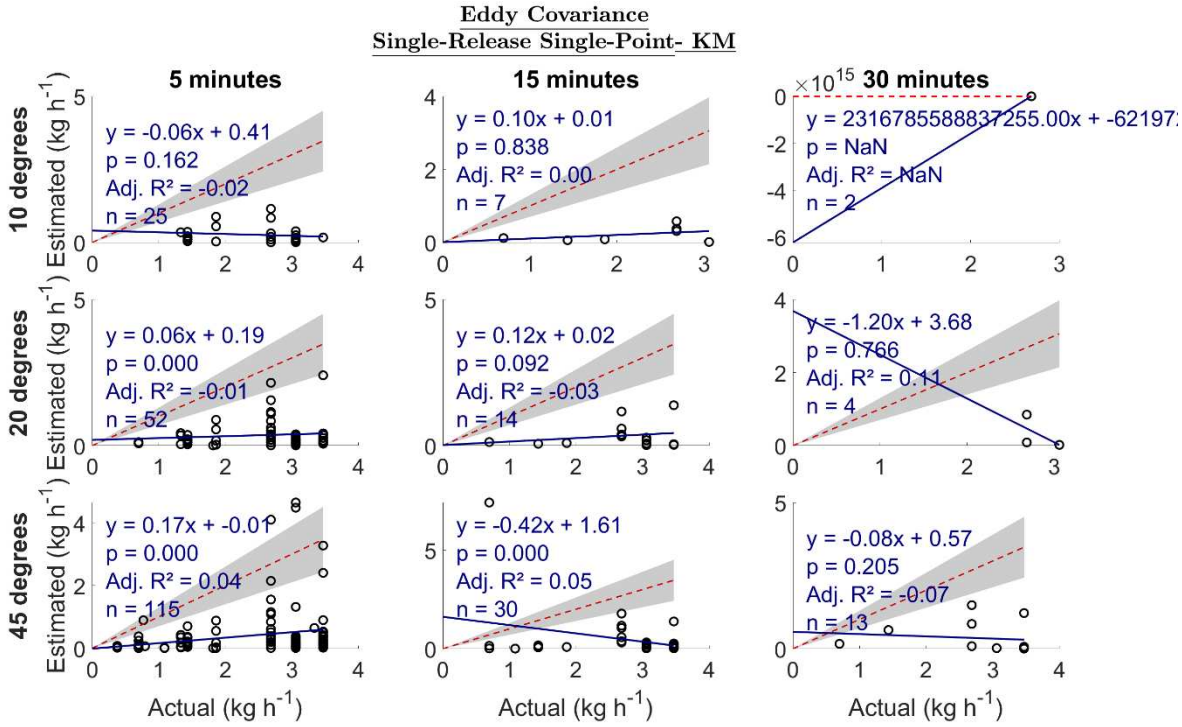

Figure A14. Estimated emission vs actual emission (kg h^{-1}) for single-release single-point emissions. The red dotted line is a 1:1 line based on actual emissions i.e. points below the line are underestimated and above are overestimated emissions. The gray region represents ±30% of the actual emission. Adj. R^2 is the adjusted R^2. The sample size is n.

A3.1.2 Multi-Release Single-Point

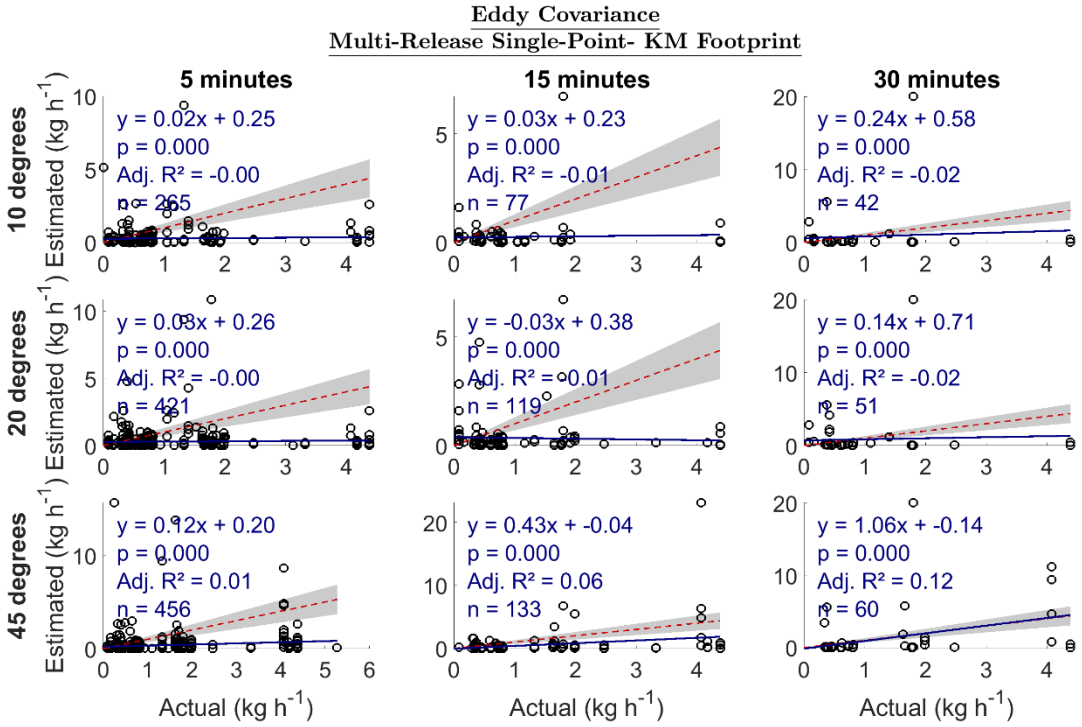

Figure A15. Estimated emission vs actual emission (kg h^{-1}) for multi-release single-point emissions. The red dotted line is a 1:1 line based on actual emissions i.e. points below the line are underestimated and above are overestimated emissions. The gray region represents ±30% of the actual emission. Adj. R^2 is the adjusted R^2. The sample size is n.

A3.2 Gaussian Plume Inverse Method: Single-Release Single-Point

A3.2.1 Scenario 1: Equation A7 & ~10 Hz sonic anemometer dispersion coefficients

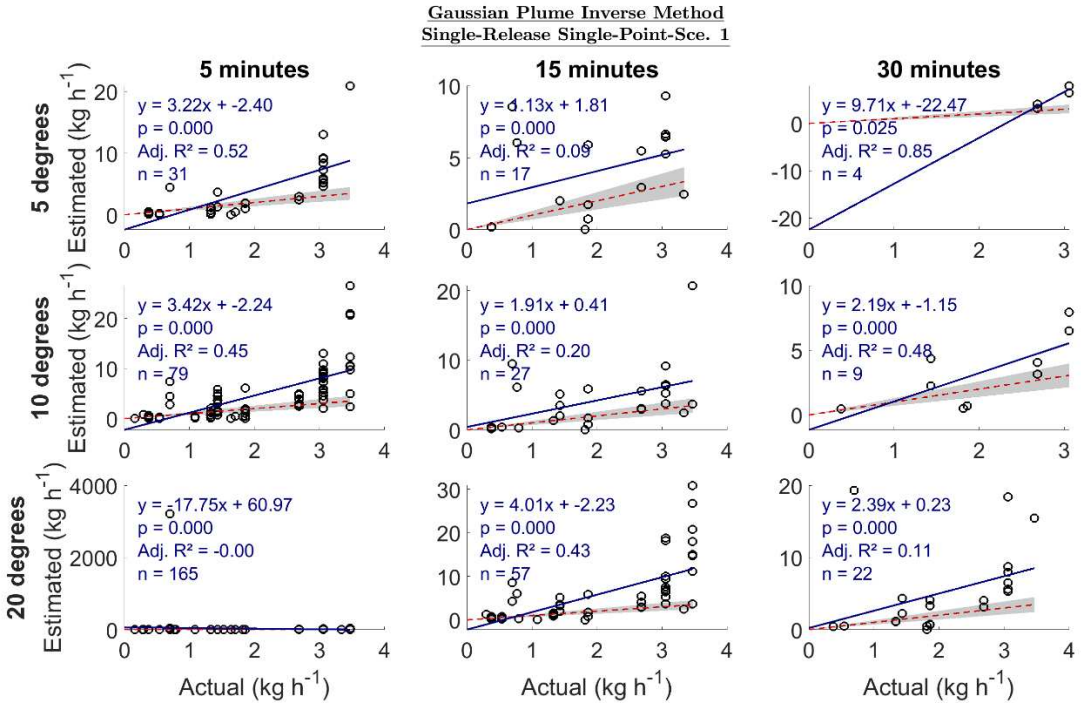

Figure A16. Estimated emission vs actual emission (kg h^{-1}) for single-release single-point emissions. The red dotted line is a 1:1 line based on actual emissions i.e. points below the line are underestimated and above are overestimated emissions. The gray region represents ±30% of the actual emission. Adj. R^2 is the adjusted R^2. The sample size is n.

A3.2.2 Scenario 2: Equation A8 & ~10 Hz sonic anemometer dispersion coefficients

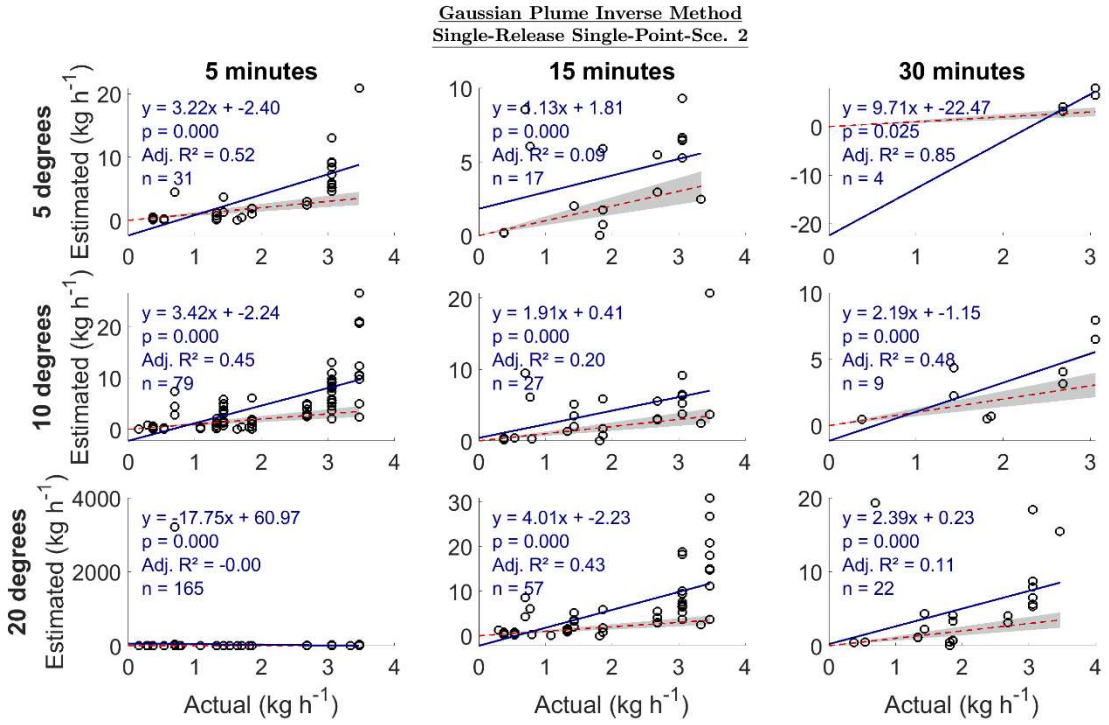

Figure A17. Estimated emission vs actual emission (kg h^{-1}) for single-release single-point emissions. The red dotted line is a 1:1 line based on actual emissions i.e. points below the line are underestimated and above are overestimated emissions. The gray region represents ±30% of the actual emission. Adj. R^2 is the adjusted R^2. The sample size is n.

A3.2.3 Scenario 3: Equation A7 & EPA 2013 dispersion coefficients

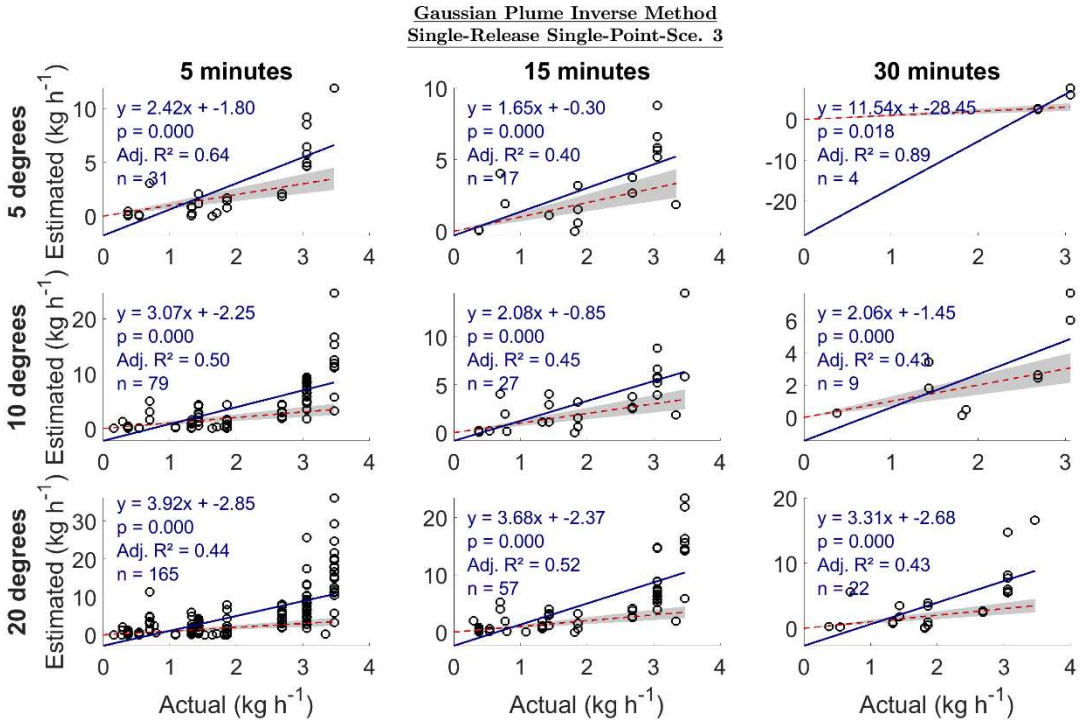

Figure A18. Estimated emission vs actual emission (kg h^{-1}) for single-release single-point emissions. The red dotted line is a 1:1 line based on actual emissions i.e. points below the line are underestimated and above are overestimated emissions. The gray region represents ±30% of the actual emission. Adj. R^2 is the adjusted R^2. The sample size is n.

A3.2.4 Scenario 4: Equation A8 & EPA 2013 dispersion coefficients

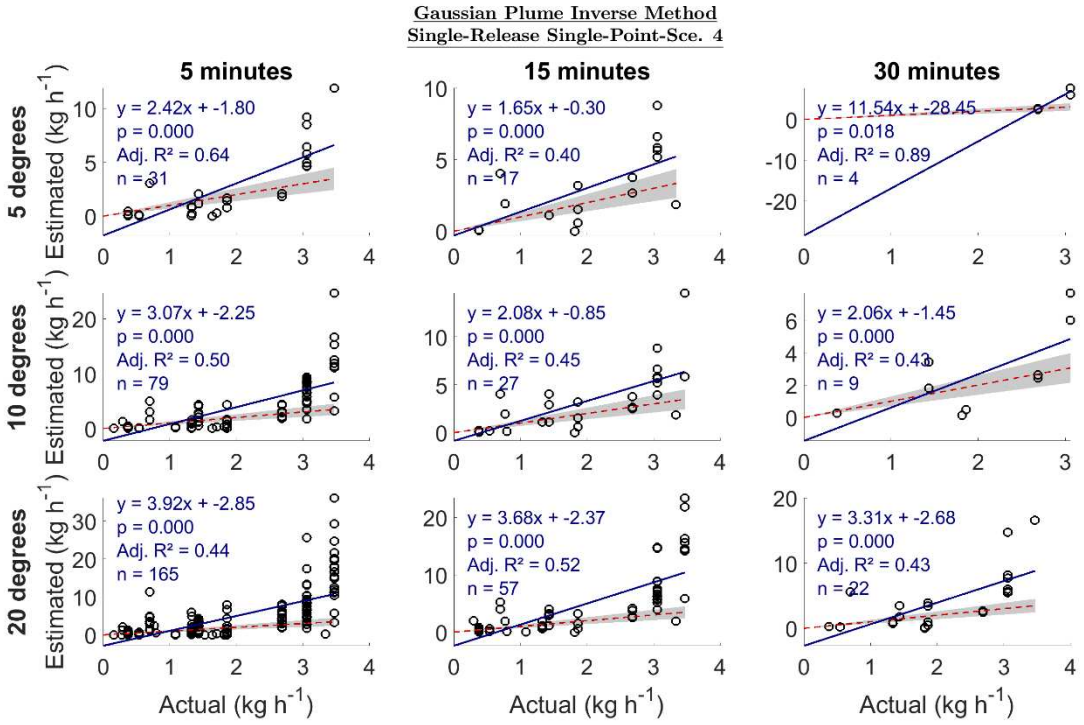

Figure A19. Estimated emission vs actual emission (kg h^{-1}) for single-release single-point emissions. The red dotted line is a 1:1 line based on actual emissions i.e. points below the line are underestimated and above are overestimated emissions. The gray region represents ±30% of the actual emission. Adj. R^2 is the adjusted R^2. The sample size is n.

A3.2.5 Scenario 5: Equation A7 & 1 Hz sonic anemometer dispersion coefficients

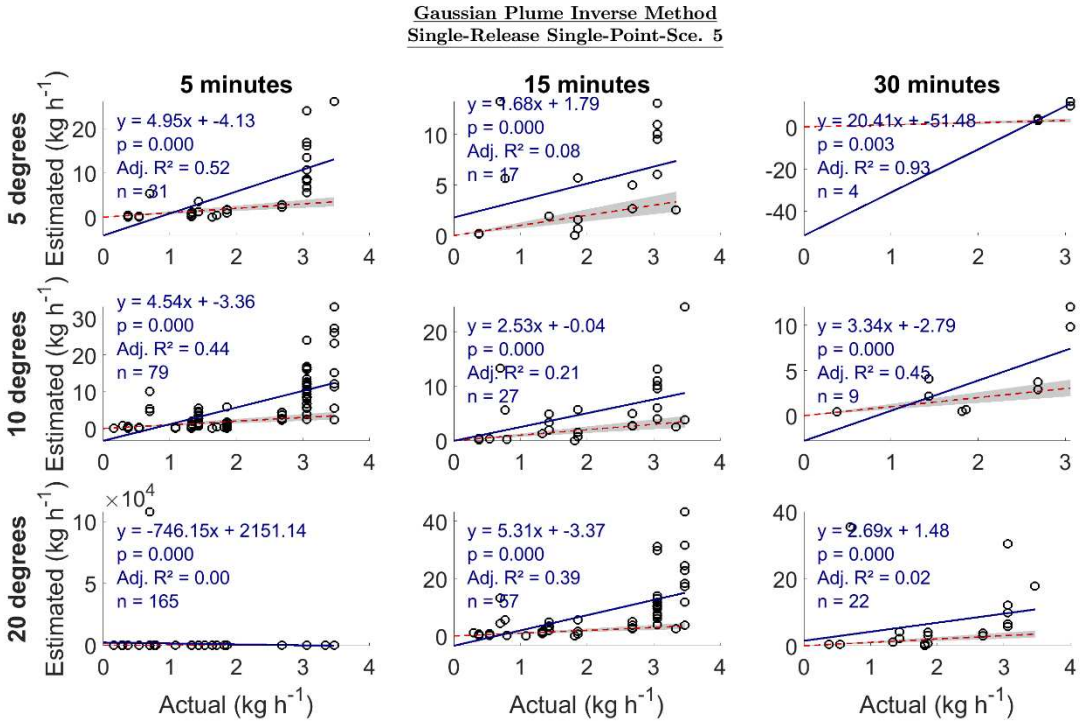

Figure A20. Estimated emission vs actual emission (kg h^{-1}) for single-release single-point emissions. The red dotted line is a 1:1 line based on actual emissions i.e. points below the line are underestimated and above are overestimated emissions. The gray region represents ±30% of the actual emission. Adj. R^2 is the adjusted R^2. The sample size is n.

A3.2.6 Scenario 6: Equation A8 & 1 Hz sonic anemometer dispersion coefficients

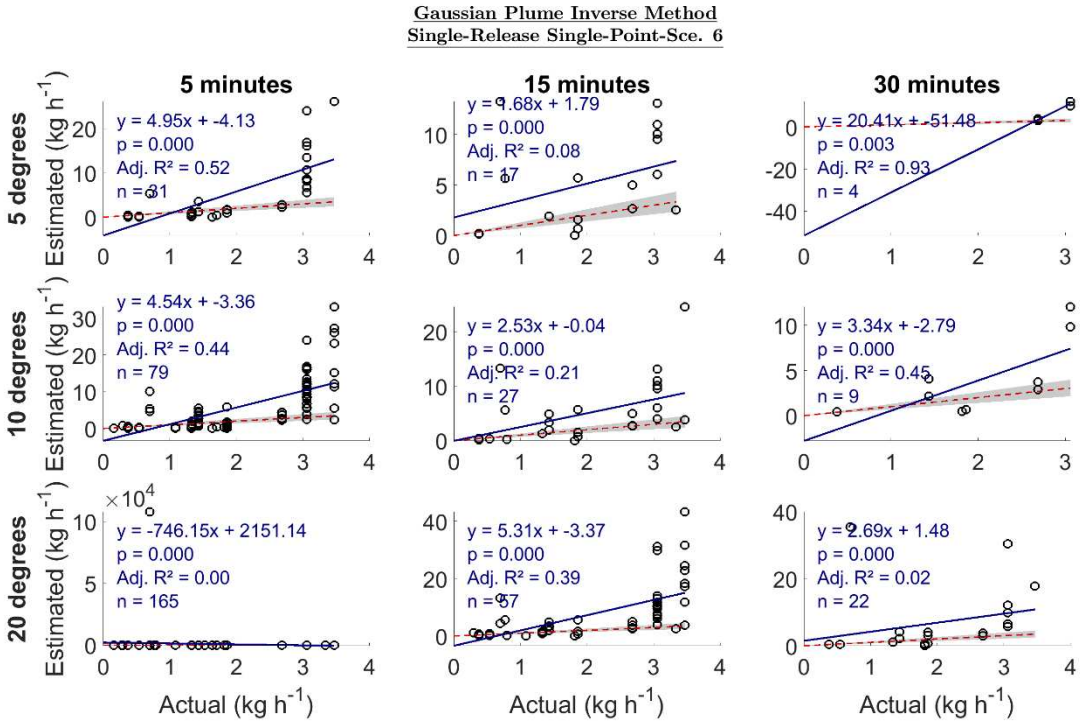

Figure A21. Estimated emission vs actual emission (kg h^{-1}) for single-release single-point emissions. The red dotted line is a 1:1 line based on actual emissions i.e. points below the line are underestimated and above are overestimated emissions. The gray region represents ±30% of the actual emission. Adj. R^2 is the adjusted R^2. The sample size is n.

A3.3 Models' Validation File

Time	Duration_HMS	EmissionPoint	Actual_Emission_kg_h	TotalEmissions	Uast	L	hs	Cb	mean_CH4_ppm	meanAT	y	mean_WS	mean_P_Pa	GPIM_Emission_kg_h	WindTrax (kg/h)	WindTrax-2_L-EC
2/13/2024 10:15	1:59:59	4T-12	2.640943924	2.640943924	0.602905	-3967.792868	4.572	2.090088	3.04428961	277.9348	1.21266	3.57080797	84128.83326	2.646264536	1.454	1.415
2/13/2024 11:00	1:59:59	4T-12	2.640943924	2.640943924	0.618549	-9046.78801	4.572	2.090088	3.970833027	277.9901	2.92143	3.131501	84132.09043	4.922171799	1.966	2.819
2/13/2024 11:15	1:59:59	4T-12	2.640943924	2.640943924	0.572507	2114.671175	4.572	2.090088	3.102874665	278.4127	6.378449	2.73867147	84115.2785	2.750184397	1.632	1.45
2/15/2024 7:00	3:59:59	4T-31	1.308861601	1.308861601	0.410045	6824.365598	4.9276	2.06483	3.078168103	269.9447	5.57591	1.14425468	84162.21079	1.269720069	0.6081	0.6716
2/17/2024 9:30	3:59:59	5S-27	1.787090411	1.787090411	0.365114	29.32349598	1.2192	2.031003	2.035164811	267.879	2.52239	0.28857985	84938.49375	0.016963131	4.60E-04	
2/18/2024 18:15	1:59:58	4S-21	0.756090336	0.756090336	1.188247	-614.2021232	1.143	2.219921	3.783770526	276.0193	0.927598	1.82489577	83613.12463	5.58015059	0.6806	
2/24/2024 5:08	1:59:59	4S-22	0.781200202	0.781200202	0.821323	-275.8862507	1.143	2.102486	2.283704848	268.3823	5.839382	1.10158416	84170.01471	0.241147207	7.72E-02	
3/1/2024 10:30	4:59:59	4W-22	3.008461053	3.008461053	0.744117	2796.196519	1.4478	2.020178	10.2390292	288.1704	0.337972	5.79619861	83654.61441	10.30154603	3.524	3.41
3/1/2024 10:45	4:59:59	4W-22	3.008461053	3.008461053	0.735233	8606.021404	1.4478	2.020178	11.26040841	288.8746	0.755437	5.31224672	83639.83807	11.01699612	3.516	4.049
3/1/2024 11:00	4:59:59	4W-22	3.008461053	3.008461053	0.72717	19976.28029	1.4478	2.020178	15.1216957	288.9612	0.500659	5.44406474	83635.93694	14.10369293	5.268	5.422
3/1/2024 11:15	4:59:59	4W-22	3.008461053	3.008461053	0.672598	5281.268141	1.4478	2.020178	11.64325554	288.8222	0.083399	5.65289374	83641.02011	12.1865376	3.936	3.604
3/1/2024 13:45	4:59:59	4W-22	3.008461053	3.008461053	0.680827	4893.486575	1.4478	2.020178	11.35895748	289.8602	0.182173	3.99380812	83522.10084	6.211436023	2.852	2.818
3/1/2024 14:15	4:59:59	4W-22	3.008461053	3.008461053	0.791826	6098.825399	1.4478	2.020178	8.138930858	290.0408	1.68032	3.28586029	83493.3752	3.996448038	1.861	1.732
3/6/2024 14:15	3:00:00	4W-32	3.283174006	3.283174006	0.747401	1234.410185	0.9652	2.07032	10.088583	285.8566	0.301888	0.82000927	83348.01754	2.524062314	0.6378	
3/12/2024 13:07	3:53:59	4S-23	1.40894685	1.40894685	0.565216	11017.69146	2.286	2.078665	4.339370646	284.403	6.168219	2.67813027	83729.79621	3.353859353	2.446	2.18
3/12/2024 13:22	3:53:59	4S-23	1.40894685	1.40894685	0.587588	-9414.698117	2.286	2.078665	4.930021252	284.3269	7.051012	2.64068699	83708.51838	4.953998857	3.35	3.24
3/12/2024 13:37	3:53:59	4S-23	1.40894685	1.40894685	0.555736	-13390.83022	2.286	2.078665	3.42845064	284.3676	1.497296	2.31789702	83689.3689	1.945601204	0.7673	
3/17/2024 12:01	4:04:46	4W-51	0.685326168	0.685326168	0.416326	-3244.967188	0.4572	1.995054	19.71393274	278.9118	0.257266	1.10704845	84794.74772	11.66200196	1.908	2.666
3/18/2024 13:41	5:19:47	4W-32	3.413249408	3.413249408	0.630694	2745.689846	0.9652	2.239865	33.42129438	285.2602	1.361598	2.63588948	84657.3863	24.65898574	7.717	
3/20/2024 7:47	3:19:59	5S-32	1.830068426	1.830068426	0.618934	866.2128433	1.0414	1.989382	3.054691455	276.3259	6.121651	2.68473116	84271.43604	5.716964626	1.652	
3/20/2024 9:02	3:19:59	5S-32	1.830068426	1.830068426	0.525049	9921.314794	1.0414	1.989382	2.167851619	279.0382	3.811796	3.10514386	84365.52937	0.686338053	0.2875	0.305
3/20/2024 9:17	3:19:59	5S-32	1.830068426	1.830068426	0.568894	5035.882458	1.0414	1.989382	2.465681074	279.0769	6.142715	2.87127818	84374.39467	1.572305175	0.8735	
3/20/2024 12:22	5:13:00	5W-32	0.368933986	0.368933986	0.692366	7213.569859	1.2446	2.005912	2.020713459	282.4805	4.092545	2.26796829	84227.28812	0.177793598	2.02E-02	
3/20/2024 12:52	5:13:00	5W-32	0.368933986	0.368933986	0.722152	774.3746734	1.2446	2.005912	2.01931774	283.2036	1.57405	1.80031194	84177.90224	0.149108588	1.25E-02	

Time	Stationarity - dev(w) [%]	Stationarity - dev(CH4) [%	Stationarity - dev (w/ch4)	Stationarity -flag (w/CH4)	CH4_flux (umol m-2 s-1	KM_Footprint Value (m-2)	EC Emission (kg/h)-KM	Klujn et	EC Emi	n (kg/h)-Klujn
2/13/2024 10:15	2	43	192	6	0.746573	0.000138583	0.311077771	0.00093	0.046343	
2/13/2024 11:00	3	24	21	2	1.39477	0.000139089	0.579051437	0.000369	0.218175	
2/13/2024 11:15	1	12	16	2	0.773093	0.000119442	0.373750577	5.34E-05	0.8353	
2/15/2024 7:00	21	39	68	4	-0.885658	0.000102204	-0.500386791	0.00013	-0.39326	
2/17/2024 9:30	68	69	91	5	-2.09E-02			0.0003	-0.00402	
2/18/2024 18:15	81	58	91	5	27.5962			0.000764	2.086441	
2/24/2024 5:08										
3/1/2024 10:30	0	54	413	7	-0.420716	0.006211989	-0.003910796	0.009513	-0.00255	
3/1/2024 10:45	0	41	37	3	-5.18482	0.007065093	-0.042376267	0.007463	-0.04012	
3/1/2024 11:00	0	30	243	6	-1.49331	0.006530287	-0.013204579	0.01301	-0.00663	
3/1/2024 11:15	1	50	363	7	-1.53558	0.006118128	-0.014493082	0.009754	-0.00909	
3/1/2024 13:45	2	83	22	2	-6.61429	0.005823846	-0.065581326	0.009869	-0.0387	
3/1/2024 14:15	12	64	371	7	0.90252	0.004111863	0.012674331	0.004801	0.010856	
3/6/2024 14:15	74	71	150	6	7.77136			0.00565	0.079428	
3/12/2024 13:07	4	6	52	4	-0.352137	0.000177795	-0.114366221	6.24E-05	-0.32598	
3/12/2024 13:22	5	58	155	6	0.135321	0.000129654	0.060268138			
3/12/2024 13:37										
3/17/2024 12:01	17	90	87	5	12.1396	0.005913262	0.11854525	0.008695	0.080623	
3/18/2024 13:41										
3/20/2024 7:47										
3/20/2024 9:02	6	57	327	7	5.42E-02	3.68E-05	0.085041507	0.000112	0.028068	
3/20/2024 9:17										
3/20/2024 12:22										
3/20/2024 12:52										

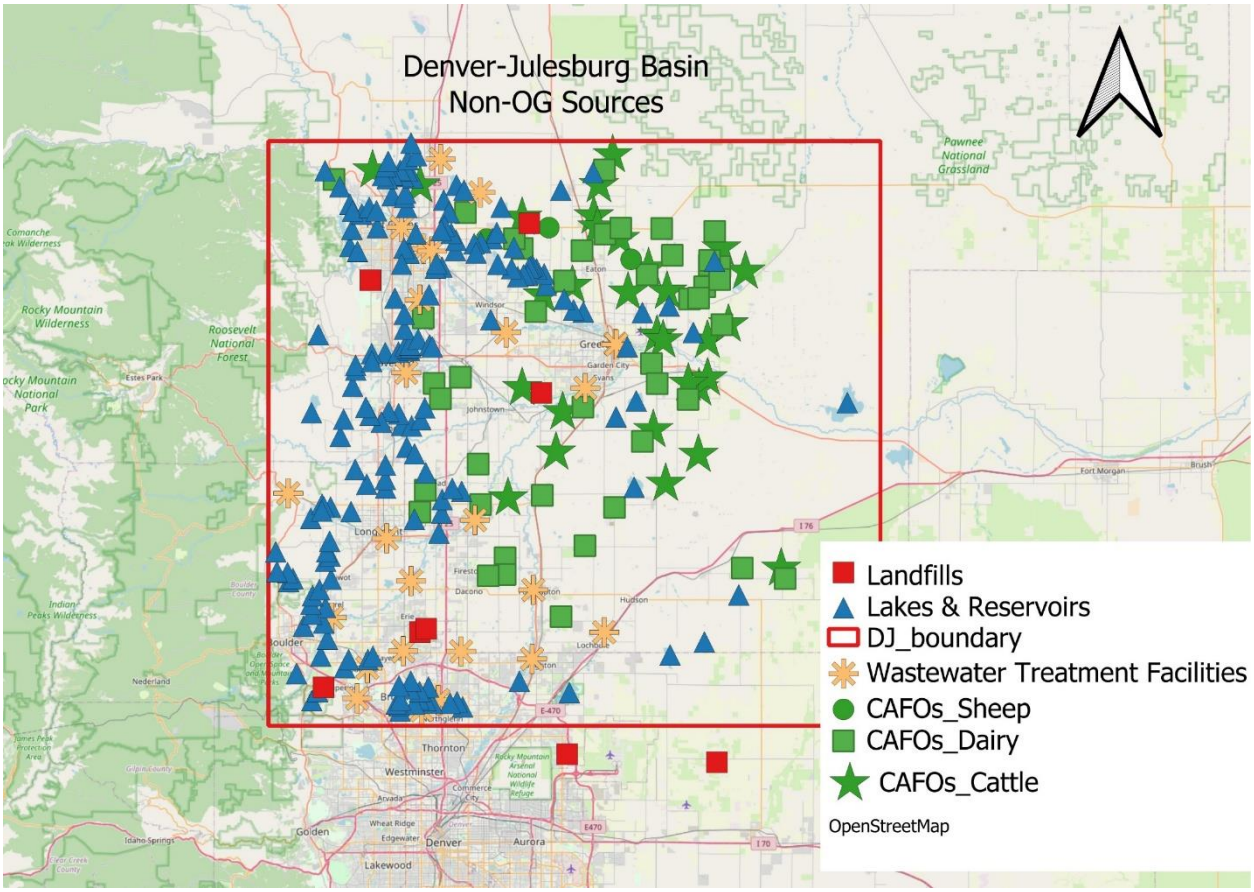

Figure A22. Location of all non-oil and gas sources in this study's DJ boundary

Figure A23. Instrument setup. Top left: Aeris Strato analyzer (sampling at 1 Hz). Top right: Airmar instrument software displaying meteorological conditions. Center: Airmar 150 WX instrument (sampling at 1 Hz). Bottom: METEC truck with the Aeris inlet tubing collocated with the Airmar instrument.

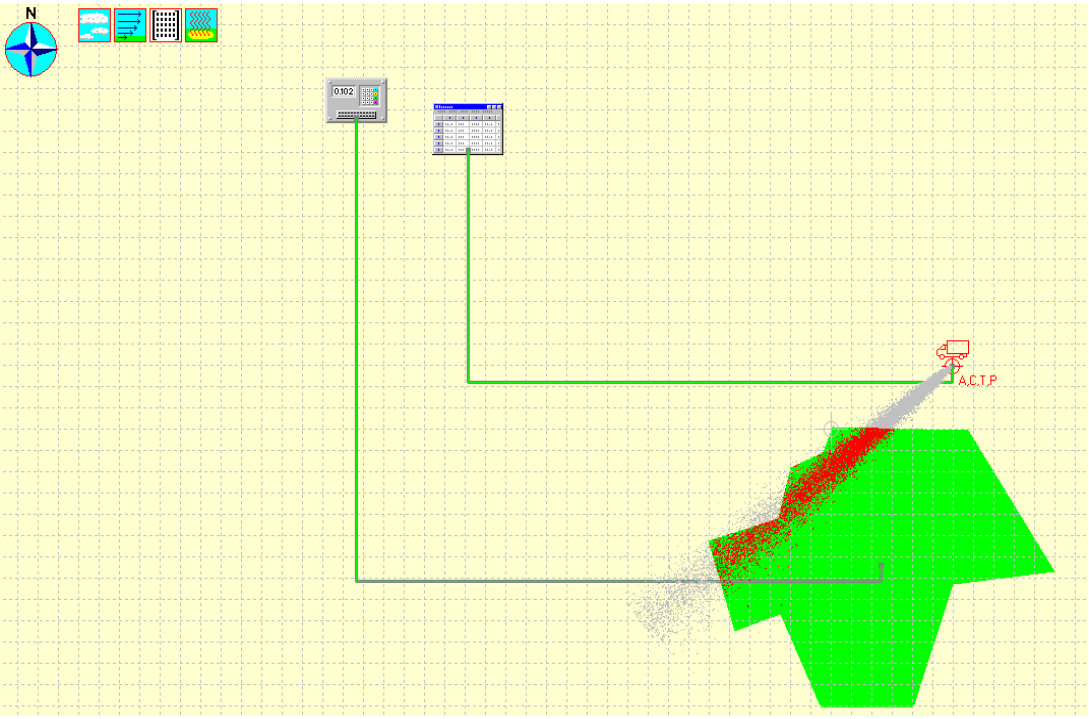

Figure A24. Sample WindTrax configuration of an area source model. The green polygon is the facility layout with size configurations from Google Maps (Google, 2025). The truck represents the METEC truck with instruments: anemometer (A), CH_4 concentration sensor (C), thermometer (T), and Pressure sensor (P).

LIST OF ABBREVIATIONS

CH_4	Methane
EF	Emission factor
EC	Eddy covariance
AFG	Aerodynamic flux gradient
GPIM	Gaussian Plume Inverse Method
bLs	Backward Lagrangian stochastic model
DJ	Denver-Julesburg
SIT	State inventory tool
IPCC	Intergovernmental Panel on Climate Change
EPA	Environmental Protection Agency
CDPHE	Colorado Department of Public Health and Environment
CAFOs	Concentrated animal feeding operations
SRSP	Single-release single-point
MRSP	Multi-release single-point
METEC	Methane Emissions Technology Evaluation Center